TIME DEPENDENT FAILURE OF THIN FILMS

Thesis by

Mullahalli V. Srinivas

California Institute of Technology

Pasadena, California

1994

(Thesis Submitted on July 28, 1993)

In Partial Fulfillment of the Requirement

for the Degree of

Mechanical Engineer

Acknowledgements

I am extremely indebted to my thesis supervisor, Professor G. Ravichandran, for his precious guidance and constant supervision throughout this work. His invaluable help and encouragement during all stages of the work has played a very significant role in the completion of this thesis. I would also like to thank Professor W.G. Knauss for helpful discussions and also for serving as one of thesis committee members. My thanks also go to the other member of my thesis committee, Professor D. Goodwin, for taking time to review the dissertation. In addition, the IBM, specifically Dr. Sundar Kamath, is to be thanked for the grant which supported this work. Finally, I am most appreciative to all the students, too numerous to mention by name, with whom I had the chance to work during my stay here.

Abstract

The prediction of time dependent failure at the interface of a thin film bonded to a substrate is considered in terms of a thermorheologically simple viscoelastic material. An initial investigation of stress distribution at the interface is carried out to understand the possible location and the mechanism of failure. Subsequently, a detailed analysis is developed to obtain not only the longitudinal stress component but also the lateral and shear stress components at the interface. Viscoelastic material behavior is included in the model to account for the stress relaxation behavior of the film. The proposed model satisfies both the edge free boundary conditions as well as the displacement and traction continuity at the interface. Using the model, the magnitude of the stresses and their relaxation behavior has been studied for the case of a polyimide film bonded to a silicon substrate. The analysis is capable of incorporating the material property at different temperatures. Using this capability, the stress evolution in a polyimide film during a typical curing process is obtained. With a view towards reducing the residual stress developed in the film, the effect of cooling rate and cooling cycle on final built in residual stresses during the curing process is studied.

Based on the stress analysis and also from experimental observations, the most likely type of failure mechanism appears to be edge decohesion. So, the problem of edge decohesion along the interface of a thin viscoelastic film bonded to an elastic substrate under tensile residual stresses is considered in the next chapter. An analytical model is developed to predict the crack growth along the interface and its velocity. The tensile residual stress in the film is replaced by a combination of edge loads and an explicit relation of strain energy with respect to time is obtained by simple beam analysis. The strain energy function is computed at small time intervals and the energy release rate is calculated using Griffith's energy balance approach; the

discretized time step is assumed to be very small so that the dissipation effects over a given time step are neglected. Crack growth along the interface is computed based on a fracture criteria. The validity of the assumptions in the analytical results is checked by performing a finite element analysis.

Table of Contents

Introductory Remark

This dissertation is organized in two complementary papers, each containing its own abstract, introduction and conclusion. The first chapter is concerned with the stress analysis at the interface of the thin film bonded to a substrate. A complete distribution of longitudinal, lateral and shear stresses at the interface is obtained using an analysis based on composite beam theory. The stress distribution for the case of a thin polyimide film bonded to an elastic substrate show that the lateral and shear stresses are concentrated at the free ends indicating that the edge decohesion is the likely type of failure to be caused at the interface. The stress evoulution in the curing process of the polyimide film is also discussed. It is shown that by employing slow cooling rates with a stepwise cooling, the final residual stresses in the film will be reduced.

The edge decohesion type of failure at the interface predicted by the stress analysis is considered in the next chapter. Strain energy release rates and crack velocity and crack growth relations are obtained by applying a Griffith energy balance to a discretized form of strain energy function. A finite element analysis is also performed and the results obtained are shown to agree well with the analytical results.

Time Dependent Interfacial Stresses in a Thin Film Bonded to a Substrate

Abstract

A viscoelastic stress analysis at the interface of a thin film and a substrate combination under thermomechanical loading is presented. A detailed analysis is developed to obtain not only the longitudinal stress component but also the lateral and shear stress components at the interface. Viscoelastic material behavior is included in the model to account for the stress relaxation behavior of the film. The proposed model satisfies both the edge free boundary conditions as well as the displacement and the traction continuity at the interface. Using the model, the magnitude of the stresses and their relaxation behavior has been studied for the case of a polyimide film bonded to a silicon substrate. The analysis is capable of incorporating the material property at different temperatures by using a shift factor. Using this capability, the stress evolution in a polyimide film during a typical curing process is obtained. With a view towards reducing the residual stress developed in the film, the effect of cooling rate and cooling cycle on final built in residual stresses during the curing process is studied.

1 Introduction

Advances in electronic packaging technology has increased the demand for devices made of many layers bonded together. Among such heterogenous structures, electronic devices such as microchips have recently received considerable attention among researchers. The increasing demand of large scale integration require exten-

sive use of multilayer technology with intermetal insulating layers. High temperature polymers are used as insulating layers [13] because of the ease of fabrication processes. Most extensively used polymer in multilayer packaging is polyimide which not only is a good insulator but also has low dielectric constant, high thermal and chemical stabilities and it is easy to apply by spin coating [22]. The majority of the applications use polymer films less than 1 mil (25 μm) in thickness while some use relatively thicker films on the order 2-3 mils such as displays and tapes.

In spite of possessing such desirable properties, the polyimide films are subjected to very high residual stress caused by thermal mismatch during the fabrication of the film. Generally, the film is deposited by spin coating onto a substrate at elevated temperatures in a stress free condition. The film and substrate are then cooled to room temperature following a certain cooling pattern. During the cooling process, the mismatch in thermal coefficients of the film and the substrate results in residual stresses. The residual stresses have been determined experimentally [7] for a polyimide film on a silicon substrate, and they are found to be of the order 50 to 70 MPa. The polymer film deposited by spin coating is not defect free. Even a carefully deposited film has certain imperfections such as voids and inclusions. These defects act as stress raisers under the influence of residual stresses and the structure may fail based on the magnitude of the residual stress. Thus, an understanding of the thermomechanical residual stresses is critical in the prediction of cracking and delamination in the multilayer structure and hence their performance and reliability in service.

Timoshenko [21] analyzed a one dimensional problem of a bi-material strip submitted to a uniform heating. He obtained a simple relation for the longitudinal stress, σ_{xx}, which was assumed to be distributed uniformly at sections remote from the free ends. The one dimensional analysis is as follows:

Consider a rod of length l and modulus E, clamped at both ends. If the temperature is reduced from T_2 to T_1, it would tend to shrink in length by an amount equal to $\alpha (T_2 - T_1) l$, where α is the co-efficient of thermal expansion. But the rod is constrained and is, therefore, effectively elongated in tension. The tensile strain is given by

$$\varepsilon = \alpha (T_2 - T_1) \tag{1.1}$$

and the corresponding thermal stress σ_o, by Hooke's law, is

$$\sigma_o = E\alpha (T_2 - T_1) \tag{1.2}$$

Consider now the film-substrate combination (Fig. 1a) which is subjected to a temperature change ΔT. The strain in the film ε_1 and the substrate ε_2 are

$$\varepsilon_1 = \alpha_1 \Delta T + \frac{F(1-\nu_1)}{E_1 h_1 w} \tag{1.3}$$

$$\varepsilon_2 = \alpha_2 \Delta T - \frac{F(1-\nu_2)}{E_2 h_2 w} \tag{1.4}$$

In the above equations, modulus E_i is replaced by $E_i/(1-\nu_i)$ in order to account for biaxial stress conditions, where i=1 refers to the film and i=2 refers to the substrate.

But strain compatability requires $\varepsilon_1 = \varepsilon_2$; therefore, the thermal mismatch force is

$$F = \frac{w(\alpha_2 - \alpha_1)\Delta T}{\left[\frac{(1-\nu_1))}{h_1 E_1}\right] + \left[\frac{(1-\nu_2))}{h_2 E_2}\right]} \tag{1.5}$$

If $h_2 E_2/(1-\nu_2) \gg h_1 E_1/(1-\nu_1)$, the thermal stress σ_o in the film is

$$\sigma_o = \frac{F}{h_1 w} = \frac{(\alpha_2 - \alpha_1)\Delta T E_1}{(1-\nu_1)} \tag{1.6}$$

Regarding the stress distribution near the free ends, it was stated that the lateral and the shear stress components were concentrated at the ends.

The one dimensional approximate model is simple and easy to incorporate in engineering applications. However, when we are interested in failure problems such as cracking and delamination, it is the lateral stress perpendicular to the interface, σ_{yy}, and the shearing stress, τ_{xy}, which are important because the longitudinal stress component, σ_{xx}, only determines the ultimate, fatigue and/or brittle strength of the material. So, a more rigorous analysis to determine, in addition, the longitudinal and shear stress is necessary from failure or life prediction point of view.

An approximate solution for a rectangular plate clamped along the edges was obtained by Aleck [1] based on the elasticity theory. The normal and shear stress components were determined at each point in the plate. A classic paper on stress distribution in the bonded joints is by Goland *et al.* [8]. They have obtained simple stress relations for two simplified cases in cemented lap joint based on structural analysis. Chen *et al.* [3] used a similar approach to obtain several simple and typical analytical models to bring out the relative importance of geometrical and material parameters. Suhir [19] extended Timoshenko's [21] theory of bimetallic strips and came up with relations for the stress components at the interface. He introduced the concept of longitudinal interfacial compliance to satisfy the stress free boundary condition of longitudinal stress component, σ_{xx}, at the free ends. Later, in another paper, Suhir [20] included in addition the transverse (through thickness) compliance to satisfy the stress free boundary condition at the free ends for both longitudinal and shear stresses.

All the works stated above have considered linear elastic material in their analysis. For a polymeric film, the material property is not linearly elastic, but it is viscoelastic

in nature, that is, if the film is subjected to stress, it tends to relax over time. Since the film failure is dependent on the magnitude of the residual stresses, the relaxation behavior could have great influence on it. It is essential to include time and temperature dependent relaxation behavior of polymeric materials to accurately model the behavior of the multi-layered structures.

It is the purpose of the present work to study the stress distribution at the interface of a thin film and substrate incorporating the viscoelastic material properties of the thin film.

2 Analysis

2.1 Problem Description

The configuration of the model problem to be analysed is shown in Fig. 1b. A thin film of thickness h_1 is bonded to a substrate of thickness h_2 and the length of this bonded structure is $2l$ such that $2l \gg h_1$. The film is deposited on the substrate at an elevated temperature, T_2, and cooled to the room temperature, T_1, following a known cooling history. Due to mismatch in thermal coefficients of the film and the substrate, residual stresses are set up in the composite structure during cooling.

The residual stresses along the interface of this structure are analysed on the basis of a plate theory. The coefficient of thermal expansion of the film and the substrate are assumed to be constant, that is, independent of temperature. The film and substrate are considered to be thermorheologically simple linearly viscoelastic materials which are characterized by a constitutive relation of the form [4], [12], [14], [16],

$$s_{ij}(\vec{x},t) = \int_{-\infty}^{t} 2G(\xi - \xi')\frac{\partial}{\partial t'}e_{ij}\,(\vec{x},\xi')\,d\xi' \tag{2.1}$$

$$\sigma_{kk}(\vec{x},t) = \int_{-\infty}^{t} 3K(\xi - \xi')\frac{\partial}{\partial t'}\varepsilon_{kk}\,(\vec{x},\xi')\,d\xi' \tag{2.2}$$

where s_{ij} and σ_{kk} are the deviatoric and dilatational components of the stress tensor $\boldsymbol{\sigma}$, e_{ij} and ε_{kk} are the deviatoric and dialtational components of the strain tensor $\boldsymbol{\varepsilon}$, and $G(t)$ and $K(t)$ are, respectively, the time dependent shear and bulk moduli of the material.

The time temperature variation of the material property is incorporated using the concept of a reduced time ξ [12], [14]

$$\xi = \int_{0}^{t} \varphi\,[T(\vec{x},\lambda)]\,d\lambda \tag{2.3}$$

where φ is a shift factor which is determined from experimental data.

2.2 Basic Equations

Figure 1b shows the forces acting on the substrate and the film at any distance x along the length of the structure. The force $T(x,t)$ is assumed to be distributed uniformly over the thickness. A correction to its actual non-uniform distribution is introduced by considering interfacial compliance as outlined by Suhir [20] in his elastic analysis.

The longitudinal stress component, $\sigma_{xx}(x,t)$, in the film at the interface is due to the axial force $T(x,t)$ and the moment $M(x,t)$ which from the elementary mechanics is given by the relation,

$$\sigma_{xx}(x,t) = \frac{T(x,t)}{h_1} + \frac{6M(x,t)}{h_1^2} \tag{2.4}$$

The shearing stress, $\tau_{xy}(x,t)$, and the lateral stress, $\sigma_{yy}(x,t)$, which occur at the interface of a thin film bonded to a substrate experiencing a temperature change, are related by the following equilibrium equation:

$$\begin{aligned} -\int_{-l}^{x}\int_{-l}^{\zeta}\sigma_{yy}(\zeta',t)d\zeta d\zeta' &= M_1(x,t)-\frac{h_1}{2}T(x,t) \\ &= -M_2(x,t)+\frac{h_2}{2}T(x,t) \end{aligned} \tag{2.5}$$

where

$$T(x,t)=\int_{-l}^{x}\tau_{xy}(\zeta,t)d\zeta \tag{2.6}$$

is the shearing force caused by thermal expansion or contraction mismatch of the materials.

It will be more convenient to construct the above equations in Laplace domain so that the convolution type of constitutive equations ((2.1) and (2.2)) become a linear function thus making the future formulations simpler. The variables in the Laplace domain are denoted by the overbar and s is the Laplace parameter. The above equations (2.5) and (2.6) in Laplace domain can be written as

$$\begin{aligned} -\int_{-l}^{x}\int_{-l}^{\zeta}\overline{\sigma}_{yy}(\zeta',s)d\zeta d\zeta' &= \overline{M}_1(x,s)-\frac{h_1}{2}\overline{T}(x,s) \\ &= -\overline{M}_2(x,s)+\frac{h_2}{2}\overline{T}(x,s) \end{aligned} \tag{2.7}$$

and

$$\overline{T}(x,s)=\int_{-l}^{x}\overline{\tau}_{xy}(\zeta,s)d\zeta \tag{2.8}$$

Let $w_1(x,t)$ and $w_2(x,t)$ be the lateral deflection of the strips, which are treated here as elongated rectangular plates. The relation between the moment $M(x,t)$ and the deflection $w(x,t)$ in the Laplace domain are [see Appendix I]:

$$\overline{M}_1(x,s) = \frac{4s\overline{\mu}_1(s)(3\overline{K}_1(s)+\overline{\mu}_1(s))h_1^3}{12(3\overline{K}_1(s)+4\overline{\mu}_1(s))}\overline{w}_1''(x,s) = \overline{D}_1(s)\overline{w}_1''(x,s) \tag{2.9}$$

$$\overline{M}_2(x,s) = \frac{4s\overline{\mu}_2(s)(3\overline{K}_2(s)+\overline{\mu}_2(s))h_2^3}{12(3\overline{K}_2(s)+4\overline{\mu}_2(s))}\overline{w}_2''(x,s) = \overline{D}_2(s)\overline{w}_2''(x,s) \tag{2.10}$$

where prime represents differentiation with respect to the spatial variable x.

Substituting the expression for $\overline{M}_1(s)$ and $\overline{M}_2(s)$ in equation (2.7) and differentiating it twice with respect to x,

$$\begin{aligned}\overline{\sigma}_{yy}(x,s) &= -\overline{D}_1(s)\overline{w}_1^{IV}(x,s) + \frac{h_1}{2}\overline{\tau}_{xy}'(x,s) \\ &= \overline{D}_2(s)\overline{w}_2^{IV}(x,s) - \frac{h_2}{2}\overline{\tau}_{xy}'(x,s)\end{aligned} \tag{2.11}$$

The lateral stress $\sigma_{yy}(x,t)$ can also be represented as

$$\sigma_{yy}(x,t) = \int_0^t K_s(t-t')(dw_1(x,t') - dw_2(x,t')) \tag{2.12}$$

where K_s is the through thickness spring constant.

The above equation in Laplace domain can be written as

$$\overline{\sigma}_{yy}(x,s) = s\overline{K}_s(s)(\overline{w}_1(x,s) - \overline{w}_2(x,s)) \tag{2.13}$$

The constant K_s is related to transverse compliance of the film and substrate which is evaluated in the following way:

The elastic solution for the lateral displacements in a long and narrow strip due to a transverse load is given by the relation [20]

$$w(x) = \frac{(1-\nu^2)h}{E\sigma_{yy}(x)} \tag{2.14}$$

Using the correspondence principle, the solution in the Laplace domain for the viscoelastic problem is

$$\overline{w}(x,s) = \frac{(3\overline{K}(s) + 4\overline{\mu}(s))h}{4s\overline{\mu}(s)(3\overline{K}(s) + \overline{\mu}(s))}\overline{\sigma}_{yy}(x,s) \tag{2.15}$$

Substituting equation (2.15) in (2.13), we obtain,

$$\overline{K}_s(s) = \left[\frac{(3\overline{K}_1(s) + 4\overline{\mu}_1(s))h_1}{4\overline{\mu}_1(s)(3\overline{K}_1(s) + \overline{\mu}_1(s))} + \frac{(3\overline{K}_2(s) + 4\overline{\mu}_2(s))h_2}{4\overline{\mu}_2(s)(3\overline{K}_2(s) + \overline{\mu}_2(s))}\right]^{-1} \tag{2.16}$$

But from equation (2.11), we have

$$\overline{w}_1^{IV}(x,s) = -\frac{\overline{D}_2(s)}{\overline{D}_1(s)}\overline{w}_2^{IV}(x,s) + \frac{(h_2+h_1)}{2\overline{D}_1(s)}\overline{\tau}'_{xy}(x,s) \tag{2.17}$$

Substituting (2.13) in the above equation,

$$\overline{w}_1^{IV}(x,s) = \frac{\overline{D}_2(s)}{s\overline{K}_s(s)\overline{D}(s)}\overline{\sigma}_{yy}^{IV}(x,s) + \frac{h}{2\overline{D}(s)}\overline{\tau}'_{xy}(x,s) \tag{2.18}$$

where $\overline{D}(s) = \overline{D}_1(s) + \overline{D}_2(s)$ is the total flexural rigidity and $h = h_1 + h_2$ is the total thickness of the bi-material strip.

Similarly,

$$\overline{w}_2^{IV}(x,s) = -\frac{\overline{D}_1(s)}{s\overline{K}_s(s)\overline{D}(s)}\overline{\sigma}_{yy}^{IV}(x,s) + \frac{h}{2\overline{D}(s)}\overline{\tau}'_{xy}(x,s) \tag{2.19}$$

From equations (2.11), (2.18) and (2.19) we obtain the following relationship between $\overline{\sigma}_{yy}(x,s)$ and $\overline{\tau}_{xy}(x,s)$

$$\overline{\sigma}_{yy}^{IV}(x,s) + 4\overline{\alpha}^4(s)\overline{\sigma}_{yy}(x,s) = 4\overline{\mu}(s)\overline{\alpha}^4(s)\overline{\tau}'_{xy}(x,s) \tag{2.20}$$

where

$$\overline{\alpha}(s) = \left[\frac{s\overline{K}_s(s)\overline{D}(s)}{4\overline{D}_1(s)\overline{D}_2(s)}\right]^{\frac{1}{4}} \qquad \overline{\mu}(s) = \frac{h_1\overline{D}_2(s) - h_2\overline{D}_1(s)}{2\overline{D}(s)}$$

Another equation for the stress components $\overline{\sigma}_{yy}(x,s)$ and $\overline{\tau}_{xy}(x,s)$ can be obtained from the continuity of longitudinal displacements $\overline{u}_1(x,s)$ and $\overline{u}_2(x,s)$ at the interface.

The displacement relations at the interface are given by:

$$\begin{aligned}\overline{u}_1(x,s) &= \alpha_1\Delta T x - \overline{\lambda}_1(s)\int_{-l}^{x}\overline{T}(\xi,s)d\xi + \overline{\kappa}_1(s)\overline{\tau}_{xy}(x,s) \\ &\quad -\frac{h_1}{2}\overline{w}_1'(x,s)\end{aligned} \tag{2.21}$$

$$\begin{aligned}\overline{u}_2(x,s) &= \alpha_2\Delta T x + \overline{\lambda}_2(s)\int_{-l}^{x}\overline{T}(\xi,s)d\xi - \overline{\kappa}_2(s)\overline{\tau}_{xy}(x,s) \\ &\quad +\frac{h_2}{2}\overline{w}_2'(x,s)\end{aligned} \tag{2.22}$$

where α_1 and α_2 are coefficients of thermal expansion of film and substrate respectively,

$$\overline{\lambda}_1(s) = \frac{3\overline{K}_1(s) + 4\overline{\mu}_1(s)}{4s\overline{\mu}_1(s)(3\overline{K}_1(s) + \overline{\mu}_1(s))}h_1$$

and

$$\overline{\lambda}_2(s) = \frac{3\overline{K}_2(s) + 4\overline{\mu}_2(s)}{4s\overline{\mu}_2(s)(3\overline{K}_2(s) + \overline{\mu}_2(s))}h_2$$

are the in-plane compliances of the strips,

$$\overline{\kappa}_1(s) = \frac{h_1}{3s\overline{\mu}_1(s)}$$

and

$$\overline{\kappa}_2(s) = \frac{h_2}{3s\overline{\mu}_2(s)}$$

are their interfacial compliances. In the above displacement equations ((2.21) and (2.22)), the first term represents the unrestricted thermal expansion, the second term is due to thermal mismatch forces $T(x,t)$ which are assumed to be uniformly distributed through its thickness, while the third term accounts for the nonuniform distribution of the aforementioned forces, and the last term is due to bending.

The continuity equation $\overline{u}_1(x,s) = \overline{u}_2(x,s)$ results in

$$\begin{aligned} \overline{\kappa}(s)\overline{\tau}_{xy}(x,s) - \overline{\lambda}_{12}(s)\int_{-l}^{x}\overline{T}(\xi,s)d\xi &= \Delta\alpha\Delta T x + \frac{h_1}{2}\overline{w}_1'(x,s) \\ &\quad + \frac{h_2}{2}\overline{w}_2'(x,s) \end{aligned} \tag{2.23}$$

where $\overline{\kappa}(s) = \overline{\kappa}_1(s)+\overline{\kappa}_2(s)$, $\overline{\lambda}_{12}(s) = \overline{\lambda}_1(s)+\overline{\lambda}_2(s)$ are the total interfacial compliance and total in-plane compliance respectively and $\Delta\alpha = \alpha_2 - \alpha_1$.

Differentiating equation (2.23) with respect to x and substituting (2.8)

$$\overline{\kappa}(s)\overline{\tau}_{xy}''(x,s) - \overline{\lambda}_{12}(s)\overline{\tau}_{xy}(x,s) = \frac{h_1}{2}\overline{w}_1'''(x,s) + \frac{h_2}{2}\overline{w}_2'''(x,s) \tag{2.24}$$

Using equations (2.18) and (2.19), equation (2.24) can be presented in the form,

$$\overline{\tau}_{xy}''(x,s) - \overline{k}^2(s)\overline{\tau}_{xy}(x,s) = \overline{m}(s)\overline{\sigma}_{yy}'''(x,s) \tag{2.25}$$

where the following notation is used:

$$\overline{k}(s) = \sqrt{\frac{\overline{\lambda}(s)}{\overline{\kappa}(s)}} \tag{2.26}$$

$$\overline{\lambda}(s) = \overline{\lambda}_{12}(s) + \frac{h^2}{4\overline{D}(s)} \tag{2.27}$$

$$\overline{m}(s) = \frac{\overline{\mu}}{s\overline{K}_s(s)\overline{\kappa}(s)} \tag{2.28}$$

Equations (2.20) and (2.25) form a system from which the stress components $\overline{\tau}_{xy}(x,s)$ and $\overline{\sigma}_{yy}(x,s)$ at the interface can be determined. In order to separate these functions, we rewrite (2.25) in the form

$$\overline{\sigma}_{yy}^{IV}(x,s) = \frac{1}{\overline{m}(s)}\left(\overline{\tau}_{xy}'''(x,s) - \overline{k}^2(s)\overline{\tau}_{xy}'(x,s)\right) \tag{2.29}$$

and by substituting this equation into (2.20) we have

$$\overline{\sigma}_{yy}(x,s) = \frac{1}{4\overline{\alpha}^4(s)\overline{m}(s)}\left((1+\overline{\epsilon}(s))\overline{k}^2(s)\overline{\tau}_{xy}'(x,s) - \overline{\tau}_{xy}'''(x,s)\right) \tag{2.30}$$

where

$$\overline{\epsilon}(s) = \frac{4\overline{\mu}(s)\overline{\alpha}^4(s)\overline{m}(s)}{\overline{k}^2(s)} = \frac{\overline{\mu}^2(s)\overline{D}(s)}{\overline{\lambda}(s)\overline{D}_1(s)\overline{D}_2(s)} \tag{2.31}$$

is a dimensionless parameter of the normal stress.

Now substituting (2.30) into (2.25), we obtain the following homogenous differential equation for the shearing stress function $\overline{\tau}_{xy}(x,s)$

$$\begin{aligned}&\overline{\tau}_{xy}^{VI}(x,s) - (1-\overline{\epsilon}(s))\overline{k}^2(s)\overline{\tau}_{xy}^{IV}(x,s) + 4\overline{\alpha}^4(s)\overline{\tau}_{xy}''(x,s)\\ &\quad -4\overline{\alpha}^4(s)\overline{k}^2(s)\overline{\tau}_{xy}(x,s) = 0\end{aligned} \tag{2.32}$$

By introducing the expression for the derivative $\overline{\tau}_{xy}'(x,s)$ from (2.20) into (2.30), we obtain the following homogenous differential equation for the normal stress $\overline{\sigma}_{yy}(x,s)$,

$$\begin{aligned}&\overline{\sigma}_{yy}^{VI}(x,s) - (1-\overline{\epsilon}(s))\overline{k}^2(s)\overline{\sigma}_{yy}^{IV}(x,s) + 4\overline{\alpha}^4(s)\overline{\sigma}_{yy}''(x,s)\\ &\quad -4\overline{\alpha}^4(s)\overline{k}^2(s)\overline{\sigma}_{yy}(x,s) = 0\end{aligned} \tag{2.33}$$

Thus, both the shearing and the lateral stresses can be determined on the basis of the same ordinary homogenous differential equation of the sixth order.

2.3 Boundary Conditions

The equilibrium condition requires that the function $\overline{\tau}_{xy}(x,s)$ must be antisymmetric with respect to the origin. Based on physical considerations, we assume that it takes the following form at the edge $x = l$.

$$\overline{\tau}_{xy}(l,s) = 0 \qquad \overline{\tau}'_{xy}(l,s) = \frac{\Delta\alpha\Delta T}{\overline{\kappa}(s)} \qquad \overline{\tau}''_{xy}(l,s) = 0 \tag{2.34}$$

The first condition follows from the equilibrium equation (2.7) which could be differentiated to be in the form

$$\begin{aligned}\int_{-l}^{x} \overline{\sigma}_{yy}(\xi,s)d\xi &= \overline{D}_1(s)\overline{w}_1'''(x,s) - \frac{h_1}{2}\overline{\tau}_{xy}(x,s) \\ &= -\overline{D}_2(s)\overline{w}_2'''(x,s) + \frac{h_2}{2}\overline{\tau}_{xy}(x,s)\end{aligned} \tag{2.35}$$

The lateral stress $\overline{\sigma}_{yy}(x,s)$ is self equilibrated and therefore the summation over the whole length ($x = l$) is zero. Since there are no concentrated lateral forces at the free end, $\overline{w}_1'''(l,s) = \overline{w}_2'''(l,s) = 0$. This leads to the condition $\overline{\tau}_{xy}(x,s) = 0$.

The second condition can be obtained from (2.24) using the fact that there are no external forces at the free edges, *i.e.*, $\overline{T}(l,s) = 0$ and that there are no bending moments in the cross section $x = l$, so that $\overline{w}_1''(l,s) = \overline{w}_2''(l,s) = 0$.

The third condition follows from (2.24) and (2.8). Since $\overline{\tau}_{xy}(l,s) = 0$ and, in addition, $\overline{w}_1'''(l,s) = \overline{w}_2'''(l,s) = 0$, then the second derivative of the shear stress must also be zero at this cross section.

The lateral stress $\overline{\sigma}_{yy}(x,s)$ must be symmetric with respect to the origin and should satisfy the equilibrium conditions for the lateral forces and bending moments:

$$\int_{-l}^{+l} \overline{\sigma}_{yy}(x,s)dx = \int_{-l}^{+l}\int_{-l}^{x} \overline{\sigma}_{yy}(\zeta,s)dxd\zeta = 0 \tag{2.36}$$

Obviously, these conditions are fulfilled automatically as long as the conditions $\overline{T}(l,s) = 0$ and $\overline{\tau}_{xy}(l,s) = 0$ are satisfied.

2.4 Solution

The differential equations (2.32) and (2.33) were solved by the method of characteristics [see Appendix II] satisfying the above mentioned boundary conditions. The normal stress $\overline{\sigma}_{yy}$ and the shear stress $\overline{\tau}_{xy}$ solutions obtained by solving the differential equations,

$$\begin{aligned}\overline{\tau}_{xy}(x,s) &= \overline{C}_1(s)\sinh\left(\overline{\beta}_1(s)x\right) + \overline{C}_3(s)\cosh\left(\overline{\gamma}_1(s)x\right)\sin\left(\overline{\gamma}_2(s)x\right) \\ &\quad +\overline{C}_5(s)\sinh\left(\overline{\gamma}_1(s)x\right)\cos\left(\overline{\gamma}_2(s)x\right)\end{aligned} \tag{2.37}$$

$$\begin{aligned}\overline{\sigma}_{yy}(x,s) &= \overline{C}_2(s)\cosh\left(\overline{\beta}_1(s)x\right) + \overline{C}_4(s)\cosh\left(\overline{\gamma}_1(s)x\right)\cos\left(\overline{\gamma}_2(s)x\right) \\ &\quad +\overline{C}_6(s)\sinh\left(\overline{\gamma}_1(s)x\right)\sin\left(\overline{\gamma}_2(s)x\right)\end{aligned} \tag{2.38}$$

where the constants $\overline{C}_1(s)$ through $\overline{C}_6(s)$ are the functions of Laplace parameter s and are given in Appendix II.

The longitudinal stress $\overline{\sigma}_{xx}$ is represented by the equation

$$\overline{\sigma}_{xx}(x,s) = \frac{\overline{T}(x,s)}{h_1} + \frac{6\overline{M}_1(x,s)}{h_1^2} \tag{2.39}$$

where $\overline{T}(x,s)$ and $\overline{M}_(x,s)$ are given by the equations (2.8) and (2.7) respectively.

The solution thus obtained in the Laplace domain is inverted back to the time domain numerically.

3 Thin Film Bonded to a Substrate

3.1 Residual Stresses in the Film

Solution to the problem of a viscoelastic thin film bonded to an elastic substrate is presented in this section. Analytical solutions established in the previous section are used to study the residual stresses and its relaxation behavior along the interface. The viscoelastic film material used in this example is a polyimide. Stress relaxation data obtained at different temperatures for the polyimide by Smith and Kim [18] is used to characterize the film material property. Master or composite curve at $30°C$ was prepared from the relaxation data available at different temperatures. Briefly, an arbitrary reference curve is selected (at $30°C$) and then the other curves are shifted horizontally along the $\log t$ axis to obtain a master curve. The master curve obtained by shifting is shown in Fig. 2, while the temperature dependence of the shift function is shown in Fig. 3. The master curve is fitted with a 13-term prony series [12] of the form

$$E(t) = E_0 + \sum_{i=1}^{13} E_i \exp\left(-\frac{t}{\tau}\right) \tag{3.1}$$

to incorporate in the numerical calculations. The constants used in the above equation (3.1) is given in Table 1. The shift function $\psi(T)$ is fitted with a linear function given below:

$$log_{10}\psi(T) = 0.06136T - 1.0697 \tag{3.2}$$

The coefficient of thermal expansion of the polyimide is temperature dependent; an average value of $1 \times 10^{-5}/°C$ between $30°C$ and $400°C$ was used as a representative value as adopted by Numata and others [15]. The initial Poisson's ratio $\nu(0)$ of

i	E (Pa)	τ (s)
0	1.9953×10^9	.....
1	1.8479×10^8	9.8286×10^{-2}
2	4.4533×10^8	6.6146
3	5.4560×10^8	4.4516×10^2
4	5.7778×10^8	2.9959×10^4
5	5.5759×10^8	2.0162×10^6
6	7.3616×10^8	1.3569×10^8
7	5.8708×10^8	9.1321×10^9
8	5.9782×10^8	6.1459×10^{11}
9	5.4039×10^8	4.1362×10^{13}
10	7.0159×10^8	2.7836×10^{15}
11	6.1711×10^8	1.8734×10^{17}
12	6.5697×10^8	1.2608×10^{19}
13	9.0950×10^8	8.4849×10^{20}

Table 1: Constants used in the prony series

polyimide is 0.29. The glass transition temperature of the polyimide is around $230°C$ [18].

The experimental data cited above is sufficient to determine the relaxation shear modulus $\mu(t)$ and the (constant) bulk modulus K, once the dilatational response of the material is assumed to be elastic. Such an assumption appears to be reasonable for high polymers such as polyimide [14]. It is more expedient, however, to express these moduli in Laplace domain and they are obtained by the relations expressed in terms of transformed tensile modulus $\overline{E}(s)$ and Poisson's ratio $\overline{\nu}(s)$ given by [14]

$$\overline{G}(s) = \frac{3K\overline{E}(s)}{9K - \eta\overline{E}(s)} \tag{3.3}$$

$$\overline{K}(s) = \frac{E(0)}{3s\,(1 - 2\nu(0))} \tag{3.4}$$

The substrate material chosen was silicon [2] whose Young's modulus value is $1.689 \times 10^{11} Pa$, Poisson's ratio is 0.2624 and coefficient of thermal expansion is $2.8 \times$

$10^{-6}/°C$.

Using these material properties, the stresses $\overline{\sigma}_{xx}(s)$, $\overline{\sigma}_{yy}(s)$ and $\overline{\tau}_{xy}(s)$ were calculated from equations (2.39), (2.38) and (2.37) along the interface for different thickness ratio with varying Laplace parameter. The stresses so obtained were numerically inverted to the time domain by the Schapery's direct method of approximation [17]. The method can be applied directly by simply multiplying the value of transformed function, say $\overline{f}(s)$ by the Laplace parameter s and evaluating the function at $s = 0.5/t$. Mathematically,

$$f(t) = \left[s\overline{f}(s)\right]_{s=s_0} \tag{3.5}$$

where $s_0 = 0.5/t$.

Figure 4 shows a plot of function $s\overline{\sigma}_{xx}(s)$ versus $\log s$ evaluated at different locations along the interface using the relation (2.39), and it is seen that the function $s\overline{\sigma}_{xx}(s)$ is practically linear. Similar behavior is observed for the stress components $s\overline{\sigma}_{yy}(s)$ and $s\overline{\tau}_{xy}(s)$ which are shown in Figs. 5 and 6 respectively. The approximate method of inversion gives good results for this kind of behavior [5] and hence the method has been used here to study the relaxation behavior of the various stress components.

3.2 Results and Discussion

The residual stresses obtained at different times and different aspect ratios were normalized with respect to the tensile modulus of the film at time $t = 0$ (glassy modulus). All the stress components were plotted against the location along the interface normalized by the length l of the film to study the relaxation behavior.

Figure 7 displays the time variations of the longitudinal stress $\sigma_{xx}(x,t)$, along the

right half of the interface. As may be expected, the stresses relax with time due to the viscoelastic nature of the film material. In the case of aspect ratio ($h_1 : l = 1 : 5$), the maximum stress occurs at the center and gradually tends to zero towards the free end. However, as the aspect ratio is decreased ($h_1 : l = 1 : 50$), the stresses remain fairly constant and suddenly drops to zero very close to the free end.

The distribution of lateral stress σ_{yy} is shown in Fig. 8 and they also relax with time. For relatively high aspect ratio the stresses near the center remain fairly constant while in the case of smaller aspect ratio, it remains nearly zero for most of its length except near the free ends. The range of length over which the stress variation occurs becomes smaller as the aspect ratio is decreased and the stresses fall very rapidly. A stress concentration occurs at the free end in both cases. A similar behavior would have been observed if a concentrated normal load was applied at the free end, thus suggesting a Saint Venant's type of behavior (rapid decay of end effects). Figure 9 shows the variation of shear stress τ_{xy} along the interface. The stresses relax as observed in the case of normal stresses. It attains a peak value gradually as we move from the center before vanishing at the free end. The location of peak stress moves closer to the free end as the aspect ratio is decreased.

The above results indicate that the stress variation at the interface is highly localized near the free ends for smaller aspect ratios. These variations do not extend more than a few film thickness. This kind of behavior is expected for the problem considered here and can be explained by considering the superposition shown in Fig. 10. In Fig. 10b, the film is under uniform misfit strain which is equivalent to the thermal strain. However, the edges are not traction free in this case. Therefore, we add a system of loads (Fig. 10c) where the edges are just subjected to stress σ_{xx} but in the opposite direction and without misfit strain, so that when superposed, the original residual stress problem (Fig. 10d) with stress free boundary conditions

at the edge is recovered.

The compressive loading in Fig.10c causes stresses σ_{xx}, σ_{yy} and τ_{xy} in the film which do not extend more than few film thickness as explained by Goodier's [10] extension of the Saint Venant's principle. The significance of this is that the thermal stress $\sigma_{xx} = E\Delta\alpha\Delta T$, $\sigma_{yy} = 0$ and $\tau_{xy} = 0$ for the interior of the plate. The stresses calculated in the numerical example above approach these values in the interior as the aspect ratio is decreased. Also, these stress values are of the same order as that obtained experimentally for a polyimide film on silicon substrate [7].

The magnitude of the longitudinal stress σ_{xx} is about 50-60 times larger than the tensile lateral stress σ_{yy} and maximum shear stress τ_{xy}. However, from a failure or reliability point of view, the interfacial stresses σ_{yy} and τ_{xy} are very important while the normal stress σ_{xx} is responsible for the ultimate, fatigue and brittle strength of the film. Thus, if there are any imperfections at the interface, the most likely location where the fracture will initiate is near the free edge because the stresses responsible for failure are concentrated in this region. Experimental observations of thin ductile films on brittle substrates [6] and brittle films on brittle substrates [11] have shown this kind of a behavior where the films decohere at the edges along the interface.

4 Effect of Cooling Rate and Cooling Cycle

The analytical model described before can also be used to calculate stresses at any temperature by incorporating the reduced time factor in the constitutive relation [12], [14]. The model with reduced time is used here to study the effect of cooling rate and cooling cycle on the final residual stresses built in the film. In most practical

applications the aspect ratio of the film is very low and so the results presented in this section is for an aspect ratio $h_1 : l$ of 1:50. Organic films such as polyimide are deposited by spin coating them onto a substrate and later subjecting it to thermal cycles to obtain the desired properties. Figure 11 shows a conventional curing cycle adopted to deposit a polyimide film [7].

Polyimide is insoluble in most commonly used solvents and therefore applied as precursor on the substrate by spin coating. The coated films are pre-baked at $80°C$ for about 30 minutes to evaporate the moisture content. Then they are heated at a constant rate to about $400°C$. During heating, a hydrolitic chemical reaction (imidization) takes place to form polyimide. The chemical reaction is associated with volume shrinkage which might build up some shrinkage stresses. The film is then subjected to final baking at $400°C$ for about 30 minutes to get rid of all the moisture and excess solvents. Finally, the film is cooled at a constant rate to the room temperature. Goldsmith and others [9] have investigated the in situ stresses generated during the final baking process. They have shown that there are no shrinkage stresses developed at final bake temperature. Thus, the residual stresses are completely due to thermal mismatch. Since our model can calculate the thermal stresses, we will use it to study the evolution of these stresses.

Given a combination of film and substrate materials and its geometry, the only parameters which affect the residual stresses during the film deposition and its curing are the cooling rate and the cooling cycle. The model developed earlier was used to study the effect of these parameters on final residual stresses built in the film.

Figure 12 shows the longitudinal stress, σ_{xx}, distribution when the film is cooled at different rates to the room temperature. The stress components are plotted at a

fixed observer time. It is seen that the final residual stress values are reduced for slow cooling rates. The reduction in residual stress is due to the fact that when the film and the substrate are cooled, the stresses are generated due to thermal mismatch along with the relaxation of the generated stress due to viscoelastic nature of the film. The observed overall stress depends on the rate of stress generated relative to the stress relaxation over the course of time. Also, the relaxation is much more pronounced at higher temperatures, as the material clock is faster than the observer clock (reduced time, equation (2.2)). Thus, at very slow rates of cooling, the stress relaxation is more compared to higher cooling rates. So, the residual stresses in the film decreases as the cooling rate is slowed down.

Figure 13 shows the stress evolution at a distance $l/4$ from the free edge when the film is cooled to room temperature in different steps. The final residual stress decreases as the number of steps are increased. At each hold time in a cooling step, the stress relaxation occurs. As more number of steps are introduced, the longer the hold time, causing more relaxation. So, the final residual stress observed will be lesser when the number of cooling steps are increased as seen in Fig. 13. In an actual curing process, an optimum number of steps with a lower rate of cooling has to be worked out. It is however desirable to have more number of cooling steps at higher temperatures as the material time scale is higher in that region.

5 Conclusions

A detailed viscoelastic interfacial stress analysis of a thin film bonded to a substrate under thermal loading was obtained. The stress analysis provided a complete distribution of lateral, longitudinal and shear stress components along the interface as a function of time. The stress components relaxed a considerable amount over time.

The longitudinal stress component, σ_{xx}, was uniformly distributed away from the free ends as in the case of one dimensional model. The shear and lateral components were concentrated near the free ends and had no effect on the interior as the aspect ratio was decreased. A stress concentration effect is observed at the free ends. The concentration of the shear and lateral stresses at the free ends indicate that the free ends are the possible location where the material is likely to fail. The model was used in studying the process where stress evolution over time occurs as in the case of curing of thin film. The effect of curing parameters such as cooling rate and cooling cycle in a typical curing process showed that the magnitude of the residual stresses in the film decreased under slow rates of cooling and also when a stepwise cooling was introduced.

Acknowledgement

We would like to thank Dr. Sundar Kamath of IBM for his interest and helpful suggestions. This work was supported by the IBM-Caltech cooperative research fund.

I Appendix I: Moment Relation

The film is modelled as a thin plate element so that the plane stress condition prevails in the y-direction (see Fig. 14). The stress components,

$$\overline{\sigma}_{yy}(x,s) = \overline{\sigma}_{xy}(x,s) = \overline{\sigma}_{yy}(x,s) = 0 \tag{I.1}$$

The curvature $(1/\overline{\rho}(x,s))$ of plate deflection can be approximated as

$$\frac{1}{\overline{\rho}(x,s)} = -\frac{d^2}{dx^2}\overline{w}(x,s) \tag{I.2}$$

where w is the deflection of the bar in the y-direction which is assumed to be smaller compared with the length of the plate l.

The strain $\varepsilon_{xx}(x,s)$ of a fiber at a distance y from the neutral axis is given by

$$\varepsilon_{xx}(x,s) = -y\frac{d^2}{dx^2}\overline{w}(x,s) \tag{I.3}$$

But from the constitutive relation (2.1) and (2.2), the strain components may be written as

$$\varepsilon_{xx}(x,s) = \left(\frac{1}{3s\overline{\mu}(s)} + \frac{1}{9s\overline{K}(s)}\right)\overline{\sigma}_{xx}(x,s) + \left(\frac{1}{9s\overline{K}(s)} - \frac{1}{6s\overline{\mu}(s)}\right)\overline{\sigma}_{yy}(x,s) \tag{I.4}$$

$$\varepsilon_{yy}(x,s) = \left(\frac{1}{3s\overline{\mu}(s)} + \frac{1}{9s\overline{K}(s)}\right)\overline{\sigma}_{yy}(x,s) + \left(\frac{1}{9s\overline{K}(s)} - \frac{1}{6s\overline{\mu}(s)}\right)\overline{\sigma}_{xx}(x,s) \tag{I.5}$$

The lateral strain $\overline{\varepsilon}_{yy}(x,s)$ in the y-direction must be zero in order to maintain the continuity in the plate during bending, from which it follows:

$$\overline{\sigma}_{yy}(x,s) = \frac{3\overline{K}(s) - 2\overline{\mu}(s)}{2\left[3\overline{K}(s) + \overline{\mu}(s)\right]}\overline{\sigma}_{xx}(x,s) \tag{I.6}$$

From equations (I.6), (I.4) and (I.3) we obtain,

$$\overline{\sigma}_{xx}(x,s) = -\frac{4s\overline{\mu}(s)\left(3\overline{K}(s)+\overline{\mu}(s)\right)}{\left(3\overline{K}(s)+\overline{\mu}(s)\right)} y \frac{d^2}{dx^2}\overline{w}(x,s) \tag{I.7}$$

The bending moment $\overline{M}(x,s)$ in the elemental strip is then evaluated by

$$\overline{M}(x,s) = -\int_{-\frac{h}{2}}^{\frac{h}{2}} \overline{\sigma}_{xx} y dy = \frac{4s\overline{\mu}(s)\left(3\overline{K}(s)+\overline{\mu}(s)\right)}{\left(3\overline{K}(s)+\overline{\mu}(s)\right)} h^3 \frac{d^2}{dx^2}\overline{w}(x,s) \tag{I.8}$$

II Appendix II: Solution to the Differential Equation

The sixth order differential equations obtained in the main text is solved here by the method of characteristics. The characteristic equation of the differential equations (2.37) and (2.38) is of the form:

$$\beta^6 - (1+\epsilon)k^2\beta^4 + 4\alpha^4\beta^2 - 4\alpha^4k^2 = 0 \tag{II.1}$$

introducing a new variable $\zeta = \beta^2 - (1+\epsilon)k^2/3$, the above equation is reduced to a simple cubic equation

$$\zeta^3 + 3q_1\zeta + 2q_0 = 0 \tag{II.2}$$

where

$$q_0 = -\frac{2}{3}(2-\epsilon)\alpha^4k^2 - \left(\frac{(1+\epsilon)}{3}k^2\right)^3 \tag{II.3}$$

$$q_1 = \frac{4}{3}\alpha^4 + \left(\frac{(1+\epsilon)}{3}k^2\right)^3 \tag{II.4}$$

The discriminant $d = q_0^2 + q_1^3$ of the equation (II.2) is always positive and hence it has one real and two conjugate complex roots:

$$\zeta_1 = a + b \tag{II.5}$$

$$\zeta_{2,3} = -\frac{(a+b)}{2} \pm i\sqrt{3}\frac{(a-b)}{2} \tag{II.6}$$

where

$$a = \left(-q_0 + \sqrt{d}\right)^{\frac{1}{3}} \tag{II.7}$$

$$b = \left(-q_0 - \sqrt{d}\right)^{\frac{1}{3}} \tag{II.8}$$

Accordingly, the characteristic equation (II.1) has the following roots:

$$\beta_{1,2} = \pm\sqrt{\zeta_1 + \frac{(1+\epsilon)}{3}k^2} \tag{II.9}$$

$$\beta_{3,4} = \pm\sqrt{\zeta_2 + \frac{(1+\epsilon)}{3}k^2} = \pm\gamma_1 \pm i\gamma_2 \tag{II.10}$$

$$\beta_{5,6} = \pm\sqrt{\zeta_3 + \frac{(1+\epsilon)}{3}k^2} = \pm\gamma_1 \mp i\gamma_2 \tag{II.11}$$

where

$$\gamma_1 = \sqrt{\frac{1}{2}\left(\sqrt{\eta_1^2+\eta_2^2}+\eta_1\right)} \tag{II.12}$$

$$\gamma_2 = \sqrt{\frac{1}{2}\left(\sqrt{\eta_1^2+\eta_2^2}-\eta_1\right)} \tag{II.13}$$

and

$$\eta_1 = -\frac{(a+b)}{2} + \frac{(1+\epsilon)}{3}k^2 \tag{II.14}$$

$$\eta_2 = \sqrt{3}\frac{(a-b)}{2} \tag{II.15}$$

Therefore the solution to the equations (2.32) and (2.33) are:

$$\begin{aligned}\overline{\tau}_{xy}(x,s) = {} & \overline{C}_1(s)\sinh\left(\overline{\beta}_1(s)x\right) + \overline{C}_3(s)\cosh\left(\overline{\gamma}_1(s)x\right)\sin\left(\overline{\gamma}_2(s)x\right) \\ & + \overline{C}_5(s)\sinh\left(\overline{\gamma}_1(s)x\right)\cos\left(\overline{\gamma}_2(s)x\right)\end{aligned} \tag{II.16}$$

$$\begin{aligned}\overline{\sigma}_{yy}(x,s) = {} & \overline{C}_2(s)\cosh\left(\overline{\beta}_1(s)x\right) + \overline{C}_4(s)\cosh\left(\overline{\gamma}_1(s)x\right)\cos\left(\overline{\gamma}_2(s)x\right) \\ & + \overline{C}_6(s)\sinh\left(\overline{\gamma}_1(s)x\right)\sin\left(\overline{\gamma}_2(s)x\right)\end{aligned} \tag{II.17}$$

The constants in the above equations can be obtained from the boundary conditions. The constants in equation (II.16) can be found using the boundary conditions (2.34). These result in the system of linear algebraic equations which are solved to obtain:

$$\overline{C}_1(s) = -\frac{\Delta\alpha\Delta T}{\overline{\kappa}(s)\overline{D}_0(s)}\left[\coth\left(2\overline{v}_1(s)\right) - \frac{\cos\left(2\overline{v}_2(s)\right)}{\sinh\left(2\overline{v}_1(s)\right)}\right]\frac{1}{\cosh\left(\overline{u}(s)\right)} \tag{II.18}$$

$$\overline{C}_3(s) = \frac{\Delta\alpha\Delta T}{\overline{\kappa}(s)\overline{D}_0(s)}\left[\frac{\sin\left(\overline{v}_2(s)\right)}{\sinh\left(\overline{v}_1(s)\right)} + \frac{3\overline{\zeta}_1(s)\cos\left(\overline{v}_2(s)\right)}{2\overline{\eta}_2(s)\cosh\left(\overline{v}_1(s)\right)}\right]\tanh\left(\overline{u}(s)\right) \tag{II.19}$$

$$\overline{C}_5(s) = \frac{\Delta\alpha\Delta T}{\overline{\kappa}(s)\overline{D}_0(s)}\left[\frac{\cos\left(\overline{v}_2(s)\right)}{\cosh\left(\overline{v}_1(s)\right)} - \frac{3\overline{\zeta}_1(s)\sin\left(\overline{v}_2(s)\right)}{2\overline{\eta}_2(s)\sinh\left(\overline{v}_1(s)\right)}\right]\tanh\left(\overline{u}(s)\right) \tag{II.20}$$

where, $\overline{u}(s) = \overline{\beta}_1(s)l$, $\overline{v}_1(s) = \overline{\gamma}_1(s)l$, $\overline{v}_2(s) = \overline{\gamma}_2(s)l$ and

$$\begin{aligned}\overline{D}_0(s) = &\left[\overline{\gamma}_1(s) + \frac{3\overline{\zeta}_1(s)}{2\overline{\eta}_2(s)}\overline{\gamma}_2(s) + \left(\overline{\gamma}_2(s) - \frac{3\overline{\zeta}_1(s)}{2\overline{\eta}_2(s)}\overline{\gamma}_1(s)\right)\frac{\sin\left(2\overline{v}_2(s)\right)}{\sinh\left(2\overline{v}_1(s)\right)}\right] \\ &\times \tanh\left(\overline{u}(s)\right) - \overline{\beta}_1(s)\left[\coth\left(2\overline{v}_1(s)\right) - \frac{\cos\left(2\overline{v}_2(s)\right)}{\sinh\left(2\overline{v}_1(s)\right)}\right]\end{aligned} \tag{II.21}$$

is the determinant of the system of equations.

The relationship between the constants with odd indices in (II.16) and the constants with the even indices in (II.17) can be obtained by substituting equations (II.16) and (II.17) into (2.20),

$$\overline{C}_2(s) = \frac{4\overline{\mu}(s)\overline{\alpha}^4(s)\overline{\beta}_1(s)}{\overline{\beta}_1^4(s) + 4\overline{\alpha}^4(s)}\overline{C}_1(s) \tag{II.22}$$

$$\overline{C}_4(s) = 4\overline{\mu}(s)\overline{\alpha}^4(s)\left(\overline{\delta}_1(s)\overline{C}_3(s) + \overline{\delta}_2(s)\overline{C}_5(s)\right) \tag{II.23}$$

$$\overline{C}_6(s) = 4\overline{\mu}(s)\overline{\alpha}^4(s)\left(\overline{\delta}_2(s)\overline{C}_3(s) - \overline{\delta}_1(s)\overline{C}_5(s)\right) \tag{II.24}$$

where,

$$\overline{\delta}_1(s) = \frac{\overline{f}_1(s)\overline{\gamma}_2(s) - \overline{f}_2(s)\overline{\gamma}_1(s)}{\overline{f}_1^2(s) + \overline{f}_2^2(s)} \tag{II.25}$$

$$\overline{\delta}_2(s) = \frac{\overline{f}_1(s)\overline{\gamma}_1(s) + \overline{f}_2(s)\overline{\gamma}_2(s)}{\overline{f}_1^2(s) + \overline{f}_2^2(s)} \tag{II.26}$$

$$\overline{f}_1(s) = \overline{\eta}_1^2(s) - \overline{\eta}_2^2(s) + 4\overline{\alpha}^4(s) \tag{II.27}$$

$$\overline{f}_2(s) = 2\overline{\eta}_1(s)\overline{\eta}_2(s) \tag{II.28}$$

References

[1] Aleck, B.J. (1949). Thermal stresses in a rectangular plate clamped along an edge. *J. Appl. Mech., Trans. ASME.* **16**, 118-122.

[2] Brantley, W.A. (1973). Calculated elastic constants for stress problems associated with semiconductor devices. *J. Appl. Phys.* **44** 534-535.

[3] Chen, W.T. and Nelson, C.W. (1979). Thermal stresses in bonded joints. *IBM J. Res. Dev.* **23**, 178-188.

[4] Christensen, R.M. (1971). *Theory of Viscoelasticity: An Introduction*, Academic Press, New York.

[5] Cost, T.L. (1964). Approximate Laplace transform inversions in viscoelastic stress analysis. *AIAA Journal.* **12**, 2157-2166.

[6] Drory, M.D., Thouless, M.D. and Evans, E.G. (1988). On decohesion of residually stressed thin films. *Acta Metall.* **36**, 2019-2028.

[7] Elsner, G. (1987). Residual stress and thermal expansion of spun-on polyimide films. *J. Appl. Poly. Sci.* **34**, 815-828.

[8] Goland, M. and Reissner, E. (1944). The stresses in cemented joints. *J. Appl. Mech., Trans. ASME.* **11**, A17-A27.

[9] Goldsmith, C., Geldermans, P., Badetti, F. and Walker, G.A. (1983). Measurement of stresses generated in cured polyimide films. *J. Vac. Sci. Tech.* **A1**, 407-409.

[10] Goodier, J.N. (1942). An extension of Saint Venant's principle with application. *J. Appl. Phys.* **13**, 167-171.

[11] Hu, M.S., Thouless, M.D. and Evans, A.G. (1988). The decohesion of thin films from brittle substrates. *Acta Metall.* **36**, 1301-1307.

[12] Knauss, W.G. and Emri, I. (1987). Volume change and the nonlinearly themoviscoelastic constitution of polymers. *Poly. Eng. Sci.* **27**, 86-100.

[13] Manzione, L.T. (1990). *Plastic packaging of microelectronic devices*, Von Nostrand Reinhold, New York.

[14] Muki, R. and Sternberg, E. (1961). On transient thermal stress in viscoelastic materials with temperature dependent properties. *J. Appl. Mech., Trans. ASME.* **31**, 101-110.

[15] Numata, S., Oohara, S., Fujisaki, K., Imaizumi, J. and Kinjo, N. (1986). Thermal expansion behavior of various aromatic polyimides. *J. Appl. Polym. Phys.* **31**, 101-110.

[16] Pipkin, A.C., (1986). *Lectures on Viscoelasticity Theory*, 2nd. Edn. Springer-Verlag, New York.

[17] Schapery, S.A. (1961). Approximate methods of transform inversion for viscoelastic stress analysis. *Proceedings of the fourth U.S. National congress on Applied Mechanics*, 1075-1085.

[18] Smith, T.L. and Kim, C.S. (1991). Thermal expansion and viscoelastic properties of a semi-rigid polyimide. *Mat. Res. Soc. Symp. Proc.* **227**, 219-223.

[19] Suhir, E. (1986). Stresses in bi-metal thermostats. *J. Appl. Mech., Trans. ASME.* **53**, 657-660.

[20] Suhir, E. (1989). Interfacial stresses in bi-metal thermostats. *J. Appl. Mech., Trans. ASME.* **56**, 595-600.

[21] Timoshenko, S.P. (1925). Analysis of bi-metal thermostats. *J. Opt. Soc. America.* **11**, 233-255.

[22] Washo, B.D. (1977). Rheology and modelling of the spin coating process. *IBM J. Res. Dev.* **21**, 190-198.

List of Figures:

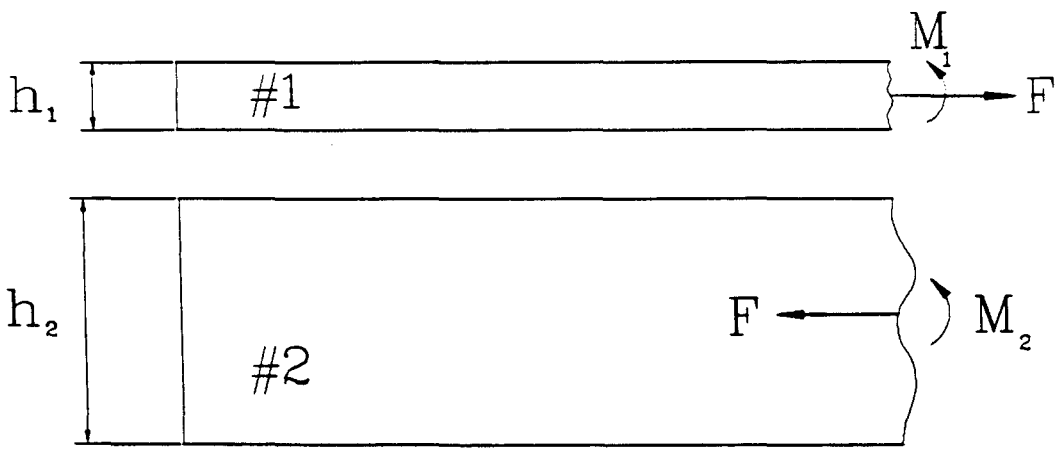
M1
h1
#1
F
h2
F
M2
#2

(a)

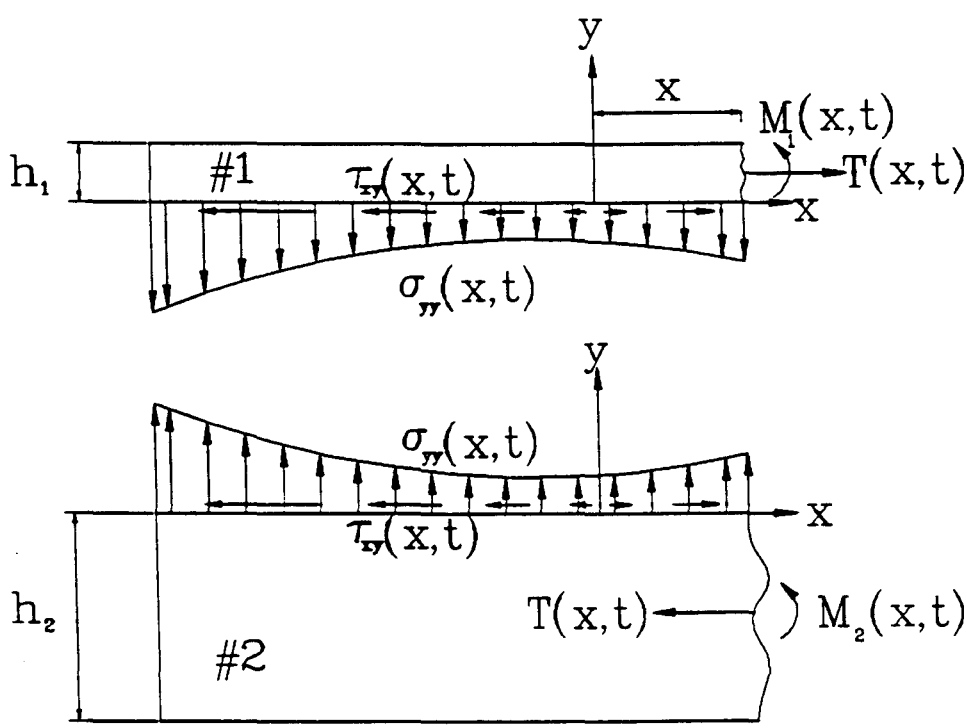
y
x
M1(x,t)
h1
#1
τxy(x,t)
T(x,t)
x
σyy(x,t)
y
σyy(x,t)
x
τxy(x,t)
h2
T(x,t)
M2(x,t)
#2

(b)

Figure 1

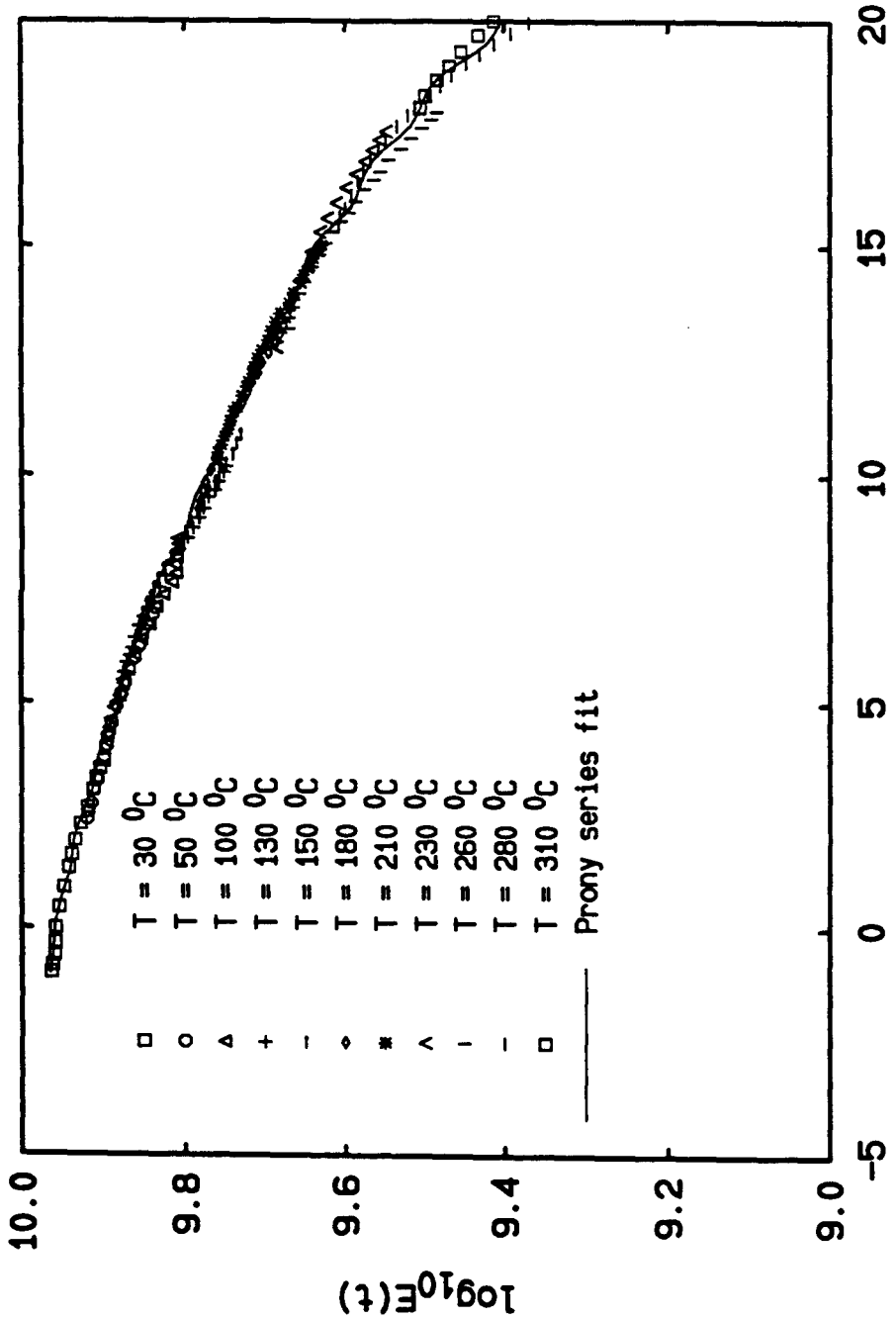
10.0
9.8
9.6
9.4
9.2
9.0
$\log_{10}E(t)$
-5
0
5
10
15
20
$\log_{10}t$
T = 30 °C
T = 50 °C
T = 100 °C
T = 130 °C
T = 150 °C
T = 180 °C
T = 210 °C
T = 230 °C
T = 260 °C
T = 280 °C
T = 310 °C
Prony series fit

Figure 2

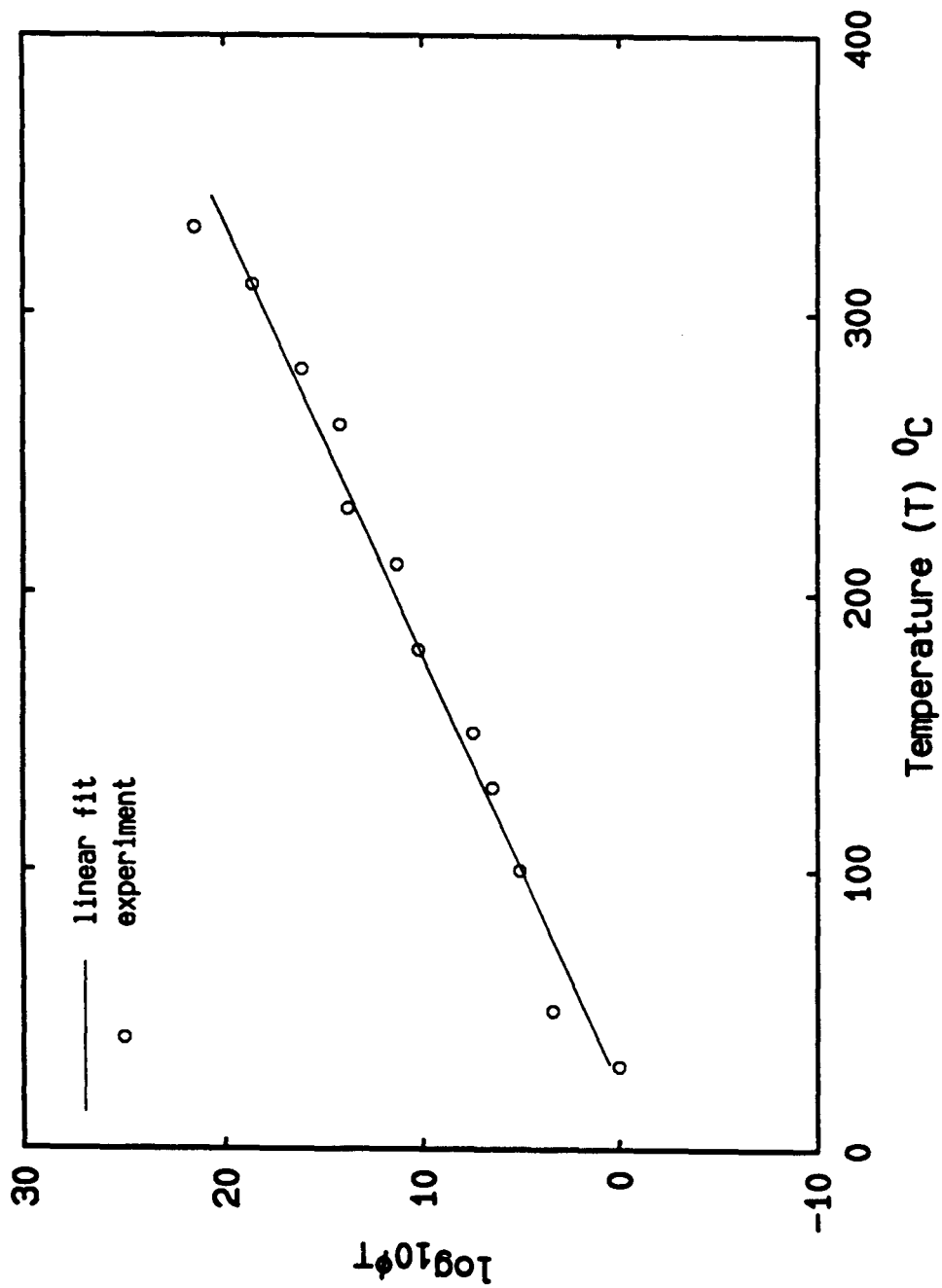
linear fit
experiment
log10φT
Temperature (T) 0C
30
20
10
0
-10
0
100
200
300
400

Figure 3

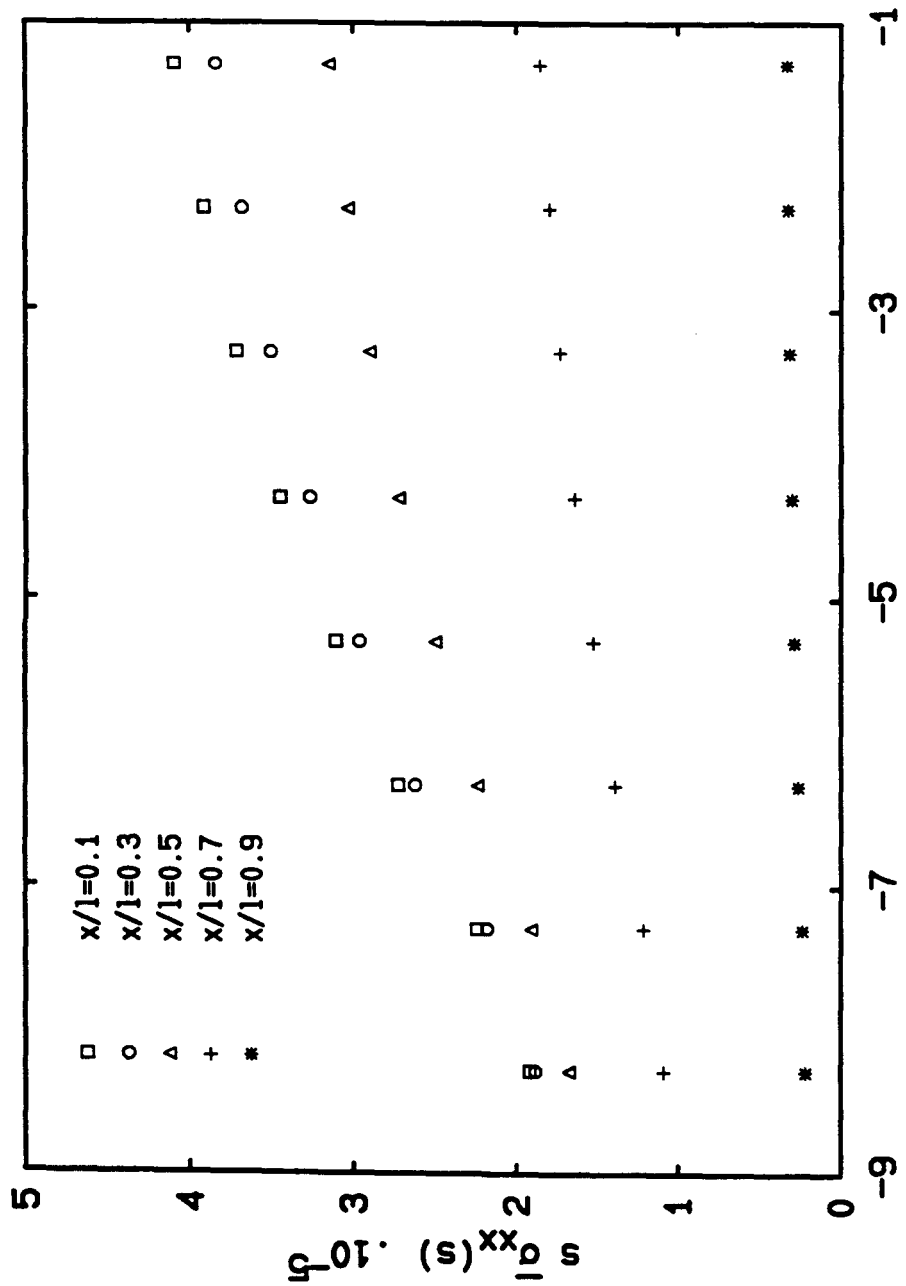

Figure 4

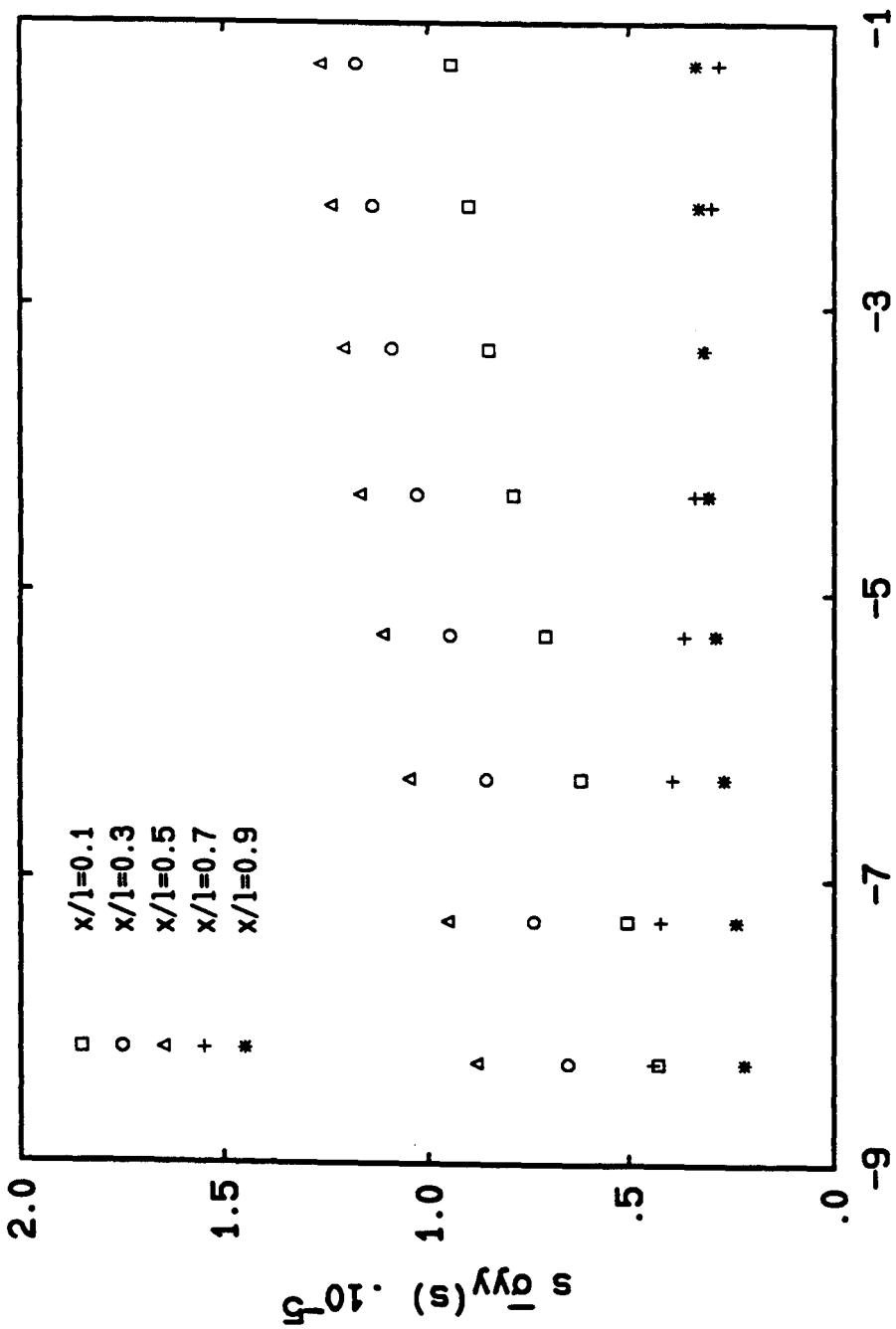

Figure 5

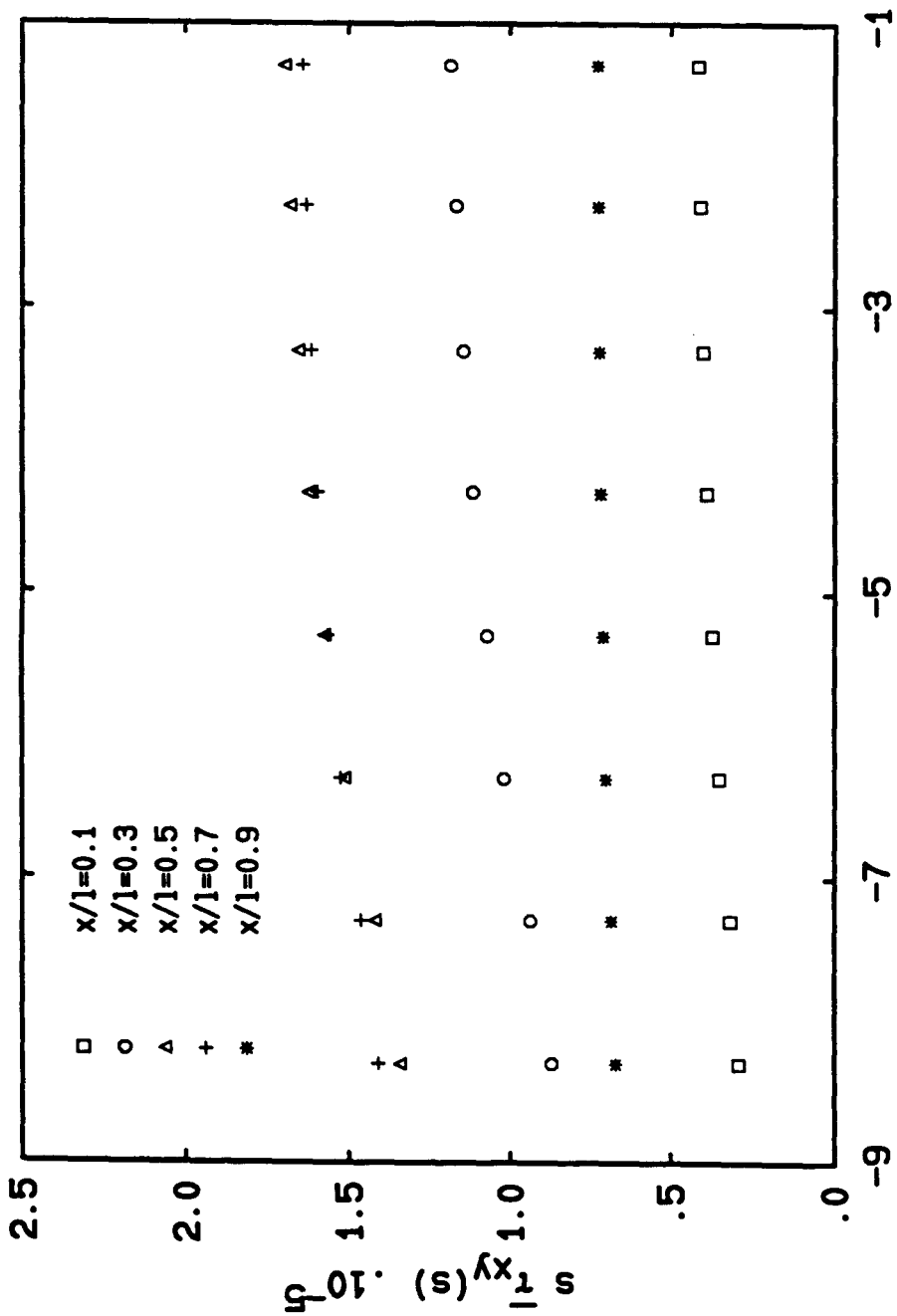
x/l=0.1
x/l=0.3
x/l=0.5
x/l=0.7
x/l=0.9
2.5
2.0
1.5
1.0
.5
.0
-9
-7
-5
-3
-1
log10s
s τ1xy(s) .10-5

Figure 6

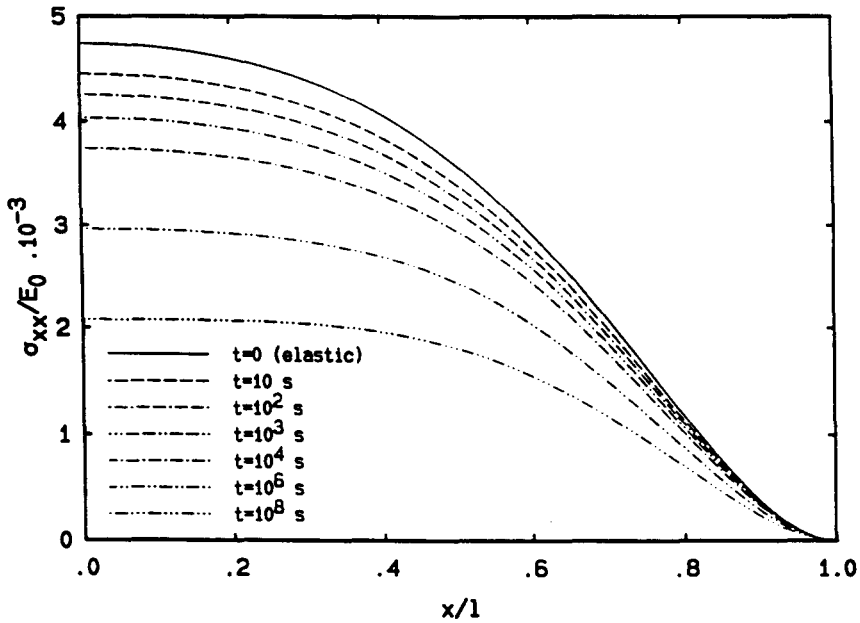
5
4
3
2
1
0
$\sigma_{xx}/E_0 \cdot 10^{-3}$
t=0 (elastic)
t=10 s
t=10^2 s
t=10^3 s
t=10^4 s
t=10^6 s
t=10^8 s
.0
.2
.4
.6
.8
1.0
x/l

(a)

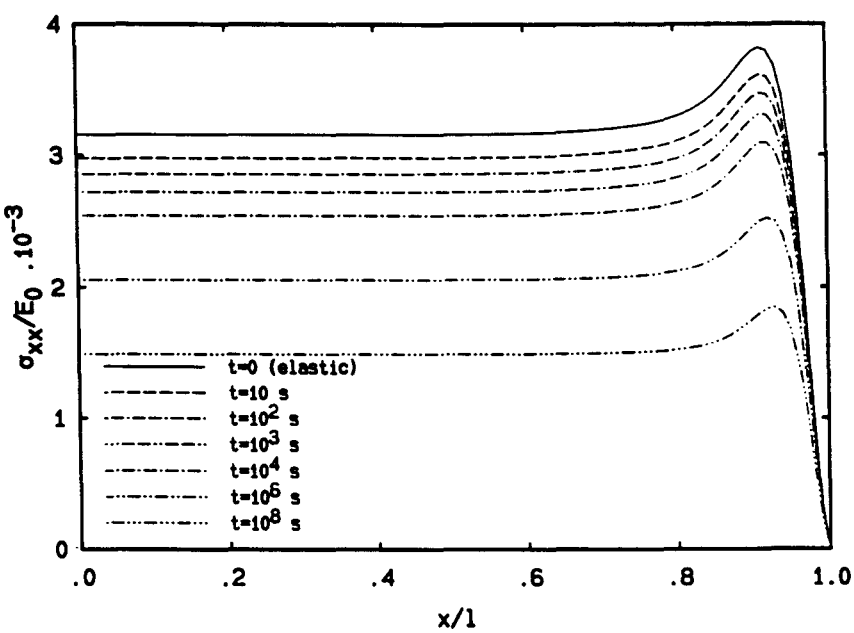
4
3
2
1
0
$\sigma_{xx}/E_0 \cdot 10^{-3}$
t=0 (elastic)
t=10 s
t=10^2 s
t=10^3 s
t=10^4 s
t=10^6 s
t=10^8 s
.0
.2
.4
.6
.8
1.0
x/l

(b)

Figure 7

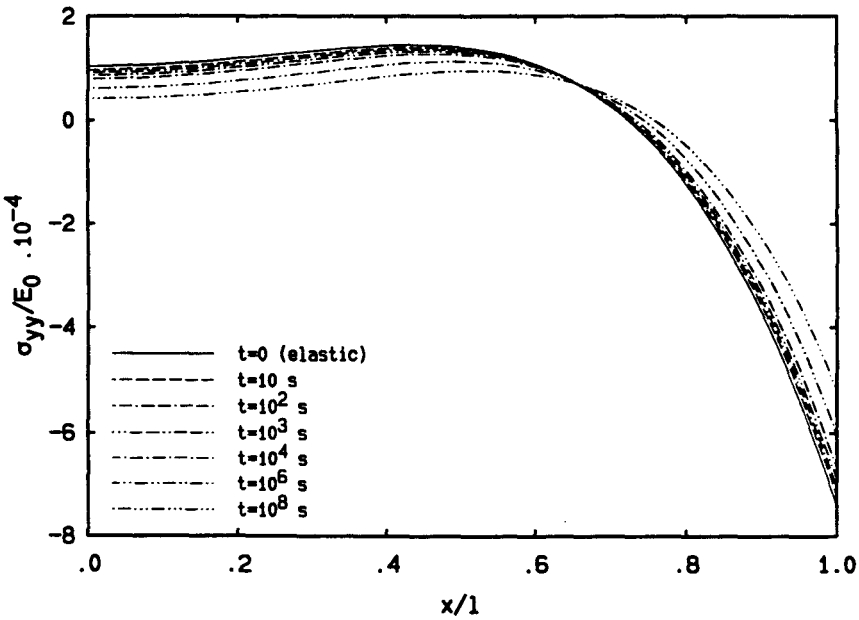
2
0
-2
-4
-6
-8
$\sigma_{yy}/E_0 \cdot 10^{-4}$
.0
.2
.4
.6
.8
1.0
x/l
t=0 (elastic)
t=10 s
t=10^2 s
t=10^3 s
t=10^4 s
t=10^6 s
t=10^8 s

(a)

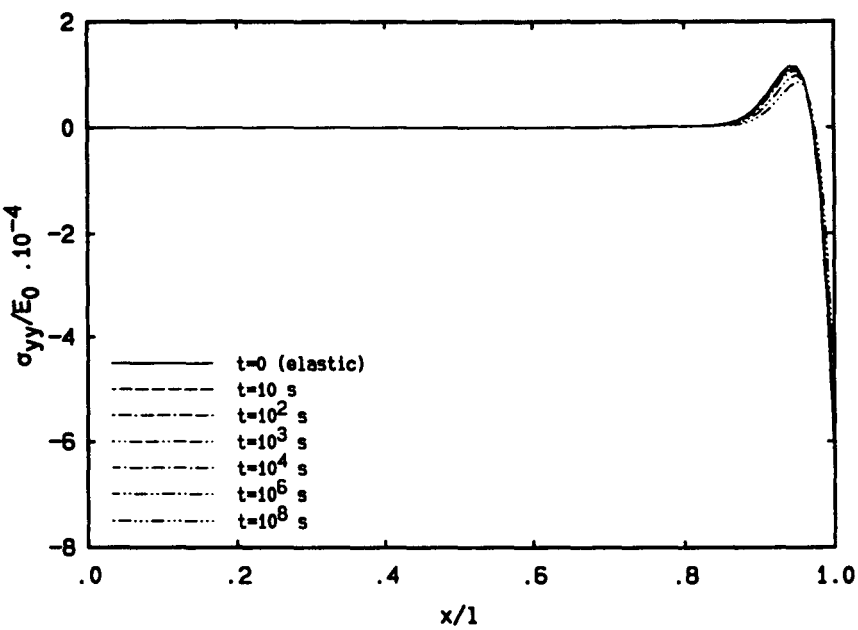
2
0
-2
-4
-6
-8
$\sigma_{yy}/E_0 \cdot 10^{-4}$
.0
.2
.4
.6
.8
1.0
x/l
t=0 (elastic)
t=10 s
t=10^2 s
t=10^3 s
t=10^4 s
t=10^6 s
t=10^8 s

(b)

Figure 8

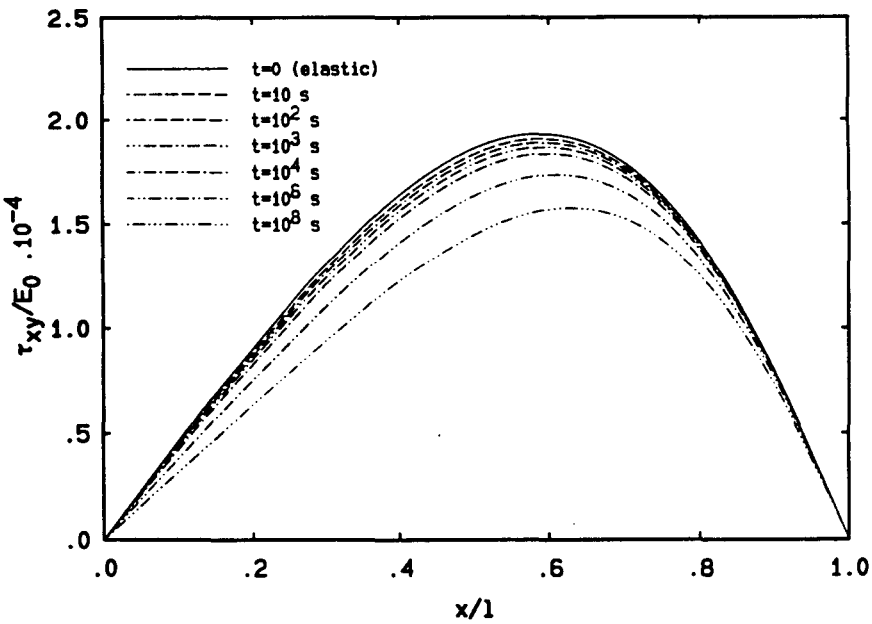
t=0 (elastic)
t=10 s
t=10^2 s
t=10^3 s
t=10^4 s
t=10^5 s
t=10^8 s
τxy/E0 .10^-4
x/l
2.5
2.0
1.5
1.0
.5
.0
.0
.2
.4
.6
.8
1.0

(a)

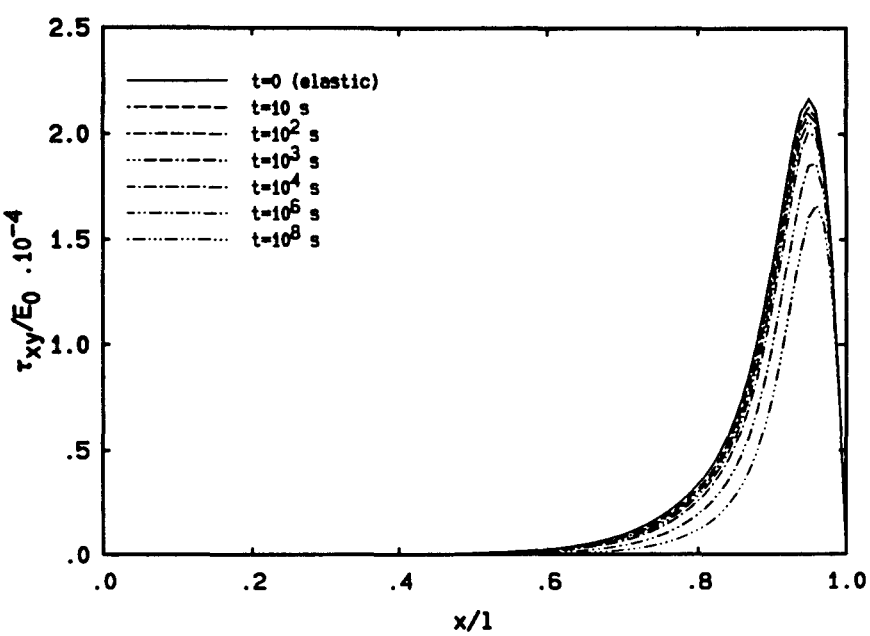
t=0 (elastic)
t=10 s
t=10^2 s
t=10^3 s
t=10^4 s
t=10^5 s
t=10^8 s
τxy/E0 .10^-4
x/l
2.5
2.0
1.5
1.0
.5
.0
.0
.2
.4
.6
.8
1.0

(b)

Figure 9

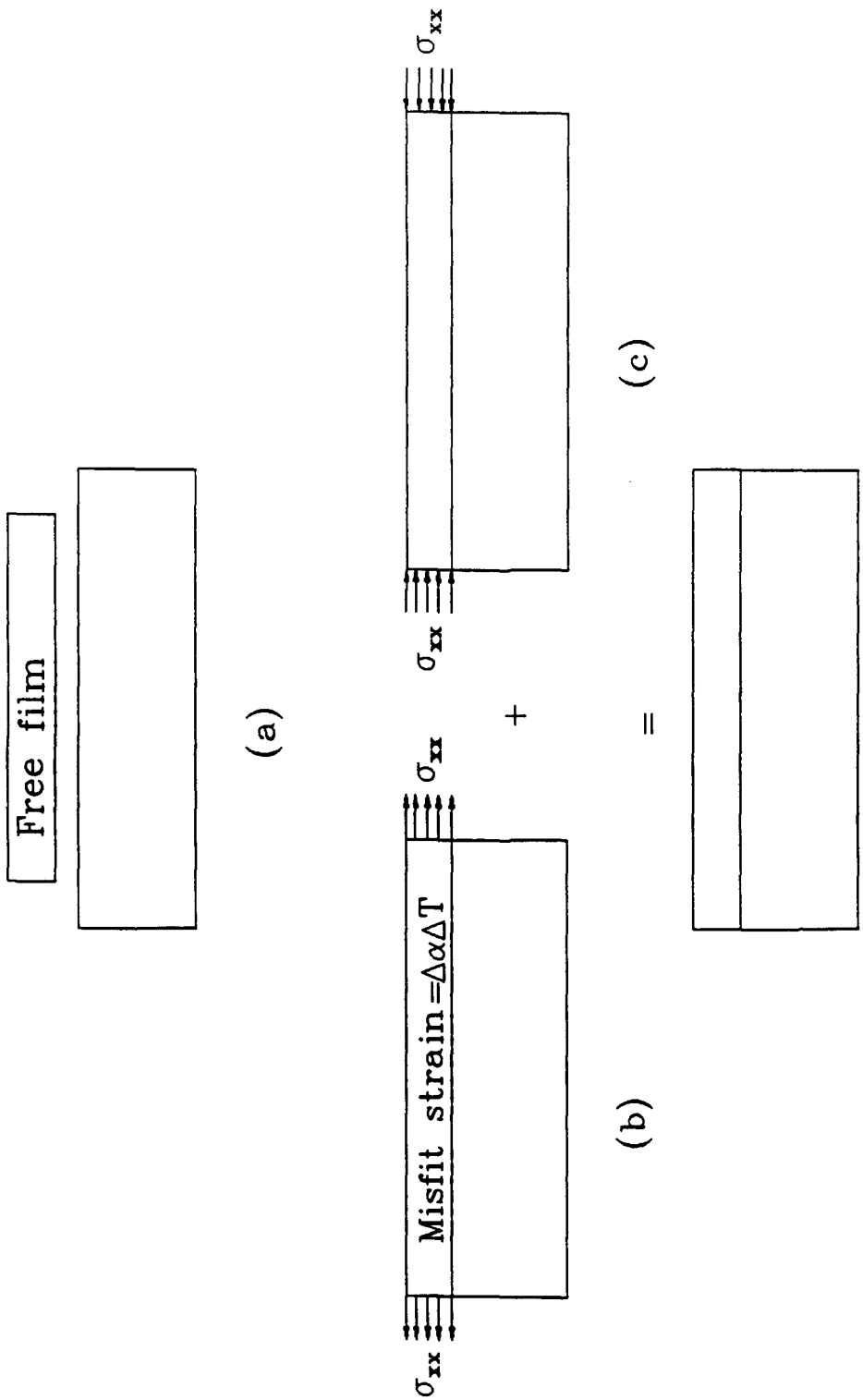
Free film
(a)
σ_{xx}
σ_{xx}
(c)
+
σ_{xx}
Misfit strain $=\Delta\alpha\Delta T$
σ_{xx}
(b)
=
(d)

Figure 10

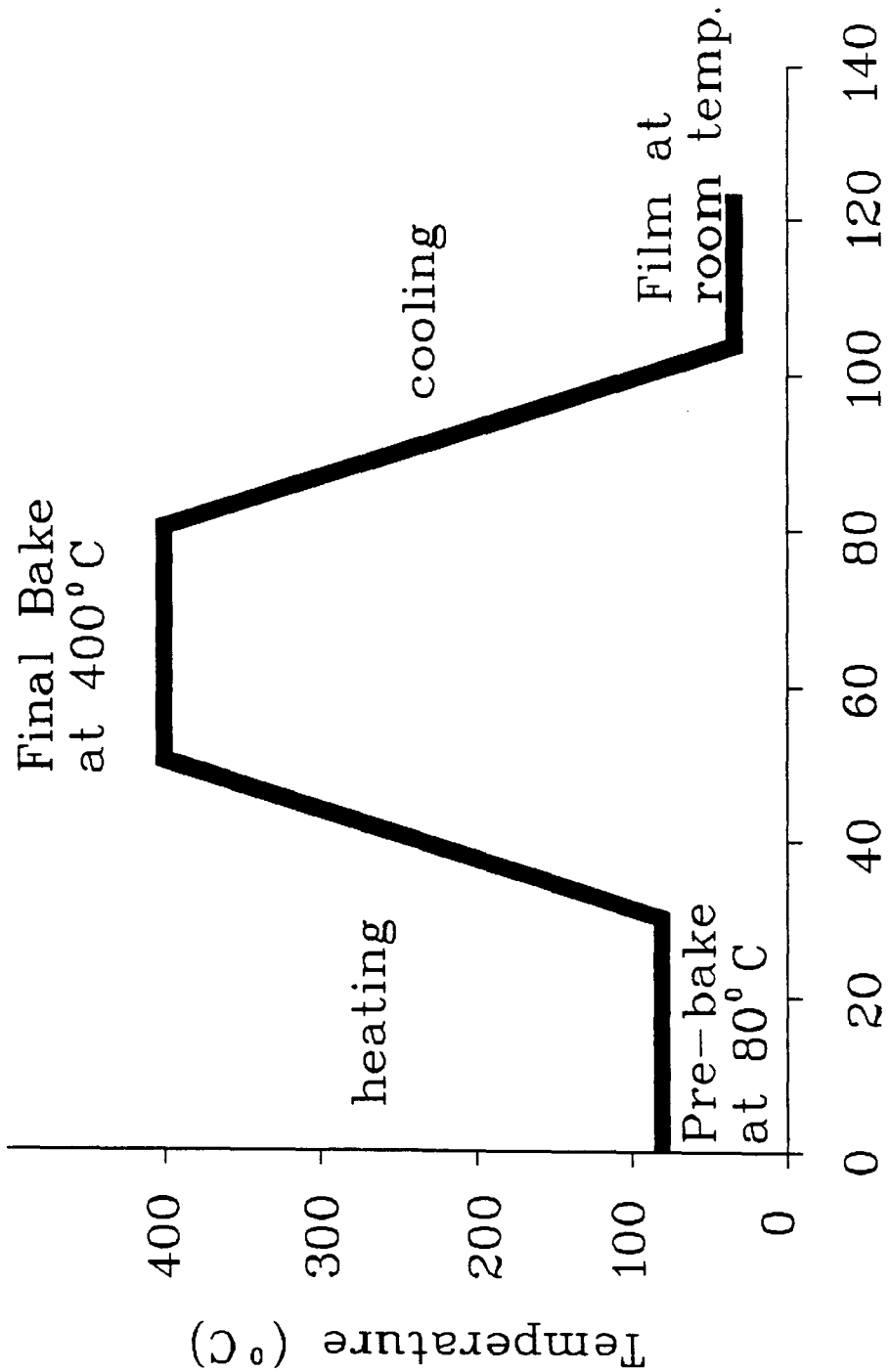
Temperature (°C)
400
300
200
100
0
Final Bake
at 400°C
heating
cooling
Pre-bake
at 80°C
Film at
room temp.
0
20
40
60
80
100
120
140
Time (mins.)

Figure 11

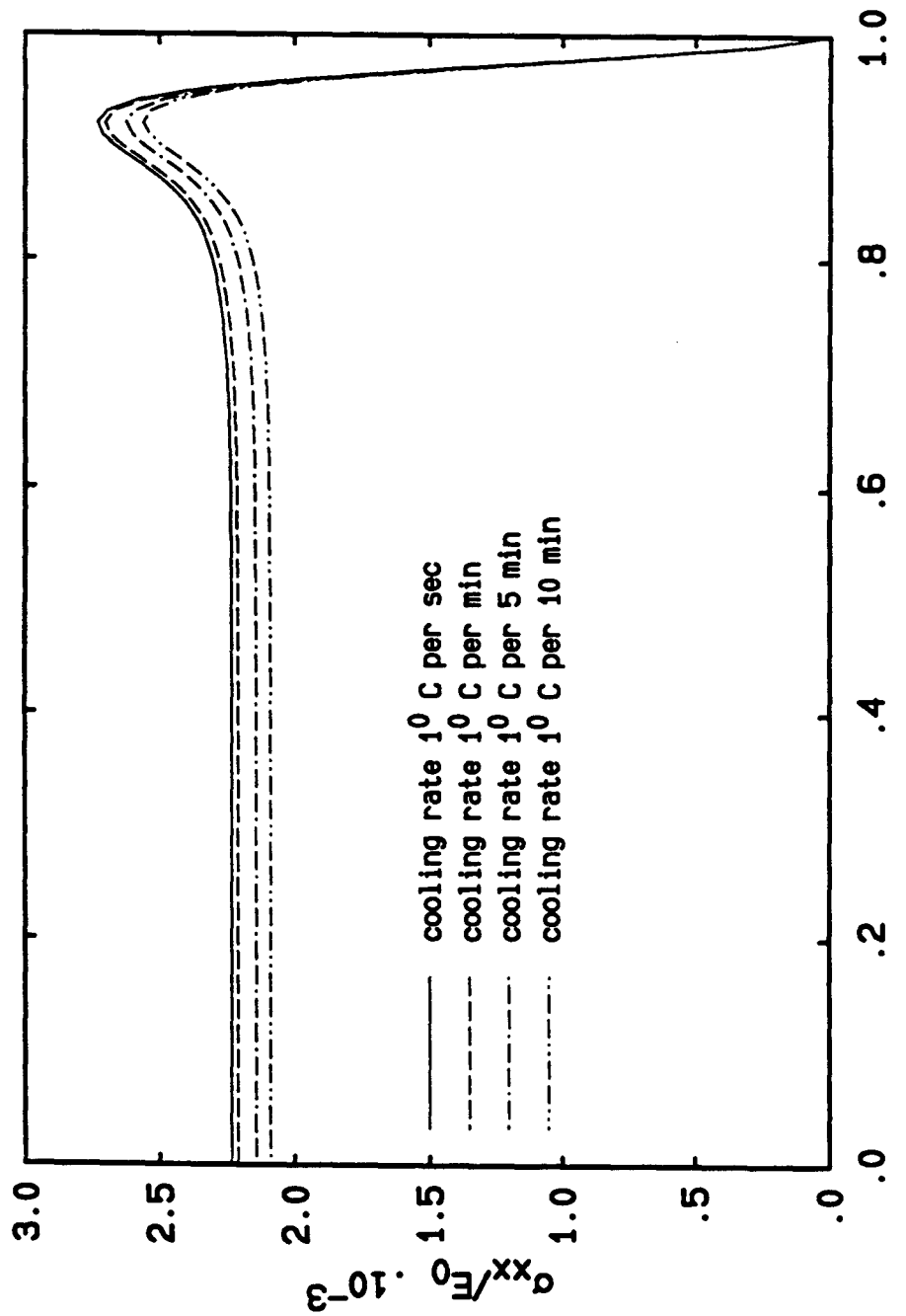
3.0
2.5
2.0
1.5
1.0
.5
.0
.0
.2
.4
.6
.8
1.0
x/l
$\sigma_{xx}/E_0 \cdot 10^{-3}$
cooling rate 1^0 C per sec
cooling rate 1^0 C per min
cooling rate 1^0 C per 5 min
cooling rate 1^0 C per 10 min

Figure 12

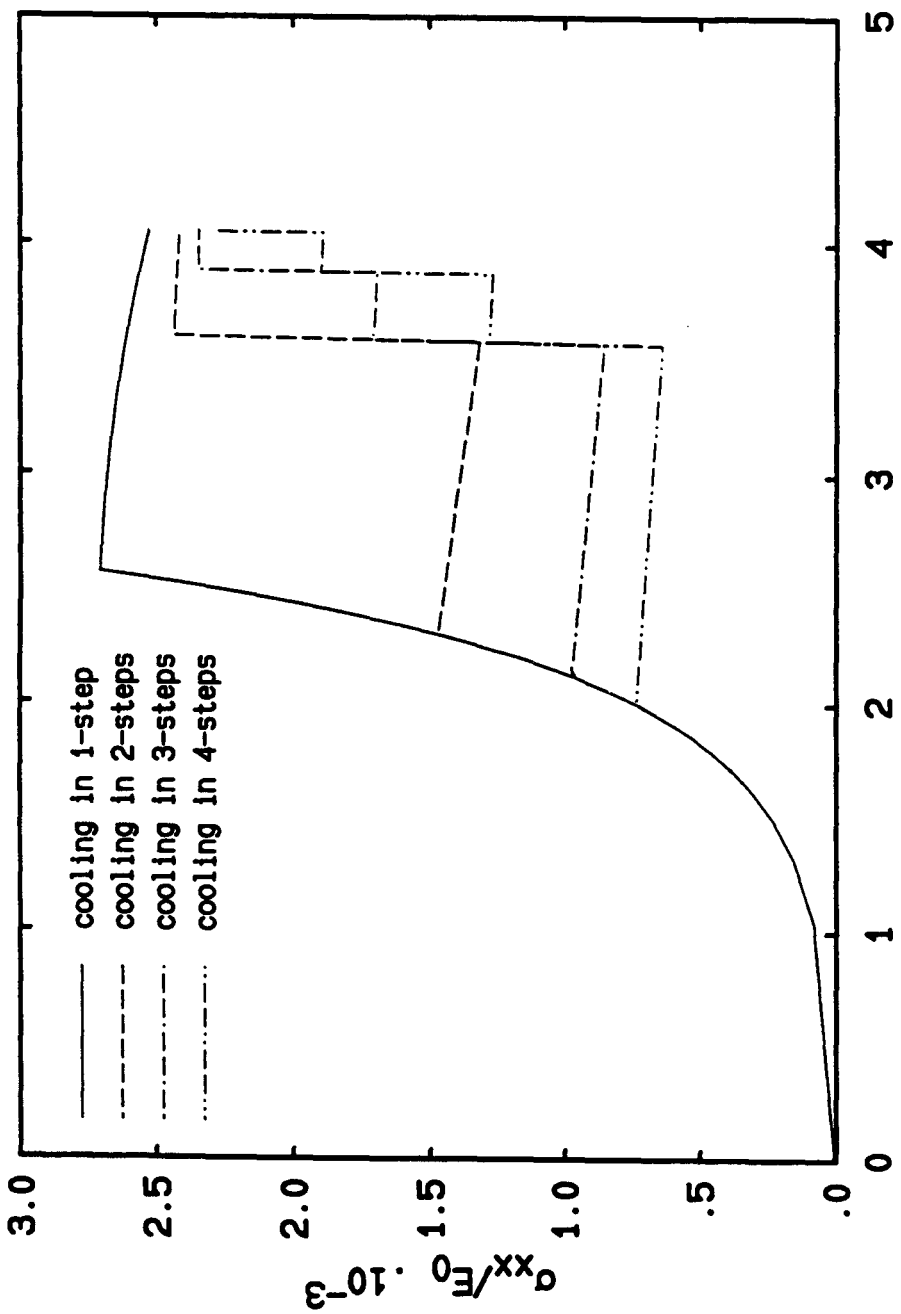
cooling in 1-step
cooling in 2-steps
cooling in 3-steps
cooling in 4-steps
$\sigma_{xx}/E_0 \cdot 10^{-3}$
$\log_{10} t$
3.0
2.5
2.0
1.5
1.0
.5
.0
0
1
2
3
4
5

Figure 13

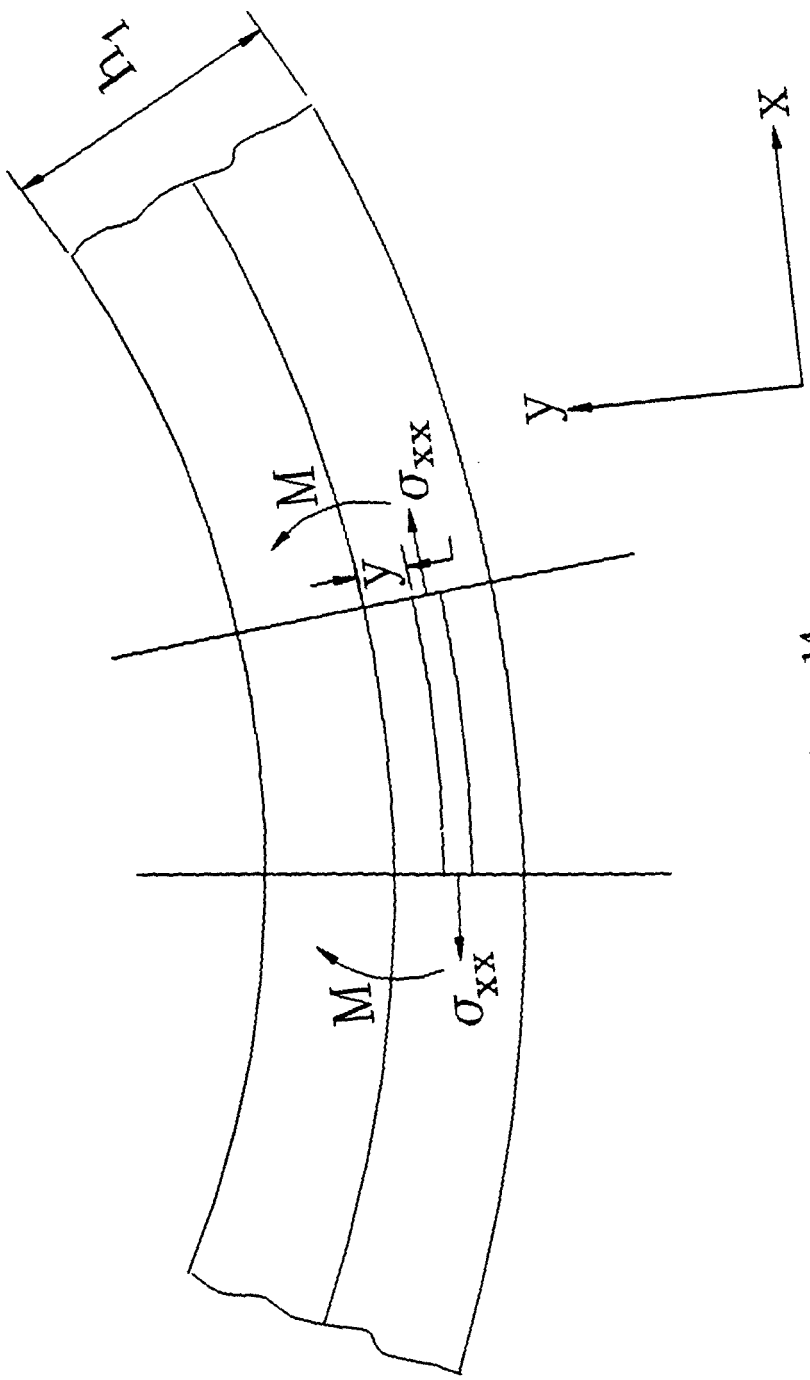

Figure 14

Interfacial Crack Propagation in a Thin Viscoelastic Film Bonded to an Elastic Substrate

Abstract

Edge decohesion along the interface of a thin viscoelastic film bonded to an elastic substrate under tensile residual stresses is considered. The tensile residual stress in the film is replaced by a combination of edge loads, and an explicit relation of strain energy with respect to time is obtained by simple beam analysis. The strain energy function is discretized into small time steps, and the energy release is calculated using Griffith's energy balance approach; the discretized time is assumed very small so that the dissipation effects over the small time steps are neglected. An analytical model is developed to predict the crack growth and its velocity. Crack growth along the interface is predicted based on a fracture criteria. The validity of the assumptions in the analytical results is checked by performing a finite element analysis.

1 Introduction

Thin films deposited on a substrate are subjected to appreciable residual stresses due to difference in the thermal coefficients. The built in residual stresses are of relatively high magnitude, which for the case of a polyimide film on a silicon substrate is of the order 40-70 MPa [7]. These residual stresses in the presence of flaws or inclusions can act as a driving force to cause failure. The type and pattern of failure mechanism is dependent on many factors which has been extensively studied in recent years [9], [12].

The failure mechanism is mainly dependent on the sign and magnitude of residual stresses and the relative strength of the film, interface and the substrate. In a compressively loaded film, any flaw in the form of interfacial separation buckles under the compressive loading, leading to delamination and eventual spalling of the film [8]. Another possibility is that the crack my propagate in the substrate in a direction perpendicular to the interface [10]. When the stresses in the film are tensile, the cracks can initiate along the interface at the free edges or at an initial crack in the film. The crack thus initiated can either continue to grow along the interface or can deviate into the film or substrate depending on the relative toughness of the constituent materials. Experimental studies in the case of brittle film on brittle substrate [11] and also for a ductile film on brittle substrate [5] reveal that the cracks, after splitting through the film, extended along the interface for a few film thickness before deviating into the substrate and travelling parallel to the interface. However, when the interface is weak in strength, the most likely form of crack growth is along the interface [23]. There are many more forms of failure mechanisms which exist in bi-material systems, and they have been reviewed by Evans [9] and by Hutchinson and Suo [12].

Polymeric thin films such as polyimide are widely used in the microelectronics industry as dielectric insulating layers. Polyimide films bonded to silicon substrate is of particular interest. This combination is of the type ductile film bonded to a brittle substrate with a weak interface. The most likely type of failure is the edge decohesion followed by crack growth along the interface. Suo and Hutchinson [22] have analysed this problem treating the film as an elastic material and have obtained the expressions for energy release rate and stress intensity factors. Polyimides in general exhibit time and temperature dependent (viscoelastic) properties and hence a time dependent fracture analysis of the bi-material system has been carried out. The focus of this paper is to study the time dependent fracture process in a bi-material

cracked along the interface.

Before proceeding to the analysis, it is useful to review the published work on crack growth and crack initiation in the viscoelastic materials. An excellent review of the experimental and theoretical papers on crack growth in viscoelastic materials is presented by Knauss [14]. Williams [25] deduced an extended Griffith criterion for the fracture of linearly viscoelastic media. By using the thermodynamic power equation for the global energy balance, he was able to solve the time history of fracture in disintegrating spherical cavity. Christensen [3] extended this method to solve an explicit case of crack geometry.

Wnuk and Knauss [26] investigated the case of a penny shaped crack in a linearly viscoelastic solid exhibiting a deformation rate sensitive yield stress to obtain the fracture initiation time. Knauss and co-workers [13], [18], [15] predicted the crack growth following initiation using the thermodynamic power relation but reducing the problem to a local energy balance in a failure zone near the cracktip. Schapery [19], [20], [21] proposed a model for crack initiation and crack growth considering the failure zone where no significant restrictions on the failing material was imposed. Schapery's criterion is equivalent to the local balance criterion [13], [18], [15] whenever the crack propagates with a uniform velocity and the deformation associated with the crack remains fixed with time. Further, McCartney [17] used the same concept of failure zone ahead of cracktip, and by assuming a constant stress distribution in this zone, he solved the problem of crack growth.

The role of conservation of energy in viscoelastic crack kinetics has been discussed in great detail. McCartney and Christensen [4] have stated that the global energy balance and local energy approaches both lead to deterministic, nontrivial failure criteria for crack growth in viscoelastic material with no inherent inconsistency

between them provided the boundedness of stresses is satisfied throughout.

In this paper the interface crack problem for a viscoelastic film on an elastic substrate with weak interface is solved to predict the crack growth and crack velocity. An explicit relation for the time-dependent strain energy of the cracked bi-material system is obtained for a Maxwell solid. The whole crack growth process is discretized into small time steps, and the energy release rate based on Griffith's approach is obtained at the beginning of each time step. The dissipation during the small time step is assumed to be negligible.

2 Problem Description

The cross section of the bi-material system with an edge crack at the interface is shown in Fig. 1. Each layer is assumed to be homogenous, isotropic and linearly viscoelastic. The uncracked interface is perfectly bonded with continuous displacements and tractions. The upper layer has a thickness h_1 and a time dependent modulus $E_1(t)$ while the lower layer has a thickness h_2 and time dependent modulus $E_2(t)$. The film and substrate materials considered here are thermorheologically simple viscoelastic materials characterized by the constitutive relation

$$s_{ij}(\vec{x},t) = \int_{-\infty}^{t} 2G(\xi-\xi')\frac{\partial}{\partial t'}e_{ij}\,(\vec{x},\xi')\,d\xi' \tag{2.1}$$

$$\sigma_{kk}(\vec{x},t) = \int_{-\infty}^{t} 3K(\xi-\xi')\frac{\partial}{\partial t'}\varepsilon_{kk}\,(\vec{x},\xi')\,d\xi' \tag{2.2}$$

where s_{ij} and σ_{kk} are the deviatoric and dilatational components of the stress tensor $\boldsymbol{\sigma}$, e_{ij} and ε_{kk} are the deviatoric and dialtational components of the strain tensor $\boldsymbol{\varepsilon}$, and $G(t)$ and $K(t)$ are, respectively, the time dependent shear and bulk moduli of the material.

The loading considered here is tensile residual stress in the film due to thermal mismatch. The film is assumed to be deposited to the substrate at an elevated temperature in a stress free condition. The film and substrate are then cooled to room temperature under a known cooling cycle. During this process, the residual stresses are built in the film due to thermal mismatch. A detailed residual stress analysis presented in the previous chapter indicates that the longitudinal stresses are almost uniformly distributed except near the free ends while the lateral and the shear stress components are concentrated near the free ends. Once the crack is initiated at the free end, the lateral and shear stresses (which are concentrated at the free ends in the case of uncracked bi-material) can be neglected and thus the only stress component in the film is the uniformly distributed longitudinal stress component, σ_{xx}. It is assumed here that the film is cooled suddenly so that a step strain, $\varepsilon_{xx}(t)$, is developed in the film which is given by

$$\varepsilon_{xx}(t) = \Delta\alpha\Delta T H(t)$$

where $\Delta\alpha$ is the difference in thermal co-efficients of the film and the substrate, ΔT is the temperature change and $H(t)$ is a heaveside step function.

The biaxial misfit stress in the film due to step strain is evaluated from the constitutive relation (2.1) and (2.2),

$$\sigma_{xx}(t) = E(t)\varepsilon_{xx}(0^+) + \left(\frac{1}{1-\nu_1}\right)\int_{0+}^{t} E(t-\xi)\frac{\partial\varepsilon(\xi)}{\partial\xi}d\xi \tag{2.3}$$

But

$$\frac{\partial\varepsilon_{xx}(\xi)}{\partial\xi} = \Delta\alpha\Delta T\delta(\xi) \tag{2.4}$$

where δ is the Dirac delta function.

For a film material, which is linearly viscoelastic and Maxwell type of solid, the extensional modulus is represented by the equation,

$$E(t) = E_1 \exp\left(-\frac{t}{\tau_1}\right) \tag{2.5}$$

Substituting (2.4) and (2.5) in (2.3) gives

$$\sigma_{xx}(t) = \frac{\Delta\alpha\Delta T}{(1-\nu_1)} E_1 \exp\left(\frac{-t}{\tau_1}\right) \tag{2.6}$$

The residual stress σ_{xx} can also be obtained by the superposition shown in Fig. 2. In Fig. 2b, the film is under uniform misfit strain corresponding to the stress σ_{xx} which is equivalent to the thermal strain. However, the edges are not traction free in this case. Therefore, we add to this a system of loads (Fig. 2b) where the edges are just subjected to the stress σ_{xx} but in the opposite direction without misfit strain, so that when superposed, the original residual problem with stress free condition (Fig. 2d) is obtained. There are no stress singularities present for the case in Fig. 2b and singularities are entirely due to loading in Fig. 2c. Thus, while analysing a problem with singularity such as the crack propagation at the interface, the residual stresses can be replaced by an equivalent loading as shown in Fig. 2c.

3 Analytical Model

3.1 General Edge Loading Problem

Figure 3a shows a general edge loading of a bilayer with an interfacial edge crack which can be used to solve several failure problems including fracture at the interface of a thin film bonded to a substrate under thermomechanical loading. The basic equations in this part are formulated in the Laplace domain. The Laplace parameter is indicated by s, and the overbar denotes the transformed variable in this domain.

Far ahead of the crack tip, the bilayer may be regarded as a composite beam. The neutral axis of the composite beam lies at a distance $(h_1\overline{\Delta}(s))$ from the bottom of

the beam. The position of this neutral axis is derived using the composite beam theory (Appendix I).

For a composite beam,

$$h_1\overline{\Delta}(s) = \frac{1 + 2\overline{\Sigma}(s)\eta + \overline{\Sigma}(s)\eta^2}{2\eta\left(1 + \overline{\Sigma}(s)\eta\right)} \tag{3.1}$$

where $\overline{\Sigma}(s) = \frac{\overline{E}_1(s)}{\overline{E}_2(s)}$ is the modulus ratio and $\eta = \frac{h_1}{h_2}$ is the thickness ratio.

Overall equilibrium in Fig. 3a requires that the three axial loads and three moments satisfy

$$\overline{P}_1(s) - \overline{P}_2(s) - \overline{P}_3(s) = 0 \tag{3.2}$$

$$\begin{aligned} -\overline{M}_1(s) + \overline{M}_2(s) + \overline{M}_3(s) \;&-\; \overline{P}_1(s)\left(\frac{1}{\eta} + 1\right)\frac{h_1}{2} \\ &+\; \overline{P}_3(s)\left(\overline{\Delta}(s) - \frac{1}{2\eta}\right)h_1 = 0 \end{aligned} \tag{3.3}$$

Therefore, only four among the six variables are independent, say, $\overline{P}_1(s)$, $\overline{P}_3(s)$, $\overline{M}_1(s)$ and $\overline{M}_3(s)$.

These four load variables can further be reduced to just two, namely $\overline{P}(s)$ and $\overline{M}(s)$, which makes the formulations much simpler in future analysis discussed later. Such a reduction is possible by a superposition of the form shown in Fig. 3. This kind of a superposition is possible since the governing equations (2.1) and (2.2) of a viscoelastic material are linear in Laplace domain. In Fig. 3b, a crack can be assumed to exist anywhere parallel to the interface since the stress components $\overline{\sigma}_{yy}(s)$ and $\overline{\tau}_{xy}(s)$ are zero so that it does not affect the stress singularity due to the presence of the crack.

The expressions for the two independent load variables $\overline{P}(s)$ and $\overline{M}(s)$ are constructed using simple beam theory in the following way.

Consider the stresses in the upper beam far behind the cracktip (Fig. 3a):

$$\overline{\sigma}_{yy}(s) = \overline{\tau}_{xy}(s) = 0 \tag{3.4}$$

The stress component $\overline{\sigma}_{xx}(s)$ due to the force $\overline{P}_1(s)$ acting alone is

$$[\overline{\sigma}_{xx}(s)]_{\overline{P}_1(s)} = \frac{\overline{P}_1(s)}{h_1} \tag{3.5}$$

The stress $\overline{\sigma}_{xx}(s)$ due to the bending moment $\overline{M}_1(s)$ acting alone is

$$[\overline{\sigma}_{xx}(s)]_{\overline{M}_1(s)} = s\overline{E}_1(s)\overline{\varepsilon}_{xx}(s) = -s\overline{E}_1(s)y_1\overline{w}_1''(s) \tag{3.6}$$

where, $\overline{w}(s)$ is the deflection of the beam and y_1 is the distance measured from the neutral axis.

In order to eliminate $\overline{w}_1''(s)$, we make use of the moment relation,

$$\overline{M}_1(s) = \int_{-\frac{h_1}{2}}^{\frac{h_1}{2}} \overline{\sigma}_{xx}(s)y_1 d\overline{A}(s) = -s\overline{E}_1(s)\frac{h_1^3}{12}\overline{w}_1''(s) \tag{3.7}$$

Combining the solutions (3.5), (3.6) and (3.7), we obtain,

$$\overline{\sigma}_{xx}(s) = \frac{\overline{P}_1(s)}{h_1} + \frac{12\overline{M}_1(s)}{h_1^3}y_1 \tag{3.8}$$

Similarly, the stresses in the lower beam far behind the cracktip (Fig. 3a) are:

$$\overline{\sigma}_{yy}(s) = \overline{\tau}_{xy}(s) = 0 \tag{3.9}$$

$$\overline{\sigma}_{xx}(s) = -\frac{\overline{P}_2(s)\eta}{h_1} - \frac{12\overline{M}_1(s)\eta^3}{h_1^3}y_2 \tag{3.10}$$

where y_2 is the distance measured from the neutral axis in the substrate.

Stresses in the beam away from the cracktip (Fig. 3a) are:

$$\overline{\sigma}_{yy}(s) = \overline{\tau}_{xy}(s) = 0 \tag{3.11}$$

The stress component $\overline{\sigma}_{xx}(s)$ due to the force $\overline{P}_3(s)$ acting alone is

$$[\overline{\sigma}_{xx}(s)]_{\overline{P}_3(s)} = \overline{\Sigma}(s)\frac{\overline{P}_3(s)}{h_1\overline{A}_3(s)} \qquad h_2 - h_1\overline{\Delta}(s) < y < h_2 - h_1\overline{\Delta}(s) + h_1 \tag{3.12}$$

$$[\overline{\sigma}_{xx}(s)]_{\overline{P}_3(s)} = \frac{\overline{P}_3(s)}{h_1\overline{A}_3(s)} \qquad -h_1\overline{\Delta}(s) < y < h_2 - h_1\overline{\Delta}(s) \tag{3.13}$$

where, $\overline{A}_3(s) = \frac{1}{\eta} + \overline{\Sigma}(s)$

The stress component $\overline{\sigma}_{xx}(s)$ due to the force $\overline{M}_3(s)$ acting alone is

$$[\overline{\sigma}_{xx}(s)]_{\overline{M}_3(s)} = s\overline{E}_1(s)\overline{\varepsilon}_{xx}(s) = -s\overline{E}_1(s)\overline{y}_3(s)\overline{w}_1''(s) \qquad h_2 - h_1\overline{\Delta}(s) < y < h_2 - h_1\overline{\Delta}(s) + h_1 \tag{3.14}$$

$$[\overline{\sigma}_{xx}(s)]_{\overline{M}_3(s)} = -s\overline{E}_2(s)\overline{\varepsilon}_{xx}(s) = -s\overline{E}_2(s)\overline{y}_3(s)\overline{w}_1''(s) \qquad -h_1\overline{\Delta}(s) < y < h_2 - h_1\overline{\Delta}(s) \tag{3.15}$$

where $\overline{y}_3(s) = y - h_1\overline{\Delta}(s)$, $\overline{w}(s)$ is the deflection of the beam, y_1 is the distance measured from the neutral axis and y is the distance measured from the bottom surface of the substrate.

The net force balance yields

$$\int_0^{h_1+h_2} \overline{\sigma}_{xx}(s)d\overline{A}(s) = 0 \tag{3.16}$$

Similarly, the net moment balance requires

$$\int_0^{h_1+h_2} \left(\overline{\sigma}_{xx}(s)d\overline{A}(s)\right)\left(y - h_1\overline{\Delta}(s)\right) = \overline{M}_3(s) \tag{3.17}$$

Substituting (3.16) in the above equation, we obtain

$$\overline{M}_3(s) = \int_0^{h_1+h_2} \left(\overline{\sigma}_{xx}(s)d\overline{A}(s)\right) y \tag{3.18}$$

But

$$\begin{aligned}\int_0^{h_1+h_2} \overline{\sigma}_{xx}(s)yd\overline{A}(s) = &- \int_0^{h_1} s\overline{E}_2(s)\left(y - h\overline{\Delta}(s)\right)\overline{w}''(s)ydy \\ &- \int_{h_2}^{h_1+h_2} s\overline{E}_2(s)\left(y - h\overline{\Delta}(s)\right)\overline{w}''(s)\overline{\Sigma}(s)ydy\end{aligned} \tag{3.19}$$

which, after further simplification, becomes

$$\overline{w}''(s) = \frac{\overline{M}_3(s)}{s\overline{E}_2(s)h_1^3\overline{I}_3(s)} \tag{3.20}$$

where

$$\begin{aligned}\overline{I}_3(s) \;=\; & \overline{\Sigma}(s)\left[\left(\overline{\Delta}(s) - \frac{1}{\eta}\right)^2 - \left(\overline{\Delta}(s) - \frac{1}{\eta}\right) + \frac{1}{3}\right] \\ & + \frac{\overline{\Delta}(s)}{\eta}\left(\overline{\Delta}(s) - \frac{1}{\eta}\right) + \frac{1}{3\eta^3}\end{aligned}$$

Combining (3.12), (3.14) and (3.20) we obtain,

$$\begin{aligned}\overline{\sigma}_{xx}(s) \;=\; & \overline{\Sigma}(s)\left[\frac{\overline{P}_3(s)}{h_1\overline{A}_3(s)} + \frac{\overline{M}_3(s)}{h_1^3\overline{I}_3(s)}y_3\right] \\ & h_2 - h_1\overline{\Delta}(s) < y < h_2 - h_1\overline{\Delta}(s) + h_1\end{aligned} \tag{3.21}$$

Similarly, from equations (3.13), (3.15) and (3.20) we obtain

$$\overline{\sigma}_{xx}(s) = \left[\frac{\overline{P}_3(s)}{h_1\overline{A}_3(s)} + \frac{\overline{M}_3(s)}{h_1^3\overline{I}_3(s)}y_3\right] \quad - h_1\overline{\Delta}(s) < y < h_2 - h_1\overline{\Delta}(s) \tag{3.22}$$

The superposition of stresses in Fig. 3a and Fig. 3b leads to the following stresses in the upper beam:

$$\overline{\sigma}_{yy}(s) = \overline{\tau}_{xy}(s) = 0$$

$$\begin{aligned}\overline{\sigma}_{xx}(s) &= \frac{\overline{P}_1(s)}{h_1} + \frac{12\overline{M}_1(s)}{h_1^3}y_1 - \frac{\overline{P}_3(s)\overline{\Sigma}(s)}{h_1\overline{A}_3(s)} \\ &\quad -\frac{\overline{M}_3(s)\overline{\Sigma}(s)}{h_1^2\overline{I}_3(s)}\left(\frac{1}{\eta}+\frac{1}{2}-\overline{\Delta}(s)\right) - \frac{\overline{\Sigma}(s)\overline{M}_3(s)}{h_1^3\overline{I}_3(s)}y_1 \end{aligned} \tag{3.23}$$

For the loading in Fig. 3c, the stresses in the upper beam are:

$$\overline{\sigma}_{yy}(s) = \overline{\tau}_{xy}(s) = 0$$

$$\overline{\sigma}_{xx}(s) = \frac{\overline{P}(s)}{h_1} + \frac{12\overline{M}(s)}{h_1^3} \tag{3.24}$$

But the stresses obtained in (3.23) and (3.24) are equivalent; therefore, equating them and separating the like powers of y on either sides of the equation, we obtain,

$$\overline{P}(s) = \overline{P}_1(s) - \frac{\overline{P}_3(s)\overline{\Sigma}(s)}{\overline{A}_3(s)} - \frac{\overline{M}_3(s)\overline{\Sigma}(s)\left(\frac{1}{\eta}+\frac{1}{2}-\overline{\Delta}(s)\right)}{h_1\overline{I}_3(s)} \tag{3.25}$$

$$\overline{M}(s) = \overline{M}_1(s) - \frac{\overline{M}_3(s)\overline{\Sigma}(s)}{12\overline{I}_3(s)} \tag{3.26}$$

Similarly, the superposition of stresses in Fig. 3a and Fig. 3b for the lower beam gives

$$\overline{\sigma}_{yy}(s) = \overline{\tau}_{xy}(s) = 0$$

$$\begin{aligned}\overline{\sigma}_{xx}(s) &= -\frac{\overline{P}_2(s)\eta}{h_1} - \frac{12\overline{M}_2(s)\eta^3}{h_1^3}y_2 - \frac{\overline{P}_3(s)}{h_1\overline{A}_3(s)} \\ &\quad + \frac{\overline{M}_3(s)}{h_1^2\overline{I}_3(s)}\left(\overline{\Delta}(s) - \frac{1}{2\eta}\right) - \frac{\overline{M}_3(s)}{h_1^3\overline{I}_3(s)}y_2 \end{aligned} \tag{3.27}$$

For the loading in Fig. 3c, the stresses in the lower beam are:

$$\overline{\sigma}_{yy}(s) = \overline{\tau}_{xy}(s) = 0$$

$$\overline{\sigma}_{xx}(s) = \frac{\overline{P}^*(s)\eta}{h_1} + \frac{12\overline{M}^*(s)\eta^3}{h_1^3}y_2 \tag{3.28}$$

Equating the equivalent stress equations (3.27) and (3.28) and comparing the like powers, we obtain

$$\overline{P}^*(s) = -\overline{P}_2(s) - \frac{\overline{P}_3(s)}{\eta\overline{A}_3(s)} + \frac{\overline{M}_3(s)}{h_1\overline{I}_3(s)\eta}\left(\overline{\Delta}(s) - \frac{1}{2\eta}\right) \tag{3.29}$$

$$\overline{M}^*(s) = -\overline{M}_2(s) + \frac{\overline{M}_3(s)}{12\eta^3\overline{I}_3(s)} \tag{3.30}$$

The variables $\overline{P}_2(s)$ and $\overline{M}_2(s)$ in (3.29) and (3.30) are eliminated by making use of equations (3.2) and (3.3) to obtain:

$$\overline{P}^*(s) = -\overline{P}_(s) \tag{3.31}$$

$$\overline{M}^*(s) = -\overline{M}(s) - \frac{\overline{P}(s)h_1(1+\eta)}{2\eta} \tag{3.32}$$

Thus the set of forces and moments acting in Fig. 3a are replaced by two independent load variables $\overline{P}(s)$ and $\overline{M}(s)$ given by the expressions (3.25) and (3.26) respectively.

3.2 Thin Film Bonded to a Substrate

In this section, the equivalent system in Fig. 3c is used to study a specific problem of fracture behavior of a thin film bonded to a substrate. The film material considered here is a linear viscoelastic Maxwell type of solid whose modulus is of the form

$$E_1(t) = E_1 \exp\left(\frac{-t}{\tau_1}\right) \tag{3.33}$$

where E_1 is the glassy elastic modulus and τ_1 is the relaxation time. The Poisson's ratio ν_1 is assumed to be a constant with respect to time and temperature. The substrate is assumed to be an elastic material whose Young's modulus is E_2.

The film which is loaded by the residual stresses can be replaced by an edge loading as discussed in section 2. The stresses acting at the edge of the film are given by the relation (2.6) which in the Laplace domain can be written as

$$\overline{\sigma}_{xx}(s) = \frac{\Delta\alpha\Delta T}{(1-\nu_1)}\frac{E_1\tau_1}{(1+\tau_1 s)} \tag{3.34}$$

The equivalent loads and moments as shown in Fig. 3c can be evaluated from the knowledge of stresses in the film.

The axial load, $\overline{P}_1(s)$, is given by

$$\overline{P}_1(s) = \overline{\sigma}_{xx}(s)h_1 = \frac{\Delta\alpha\Delta T}{(1-\nu_1)}h_1\frac{E_1\tau_1}{(1+\tau_1 s)} \tag{3.35}$$

Similarly,

$$\overline{P}_3(s) = \frac{\Delta\alpha\Delta T}{(1-\nu_1)}h_1\frac{E_1\tau_1}{(1+\tau_1 s)} \tag{3.36}$$

The bending moment, $\overline{M}_3(s)$, is represented by

$$\overline{M}_3(s) = \overline{P}_3(s)h_1\left(\frac{1}{\eta}+\frac{1}{2}-\overline{\Delta}(s)\right) = \frac{\Delta\alpha\Delta T}{(1-\nu_1^2)}h_1^2\frac{E_1E_2(1+\eta)\tau_1}{2\eta\left[E_2+(E_2+\eta E_1)\tau_1 s\right]} \tag{3.37}$$

All other load variables,

$$\overline{P}_2(s) = \overline{M}_1(s) = \overline{M}_2(s) = 0 \tag{3.38}$$

Substituting the above load equations and the material variables (Appendix II) in (3.25) and (3.26), we obtain

$$\overline{P}(s) = \frac{\Delta\alpha\Delta T h_1}{(1-\nu_1)}\left[\frac{E_1\tau_1}{(1+\tau_1 s)}-\frac{E_1\tau_1\eta s}{(1+\tau_1 s)(E_2+C_6 s)} - \frac{E_1^2E_2^2\tau_1^2 6\eta^3(1+\eta)^2 s(1+\tau_1 s)}{(C_4+C_5 s)(C_9+C_{10}s+C_{11}s^2)}\right] \tag{3.39}$$

$$\overline{M}(s) = \frac{\Delta\alpha\Delta T h_1^2 E_1^2 E_2\tau_1^2\eta^3(1+\eta)}{2(1-\nu_1)}\left[\frac{s}{12(C_9+C_{10}s+C_{11}s^2)}\right] \tag{3.40}$$

Equations (3.39) and (3.40) are inverted analytically back to the time domain to obtain

$$P(t) = C_{12}\exp(-C_{13}t)+C_{14}\exp(-C_{15}t) \tag{3.41}$$

$$M(t) = C_{16}\exp(-C_{13}t)+C_{17}\exp(-C_{15}t) \tag{3.42}$$

where the constants C_{12} through C_{17} are given in Appendix II.

The stress components in the film due to the axial load $P(t)$ and the bending moment $M(t)$ are:

$$\begin{aligned}\sigma_{xx}(t) &= \left(\frac{C_{12}}{h_1}+\frac{12C_{16}}{h_1^3}y_1\right)\exp\left(-C_{13}t\right)\\ &\quad+\left(\frac{C_{14}}{h_1}+\frac{12C_{17}}{h_1^3}y_1\right)\exp\left(-C_{15}t\right)\end{aligned} \tag{3.43}$$

while all the other stress components are zero.

The strain component ε_{xx} in the film can be calculated from the constitutive relation (2.1) and (2.2), which gives

$$\varepsilon_{xx}(t) = D(t)\sigma_{xx}(0) + \int_{0+}^{t} D\left(t-\xi\right)\frac{\partial\sigma_{xx}}{\partial\xi}d\xi \tag{3.44}$$

where $D(t)$ is the creep compliance of the material. But for a Maxwell type of solid, the creep compliance is given by

$$D(t) = \frac{1}{E_1}\left(\frac{t}{\tau}+1\right) \tag{3.45}$$

Substituting equations (3.43) and (3.45) in (3.44), we obtain

$$\begin{aligned}\varepsilon_{xx} &= \frac{1}{E_1\tau_1}\left[\left(\tau_1-\frac{1}{C_{13}}\right)\left(\frac{C_{12}}{h_1}+\frac{12C_{16}}{h_1^3}y_1\right)\exp\left(-C_{13}t\right)\right.\\ &\quad+\left(\tau_1-\frac{1}{C_{15}}\right)\left(\frac{C_{14}}{h_1}+\frac{12C_{17}}{h_1^3}y_1\right)\exp\left(-C_{15}t\right)\\ &\quad\left.+\left(\frac{C_{12}}{h_1C_{13}}+\frac{12C_{16}}{h_1^3C_{13}}y_1+\frac{C_{14}}{h_1C_{15}}+\frac{12C_{17}}{h_1^3C_{15}}y_1\right)\right]\end{aligned} \tag{3.46}$$

3.3 Energy Release Rate

The fracture analysis in this part is based on the Griffith's energy balance approach. The energy balance for a crack in a media of length a is given by the relation,

$$I - U - S = 0 \tag{3.47}$$

where I is the energy input at the boundary, U is the strain energy density and S is the surface energy per unit area.

However, when the material is considered to be elastic, the above equation can be written in the form

$$G = S \tag{3.48}$$

where G is defined as the energy release rate which is given by the well known relation,

$$G = -\frac{\partial U}{\partial a} \tag{3.49}$$

In the following analysis for the viscoelastic material, for the sake of simplicity, the whole process of crack propagation is assumed to take place in a stepwise manner. That is, at any instant t_j the crack is assumed to be of length a and the crack is then assumed to grow by an amount Δa in a small interval of time Δt. The time interval Δt is assumed to be so small such that the stress variations in this time can be considered to be negligible so that the dissipation effects are neglected over this small time step. In order to calculate the strain energy release rate, the stresses are allowed to relax up to any time $t = t_j$ and then during the small time interval ($t = t_j$ to $t = t_j + \Delta t$) the process is assumed to have negligible dissipation of energy due to viscous effects, and therefore the elastic strain energy release rate relationship (3.49) can be used in this timestep.

The strain energy density in the film as a function of time in the film is given by the relation

$$U_1 = \int_{-\frac{h_1}{2}}^{\frac{h_1}{2}} \int_0^a \frac{\sigma_{xx}^2}{2E_1} dx dy \tag{3.50}$$

Substituting (3.43) in the above equation results in

$$\begin{aligned} U_1 &= \frac{a}{2E_1}\left[\left(\frac{C_{12}^2}{h_1}+\frac{12C_{16}^2}{h_1^3}\right)\exp\left(-2C_{13}t\right)\right. \\ &+\left(\frac{C_{14}^2}{h_1}+\frac{12C_{17}^2}{h_1^3}\right)\exp\left(-2C_{15}t\right) \\ &\left.+\left(\frac{C_{12}C_{14}}{h_1}+\frac{12C_{16}C_{17}}{h_1^3}\right)\exp\left\{-\left(C_{13}+C_{15}\right)t\right\}\right] \end{aligned} \tag{3.51}$$

The strain energy function is then discretised in terms of small timesteps Δt. The discretized form of the strain energy at any time $(t+\Delta t)$ is

$$\begin{aligned} U_1(t_j+\Delta t) &= a(t_j+\Delta t)\left[C_{18}\exp\left\{-2C_{13}\left(t_j+\Delta t\right)\right\}\right. \\ &+C_{19}\exp\left\{-2C_{15}\left(t_j+\Delta t\right)\right\} \\ &\left.+\,C_{20}\exp\left\{-\left(C_{13}+C_{15}\right)\left(t_j+\Delta t\right)\right\}\right] \end{aligned} \tag{3.52}$$

First of all, consider a crack of length a at time $t=t_j$, which doesn't grow further in the next time interval ($t=t_j$ to $t=t_j+\Delta t$) so that the strain energy U_1 in this system at the end of time $t=t_j+\Delta t$ will be

$$\begin{aligned} U_{11}(t_j+\Delta t) &= a(t_j)\left[C_{18}\exp\left\{-2C_{13}\left(t_j+\Delta t\right)\right\}\right. \\ &+C_{19}\exp\left\{-2C_{15}\left(t_j+\Delta t\right)\right\} \\ &\left.+\,C_{20}\exp\left\{-\left(C_{13}+C_{15}\right)\left(t_j+\Delta t\right)\right\}\right] \end{aligned} \tag{3.53}$$

Now consider the same crack of length a, at time $t = t_j$, and let it be allowed to grow by an amount $(a + \Delta a)$ in the time interval ($t = t_j$ to $t = t_j + \Delta t$), so that the strain energy U_2 at the end of time $t = t_j + \Delta t$ will be

$$\begin{aligned} U_{12}(t_j + \Delta t) &= (a(t_j) + \Delta a)\,[C_{18} \exp\{-2C_{13}\,(t_j + \Delta t)\} \\ &+ C_{19} \exp\{-2C_{15}\,(t_j + \Delta t)\} \\ &+ C_{20} \exp\{-(C_{13} + C_{15})\,(t_j + \Delta t)\}] \end{aligned} \tag{3.54}$$

The energy difference $\Delta U = U_{11} - U_{12}$ is the energy utilized in creating the new surface and hence the strain energy release rate G in this small timestep will be

$$\begin{aligned} G_1 &= -\frac{\partial U}{\partial a} = -\frac{\Delta U}{\Delta a} \\ &= [C_{18} \exp\{-2C_{13}\,(t_j + \Delta t)\} + C_{19} \exp\{-2C_{15}\,(t_j + \Delta t)\} \\ &\quad + C_{20} \exp\{-(C_{13} + C_{15})\,(t_j + \Delta t)\}] \end{aligned} \tag{3.55}$$

where the constants C_{18} through C_{20} are given in Appendix II.

The substrate material is elastic and therefore the elastic energy release rate relation can be used at all times. The expression for the strain energy in the substrate is given by

$$U_2 = \frac{a(t)}{2E_2}\left[\frac{\eta P^2(t)}{h_1} + \frac{12\eta^3}{h_1^3}\left\{M(t) + \frac{P(t)h_1\,(1+\eta)}{2\eta}\right\}^2\right] \tag{3.56}$$

By using the relation (3.49), the energy release is evaluated as

$$G_2 = \frac{1}{2E_2}\left[\frac{\eta P^2(t)}{h_1} + \frac{12\eta^3}{h_1^3}\left\{M(t) + \frac{P(t)h_1\,(1+\eta)}{2\eta}\right\}^2\right] \tag{3.57}$$

The above equation is discretized into small time steps so that it can be used with the energy release rate relation (3.55) obtained for the film.
The total energy release rate G, in the film, is given by

$$G(t + \Delta t) = G_1(t + \Delta t) + G_2(t + \Delta t) \tag{3.58}$$

However, in most practical applications the substrate material is considered to be almost rigid ($E_2 \gg E_1$). In such a case the energy release rate contribution from the substrate is negligible compared to that of the film. We make use of this condition in the future calculations.

3.4 Crack Propagation

The crack once initiated can propagate further if it can overcome the fracture resistance at the interface. The fracture resistance is strongly dependent on the toughness or the adhesive fracture energy, Γ, of the interface. The adhesive fracture energy can be interpreted as the energy required to break the bonds at the interface. The magnitude of this energy depends on the number of bonds per unit surface area and the energy required to break each bond. Therefore, a fracture criteria has to be imposed to determine the crack growth.

In the case of interfacial crack growth, mixed mode conditions prevail at the crack tip [12], [23]. When dealing with such mixed mode conditions, the adhesive fracture energy is found to depend strongly on the mode mixity. Anderson and others [1] conducted experiments at different modes and found that in the case of mode II and mode III type of deformations, the adhesive fracture energy was more than that of mode I.

In wide class of plane elasticity problems, Dundurs [6] has observed that the mode

mixity depends only on two non-dimensional parameters, α and β, which account for the mismatch of the material properties in the two materials. The parameter α accounts for the mismatch in tensile elastic modulus and is given by

$$\alpha = \frac{\mu_1(\kappa_2 + 1) - \mu_2(\kappa_1 + 1)}{\mu_1(\kappa_2 + 1) + \mu_2(\kappa_1 + 1)} \tag{3.59}$$

while the parameter β which accounts for the mismatch in bulk modulus and is given by,

$$\beta = \frac{\mu_1(\kappa_2 - 1) - \mu_2(\kappa_1 - 1)}{\mu_1(\kappa_2 + 1) + \mu_2(\kappa_1 + 1)} \tag{3.60}$$

where $i = 1$ denotes the upper layer and $i = 2$ denotes the lower layer; μ_i refers to the shear modulus of the upper or lower layer, and κ_i, which is expressed in terms of the poisson ratio ν_i, is $\kappa_i = (3 - 4\nu_i)$ for plane strain, and in plane stress $\kappa_i = (3 - 4\nu_i)/(1 + \nu_i)$.

Hutchinson and Suo [12] have shown that in a special case of $\beta = 0$, the relative amount of mode II and mode I can be separated, and a measure of mode mixity is defined by

$$\psi = tan^{-1}\left(\frac{K_{II}}{K_I}\right) \tag{3.61}$$

where K_I is the mode I stress intensity factor and K_{II} is the mode II stress intensity factor. Further, they have stated the fracture criteria for initiation of crack advance under mixed mode condition as

$$G = \Gamma(\psi) \tag{3.62}$$

Several experimental studies such as scarf joint experiments by Trantina [24], cone, peel and blister tests by Anderson and others [1], blister tests by Liechti and Hanson [16] and the asymmetric and symmetric double cantilever beam method by Cao and

Evans [2] have shown that the adhesive fracture strength Γ is a function of mode mixity ψ, thus supporting the fracture criteria stated in (3.62).

However, in the case of viscoelastic material, the time dependent variation of the mode mixity will cause the adhesive fracture energy to vary with time. In most cases for example [18], this variation is neglected. In the present analysis, the time variation of adhesive fracture energy is neglected and the adhesive fracture energy used at all times is the elastic adhesive fracture energy at time $t = 0$. Suo and Hutchinson [22] in an elastic analysis of interface debonding have shown that the mode mixity varies as a function of both thickness ratio and the modulus ratio. Thus, for a selected geometry and modulus ratio, the adhesive fracture energy can be assumed to be a constant, Γ_o, in which case the failure criteria becomes

$$G = \Gamma_o \tag{3.63}$$

Therefore, Γ_o is a measure of the critical energy which has to be overcome for the crack to grow. In other words, the crack that has initiated at the edge will grow further only if the energy release rate is more than or equal to the adhesive energy.

Once the crack which is introduced along the interface at the edge satisfies the fracture criteria and starts to grow, it is important to know at what speed it will grow and how far it grows. In order to calculate its speed of propagation, we make use of the velocity relation,

$$v = \frac{\partial a}{\partial t} \approx \frac{\Delta a}{\Delta t} \tag{3.64}$$

But the energy release rate during a small time step is given by (3.49),

$$G(t_j + \Delta t) = -\frac{\partial}{\partial a} U(t_j + \Delta t) \approx -\frac{\Delta U(t_j + \Delta t)}{\Delta a} \tag{3.65}$$

where $\Delta U = U_{11} - U_{12}$. Substituting these quantities U_{11} and U_{12} from equations (3.53) and (3.54) along with the expression for Δa from (3.64) in equation (3.65), we get

$$\begin{aligned} G(t_j + \Delta t) &= [C_{18} \exp\{-2C_{13}(t_j + \Delta t)\} + C_{19} \exp\{-2C_{15}(t_j + \Delta t)\} \\ &+ C_{20} \exp\{-(C_{13} + C_{15})(t_j + \Delta t)\}] \\ &+ \frac{a(t_j + \Delta t)}{v(t_j)} [2C_{13}C_{18} \exp\{-2C_{13}(t_j + \Delta t)\} \\ &+ 2C_{15}C_{19} \exp\{-2C_{15}(t_j + \Delta t)\} \\ &+ (C_{13} + C_{15}) C_{20} \exp\{-(C_{13} + C_{15})(t_j + \Delta t)\}] \end{aligned} \tag{3.66}$$

Making use of the criteria for crack growth (3.63) and substituting the expression for G (3.66) in this equation, we obtain the following equation for crack velocity v over a small time step Δt.

$$v = \frac{F_1(t)}{F_2(t)} \tag{3.67}$$

where

$$\begin{aligned} F_1(t) &= a(t_j) [2C_{13}C_{18} \exp\{-2C_{13}(t_j + \Delta t)\} \\ &+ 2C_{15}C_{19} \exp\{-2C_{15}(t_j + \Delta t)\} \\ &+ (C_{13} + C_{15}) C_{20} \exp\{-(C_{13} + C_{15})(t_j + \Delta t)\}] \end{aligned} \tag{3.68}$$

and

$$\begin{aligned} F_2(t) &= \Gamma_o + [C_{18} \exp\{-2C_{13}(t_j + \Delta t)\} + C_{19} \exp\{-2C_{15}(t_j + \Delta t)\} \\ &+ C_{20} \exp\{-(C_{13} + C_{15})(t_j + \Delta t)\}] \\ &+ [2C_{13}C_{18} \exp\{-2C_{13}(t_j + \Delta t)\} + 2C_{15}C_{19} \exp\{-2C_{15}(t_j + \Delta t)\} \\ &+ (C_{13} + C_{15}) C_{20} \exp\{-(C_{13} + C_{15})(t_j + \Delta t)\}] \end{aligned} \tag{3.69}$$

The above equation is valid as long as the fracture criteria (3.63) is satisfied, and at all other times the velocity will be zero.

Having obtained the velocity of crack v over a small time step, the crack growth at the end of this time step is calculated from the relation,

$$a(t_j + \Delta t) = a(t_j) + v\Delta t \tag{3.70}$$

Again, the above equation is valid as long as the fracture criteria is satisfied and it ceases to grow when the energy is below the critical level for fracture.

4 Finite Element Analysis

4.1 Motivation

In order to examine the validity of our assumptions and the analytical results obtained in the previous section, a numerical calculation using finite element technique was performed. Before attempting the actual problem described in the previous section, it is advantageous in an initial investigation to consider the simplest possible situation. Such a situation is provided by the plane stress steady crack growth of a large crack $a > 1.5b$ (Fig. 4), along the center line of an infinitely long viscoelastic strip under constant lateral strain ε_o. Analytical solution to this problem has been obtained by Mueller and Knauss [18], and therefore the finite element solutions can be compared with this solution.

A finite element analysis was performed for this problem using ABAQUS [1] code incorporating the viscoelastic material library. Due to symmetry in both x and y directions, only one quarter of the geometry was considered. An initial crack of

[1] Abaqus by Hibbit, Karlsson and Sorenson, Providence, R.I.

length a (such that $a << l$) was introduced at the center and the whole strip was discretized using eight noded plane stress elements. A focussed mesh was used near the cracktip with independent displacements allowed at all the nodes in the crack front nodal position. In addition, the mid-side nodes of the cracktip elements were moved to the quarter point position to capture the singularity near the cracktip. A typical finite element mesh near the cracktip is shown in Fig. 5. The upper end of the quarter strip was subjected to a constant lateral strain ε_o while the displacement in the longitudinal direction was constrained. Symmetry boundary conditions were imposed along the lines of symmetry.

The finite element calculations were performed for a particular crack length a to obtain the strain energy density U_1 of the complete system at different time steps. The crack length was then changed by a very small amount Δa (such that $\Delta a/l = 1 : 500$) and again the strain energy density of the whole system U_2 at the same time steps were calculated. The strain energy release rate G for the crack length a was calculated by the Griffith's energy relation,

$$G = -\frac{\partial U}{\partial a} \approx -\frac{\Delta U}{\Delta a} \tag{4.1}$$

The analytical relation for the energy release rate G obtained by Mueller and Knauss [18] is given by the relation,

$$G = \frac{\varepsilon_o^2 E^2(t)}{2\,(1-\nu^2)} F\,(\Delta t) \tag{4.2}$$

where $E(t)$ is the extensional relaxation modulus, ν is the Poisson's ratio and the function F is given by

$$F(t) = 2\left[D^{(1)}(t) - \frac{1}{2}D^{(2)}(t)\right]$$

Here, $D^{(n)}(t)$ are the time weighted averages of the creep compliance $D(t)$ defined by

$$
\begin{aligned}
D^{(n)}(t) &= \frac{n}{t^n}\int_0^t \tau^{n-1} D(\tau)\, d\tau \qquad n = 1, 2 \\
&= D(t) \qquad\qquad\qquad n = 0
\end{aligned}
$$

The energy release rate is thus calculated analytically at different time intervals. Figure 6 shows a plot of normalized energy release rate obtained by both the analytical and finite element method at different times. The plot indicates that the energy release rate obtained by the finite element method agrees closely with the analytical result. Motivated by this, finite element analysis of the actual problem discussed in Section 2 was performed to verify our analytical results presented in Section 3 and also to check the validity of our assumptions.

4.2 Viscoelastic Thin Film Bonded to an Elastic Substrate

Numerical computations were then performed for a viscoelastic thin film bonded to an elastic substrate. The modulus ratio of the film and the substrate considered in this case was $E_1(0) : E_2 = 1 : 100$ so that the substrate can almost be considered as rigid. In most practical applications the film thickness will be very small compared to its length; therefore, a film geometry with aspect ratio $(h_1 : l)$ equal to (1:100) was considered. Initially, the influence of the film geometry on the deformation near the cracktip was explored.

The thermal co-efficient of the film had a higher value than the substrate so that the tensile stresses were built in the film when cooled during fabrication. The film was assumed to be deposited at 400° C under stress free condition and cooled to the room temperature at a high cooling rate so that the stresses in the film were given by the equation (2.6). The film was discretized using eight noded plane strain elements, and the focussed mesh with capability of capturing singularity was used

near the cracktip as in the previous case. The loading in the film was introduced by applying a traction (σ_{xx}) at the film edges. A fixed boundary condition in all degrees of freedom was introduced at the points along the interface where the film was still bonded to the substrate. Such a condition was imposed because the substrate was considered to be almost rigid compared to the film.

For a given crack length a, the energy release rate was calculated as described in the case of the viscoelastic strip problem, and the results were obtained for different crack lengths at finite time steps. Figure 7 shows a plot of the normalized energy release rate with respect to normalized crack length at different time steps. Trends in the plot show that for each time step the energy release rate is nearly independent of the crack length. Thus the crack length has no influence on the cracktip geometry for larger crack lengths away from the free edge at all times. This is reflected in our analytical result for the energy release rate G (3.55) which is independent of the crack length. A similar conclusion was reached in the case of elastic analysis of debonding along an interface of a thin film bonded to a thick substrate [5]

Another important information regarding the active modes of failure is obtained by looking at the deformation pattern. Figure 8 shows the deformation in the film at time $t/\tau = 1.0$. The displacement has both opening and sliding components indicating that both mode-I and mode-II types of deformation are active.

5 Analytical Results

The analytical expressions obtained in Section 3 are used here to study the failure behavior in some specific geometries. The film considered here is a Maxwell type of viscoelastic solid, and the substrate is an elastic material. The material prop-

erties used in these calculations were the same as that used in the finite element calculations except that the thickness ratios used here are different.

The strain energy release rate was calculated from equation (3.55) at different times using a time step $\Delta t = 10^{-3}$ for different thickness ratios. Figure 9 shows the variation of normalized energy release rate with time. The energy release is observed to remain constant at all time steps as the thickness ratio is increased. In all the cases, the energy release rate is observed to be a monotonically decreasing function which is quite clear from the relaxation behavior of the film. So, to begin with at time $t = 0$, if the energy release rate is more than the adhesive energy Γ_o, the crack starts growing before it reaches a stage where the energy level drops below that of Γ_o and then it ceases to grow. In another situation, right at the beginning, if the energy release rate is below the critical value, the crack will never grow.

The energy release rate obtained by finite element calculations for a thickness ratio of $h_1 : h_2 = 1 : 100$ is compared with the analytical results in Figure 10. The finite element results agree closely with the analytical results further validating our assumptions in the analytical model.

The crack velocity and crack growth were also calculated at different times using a timestep $\Delta t = 10^{-3}$ for a thickness ratio of $h_1 : h_2 = 1 : 100$ from the relations (3.67) and (3.70) respectively. An initial crack length of $a/h = 40$ was used in our computations. The critical energy used in this case were fractions of elastic energy release rate at time $t = 0$. Figure 11 shows a plot of crack velocity as a function of time. The trend shows that the crack velocity increases with time and levels off until it ceases to grow. The crack velocity increases with the decrease in surface energy. The crack growth with respect to time is shown in Fig. 12 for different critical energy release rates Γ_o. It is seen that the amount of crack growth increases

with the decrease in critical energy as it takes a longer time for the energy release to drop below the critical value. Also, the crack growth is almost linear in all the cases considered here.

Conclusion

A simple theory has been developed for studying a crack growing along the interface. The edge load analysis in Laplace domain gave simple expressions for equivalent load variables which were inverted analytically to time domain for a Maxwell type of solid. It has been demonstrated that by discretizing the strain energy function, the energy release rate is obtained during small time steps using a Griffith's energy balance approach which showed good agreement with the finite element results. The energy release rate for the Maxwell solid was observed to be a monotonically decreasing function which suggests that the crack which starts to grow has to arrest after a while when it falls below the critical energy release rate or the crack might not grow right from the beginning if the critical energy release rate is not reached at the beginning. The analytical results showed that the strain energy release rate was independent of crack length, and the same behavior was also predicted by finite element analysis which corroborates the analytical model. The energy release rate was also seen to be independent of the thickness ratio. It was also possible to obtain explicit relations for the crack growth and its velocity. However, there was no basis currently available to check the accuracy of crack growth and its velocity.

The general nature of the edge loading problem is helpful in studying many viscoelastic fracture problems. The analysis can further be extended to include general viscoelastic material by expressing the material properties in the form of a prony series. The present approach gives a rational tool for understanding the interfacial crack propagation in a viscoelastic film bonded to a rigid substrate.

Acknowledgements

We would like to thank Professor W.G. Knauss for several helpful discussions. Also, we would like to thank Dr. Sundar Kamath of IBM for his interest and helpful suggestions. This work was supported by the IBM-Caltech cooperative research fund.

I Appendix I: Composite Beam Theory

Consider a composite beam of two different materials bonded together as shown in Fig. 13. It is convenient to replace the material in the upper layer by an equivalent area of lower layer material. However, the bonding strength should be retained in the equivalent section, *i.e.*, the moment in any section must be the same in the equivalent section as in the original section so that the force at any given element of thickness dy in the equivalent beam must be equal to that at the strip it replaces. Therefore,

$$\sigma b dy = \sigma' b' dy \tag{I.1}$$

or

$$\sigma b = \sigma' b' \tag{I.2}$$

where the primed variables refer to the equivalent section while unprimed variables refer to the original section.

Making use of the constitutive relation (2.1) and (2.2), the above equation can be written as

$$\int_0^t E(t-\tau)\frac{d\varepsilon(\tau)}{d\tau}b = \int_0^t E'(t-\tau)\frac{d\varepsilon'(\tau)}{d\tau}b' \tag{I.3}$$

For true similarity, the strains in both the sections have to be equal. Therefore,

$$\int_0^t E(t-\tau)\frac{d\varepsilon(\tau)}{d\tau}b = \int_0^t E'(t-\tau)\frac{d\varepsilon(\tau)}{d\tau}b' \tag{I.4}$$

or in the Laplace domain,

$$s\overline{E}(s)\overline{\varepsilon}(s)b = s\overline{E}'(s)\overline{\varepsilon}(s)b' \tag{I.5}$$

Thus the width of the equivalent section is given by

$$b' = b\frac{\overline{E}(s)}{\overline{E}(s)} \tag{I.6}$$

So, a composite beam can be treated as a homogenous beam provided the new width given by (I.6) is replaced.

II Appendix II: Time Dependent Material Constants

The relevant material variables appearing in the equations (3.25) and (3.26) for this specific combination of film and substrate material are given by

$$\overline{\Sigma}(s) = \frac{C_1 s}{E_2 + C_2 s} \tag{II.1}$$

$$\overline{\Delta}(s) = \frac{E_2 + C_3 s}{C_4 + C_5 s} \tag{II.2}$$

$$\overline{A}_3(s) = \frac{E_2 + C_6 s}{C_7 + C_8 s} \tag{II.3}$$

$$\overline{I}_3(s) = \frac{C_9 + C_{10} s + C_{11} s^2}{(E_2 + C_2 s)(C_4 + C_5 s)} \tag{II.4}$$

where

$$C_1 = E_1 \tau_1 \tag{II.5}$$

$$C_2 = E_2 \tau_1 \tag{II.6}$$

$$C_3 = \left(E_2 + 2\eta E_+ 1 + \eta^2 E_1\right) \tau_1 \tag{II.7}$$

$$C_4 = 2\eta E_2 \tag{II.8}$$

$$C_5 = \left(2\eta E_2 + 2\eta^2 E_1\right) \tau_1 \tag{II.9}$$

$$C_6 = (E_2 + E_1 \eta) \tau_1 \tag{II.10}$$

$$C_7 = \eta E_2 \tag{II.11}$$

$$C_8 = \eta E_2 \tau_1 \tag{II.12}$$

$$C_9 = E_2^2 \eta \tag{II.13}$$

$$C_{10} = 2\eta E_2^2 \tau_1 + 2\eta^2 E_1 E_2 \tau_1 \left(2\eta^2 + 3\eta + 2\right) \tag{II.14}$$

$$C_{11} = E_1^2 \tau_1^2 \eta^5 + E_2^2 \tau_1^2 \eta + 2\eta^2 E_1 E_2 \tau_1^2 \left(2\eta^2 + 2\eta + 2\right) \tag{II.15}$$

The other constants used in the main text are:

$$C_{12} = -\frac{D_1 D_3}{C_{11} C_5} \tag{II.16}$$

$$C_{13} = \frac{C_{10} + \sqrt{C_{10}^2 - 4C_9 C_{11}}}{2C_{11}} \tag{II.17}$$

$$C_{14} = -\frac{D_1 D_4}{C_{11} C_5} \tag{II.18}$$

$$C_{15} = \frac{C_{10} - \sqrt{C_{10}^2 - 4C_9 C_{11}}}{2C_{11}} \tag{II.19}$$

$$C_{16} = -\frac{D_2 C_{13}}{\sqrt{C_{10}^2 - 4C_9 C_{11}}} \tag{II.20}$$

$$C_{17} = -\frac{D_2 C_{15}}{\sqrt{C_{10}^2 - 4C_9 C_{11}}} \tag{II.21}$$

$$C_{18} = \frac{D_5^2 h_1}{2E_1} + \frac{D_6^2 h_1^3}{24E_1} \tag{II.22}$$

$$C_{19} = \frac{D_7^2 h_1}{2E_1} + \frac{D_8^2 h_1^3}{24E_1} \tag{II.23}$$

$$C_{20} = \frac{D_5 D_7 h_1}{E_1} + \frac{D_6 D_8 h_1^3}{12E_1} \tag{II.24}$$

where

$$D_1 = \frac{6\Delta\alpha\Delta T h_1 E_1^2 E_2^2 \tau_1^2 \eta^3 (1+\eta)^2}{(1-\nu_1)} \tag{II.25}$$

$$D_2 = \frac{h_1 E_2 D_1}{3(1+\eta)} \tag{II.26}$$

$$D_3 = \frac{C_{13}\tau_1 - 1}{C_{13} - C_{15}} \tag{II.27}$$

$$D_4 = \frac{C_{15}\tau_1 - 1}{C_{15} - C_{13}} \tag{II.28}$$

$$D_5 = -\frac{D_1 D_3}{h_1 C_5 C_{11}} \tag{II.29}$$

$$D_6 = -\frac{12 D_2 C_{13}}{h_1^3 \sqrt{C_{10}^2 - 4 C_9 C_{11}}} \tag{II.30}$$

$$D_7 = -\frac{D_1 D_4}{h_1 C_5 C_{11}} \tag{II.31}$$

$$D_6 = \frac{12 D_2 C_{15}}{h_1^3 \sqrt{C_{10}^2 - 4 C_9 C_{11}}} \tag{II.32}$$

References

[1] Anderson, G.P., DeVries, K.L. and Williams, M.L. (1974). Mixed mode stress field effect in adhesive fracture. *Int. J. Fracture.* **10**, 565-583.

[2] Cao, H.C. and Evans, A.G. (1989). An experimental study of the fracture resistance of bimaterial interfaces. *Mechanics of Materials.* **7**, 295-305.

[3] Christensen, R.M. (19179). A rate-dependent criterion for crack growth. *Int. J. Fracture.* **15**, 3-21.

[4] Christensen, R.M. and McCartney,L.N. (1983). Viscoelastic crack growth. *Int. J. Fracture.* **23**, R11-R13.

[5] Drory,M.D., Thouless, M.D. and Evans, A.G. (1988). On decohesion of residually stressed thin films. *Acta Metall.* **36**, 2019-2028.

[6] Dundurs, J. (1969). Edge-bonded dissimilar orthogonal elastic wedges. *J. Appl. Mech.* **36**, 650-652.

[7] Elsner, G. (1987). Residual stress and thermal expansion of spun-on polyimide films. *J. Appl. Poly. Sci.* **12**, 2157-2166.

[8] Evans, A.G. and Hutchinson, J.W. (1984). On the mechanics of delamination and spalling in compressed films. *Int. J. Fracture.* **20**, 455-466.

[9] Evans, A.G., Drory, M.D. and Hu, M.S. (1988). The cracking and decohesion of thin films. *J. Mater. Res.* **3**, 1043-1049.

[10] Gruninger, M.F., Lawn, B.R., Farabaugh, E.N. and Wachtman, Jr., J.B. (1987). Measurement of residual stresses in coatings on brittle substrates by indentation fracture. *J. Am. Ceram. Soc.* **70**, 344-348.

[11] Hu, M.S., Thouless, M.D. and Evans, A.G. (1988). The decohesion of thin films from brittle substrates. *Acta Metall.* **36**, 1301-1307.

[12] Hutchinson, J.W. and Suo, Z. (1991). Mixed mode cracking in layered materials. *Adv. Appl. Mech.* **29**, 63-191.

[13] Knauss,W.G. (1970). Delayed fracture - The Griffith problem for linearly viscoelastic materials. *Int. J. Fracture.* **6**, 7-20.

[14] Knauss, W.G. (1973). The mechanics of polymer fracture. *Appl. Mech. Rev.* **26**, 1-17.

[15] Knauss, W.G. and Dietmann, H. (1970). Crack propagation under variable load histories in linearly viscoelastic solids. *Int. J. Engng. Sci.* **8**, 643-653.

[16] Liechti, K.M. and Hanson, E.C. (1988). Nonlinear effects in mixed-mode interfacial delaminations. *Int. J. Fracture.* **36**, 199-217.

[17] McCartney, L.N. (1977). Crack propagation, resulting from a monotonic increasing applied stress, in a linear viscoelastic material. *Int. J. Fracture.* **13**, 641-654.

[18] Mueller, H.K. and Knauss, W.G. (1971). Crack propagation in a linearly viscoelastic strip. *J. Appl. Mech.* **38**, 483-488.

[19] Schapery, R.A. (1975). A theory of crack initiation and growth in viscoelastic media. I. Theoretical development. *Int. J. Fracture.* **11**, 141-159.

[20] Schapery, R.A. (1975). A theory of crack initiation and growth in viscoelastic media. II. Approximate methods of analysis. *Int. J. Fracture.* **11**, 369-388.

[21] Schapery, R.A. (1975). A theory of crack initiation and growth in viscoelastic media. I. Analysis of continuous growth. *Int. J. Fracture.* **11**, 549-562.

[22] Suo, Z. and Hutchinson, J.W. (1990). Interface crack between two elastic layers. *Int. J. Fracture* **43**, 1-18.

[23] Thouless, M.D., Evans,A.G., Ashby, M.F. and Hutchinson, J. W. (1987). *Acta Metall.* **35**, 1333-1341.

[24] Trantina, G.C. (1972). Combined mode crack extension in adhesive joints. *J. Composite Materials.* **6**, 271-285.

[25] Williams, M.L. (1965). Initiation and growth of viscoelastic fracture. *Int. J. Fracture* **1**, 292-310.

[26] Wnuk, M.P. and Knauss, W.G. (1970) Delayed fracture in viscoelastic - plastic solids. *Int. J. Solids Structures.* **6**, 7-20.

List of Figures

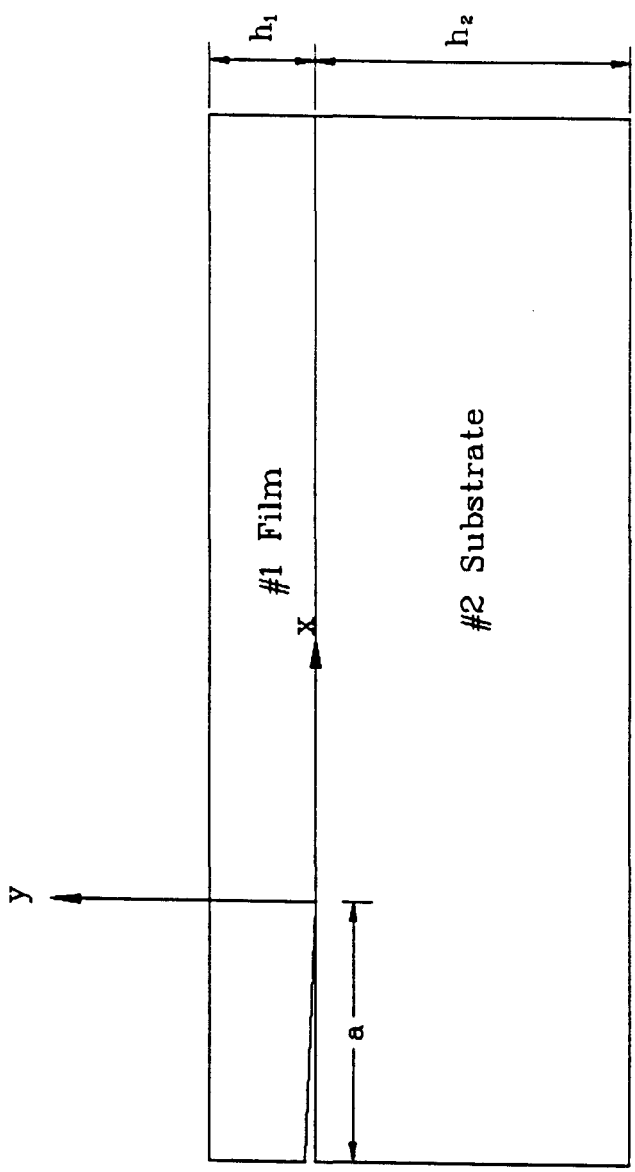

Figure 1

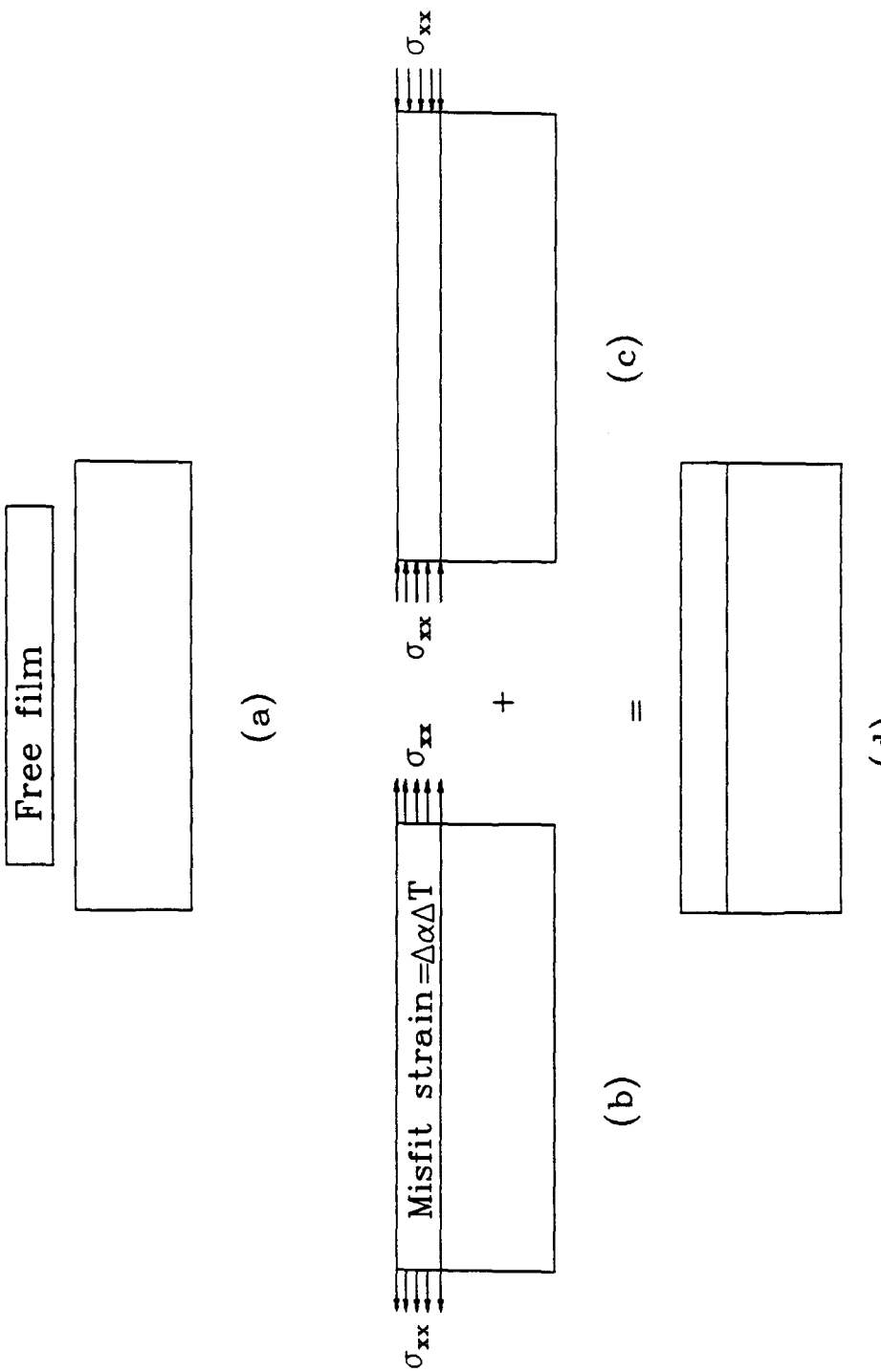
Free film
(a)
σ_{xx}
σ_{xx}
(c)
σ_{xx}
Misfit strain=$\Delta\alpha\Delta T$
σ_{xx}
(b)
+
=
(d)

Figure 2

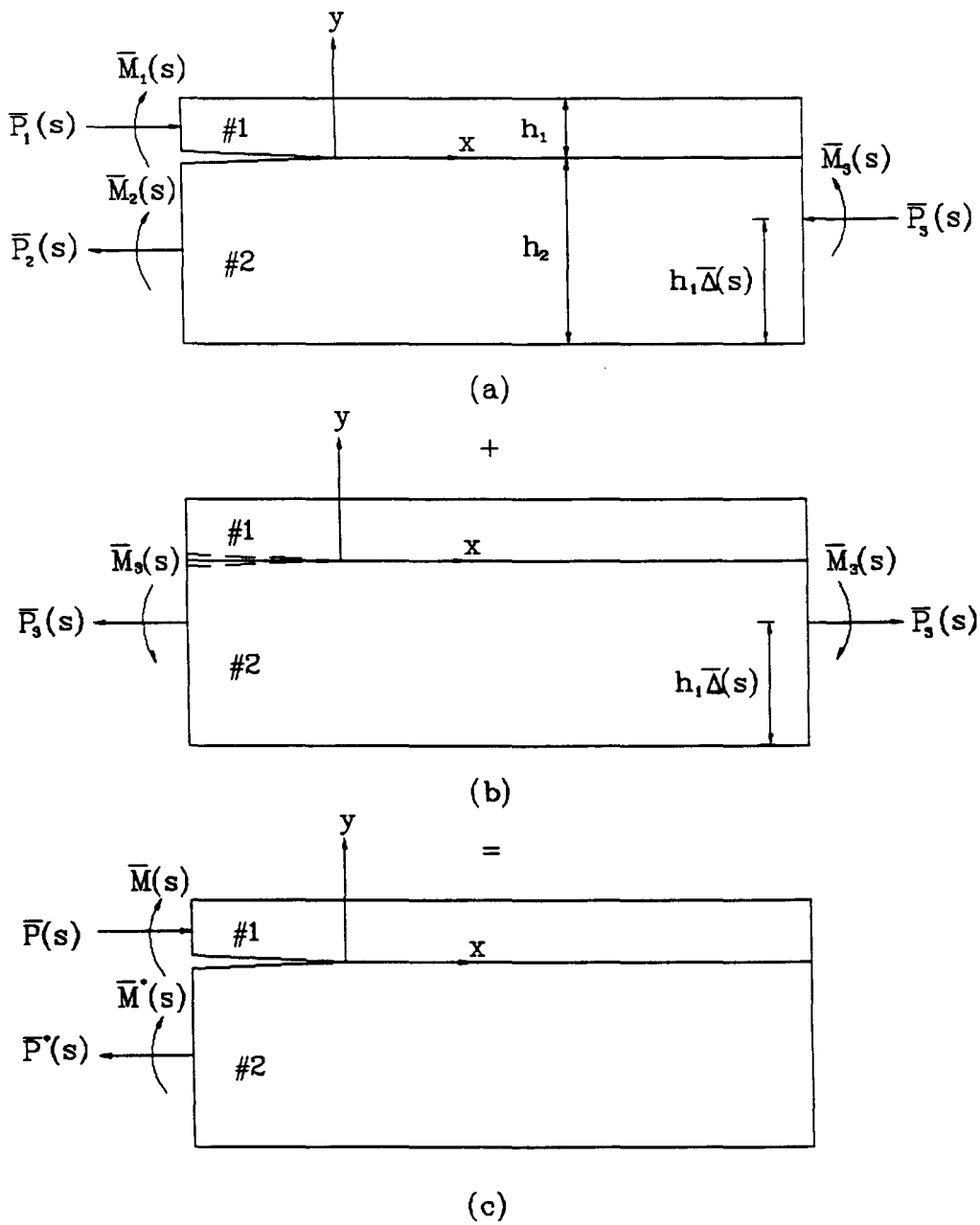
y
$\overline{M}_1(s)$
$\overline{P}_1(s)$
#1
x
h_1
$\overline{M}_3(s)$
$\overline{M}_2(s)$
$\overline{P}_3(s)$
$\overline{P}_2(s)$
#2
h_2
$h_1\overline{\Delta}(s)$
(a)
y
+
#1
x
$\overline{M}_3(s)$
$\overline{M}_3(s)$
$\overline{P}_3(s)$
$\overline{P}_3(s)$
#2
$h_1\overline{\Delta}(s)$
(b)
y
=
$\overline{M}(s)$
$\overline{P}(s)$
#1
x
$\overline{M}^*(s)$
$\overline{P}^*(s)$
#2
(c)

Figure 3

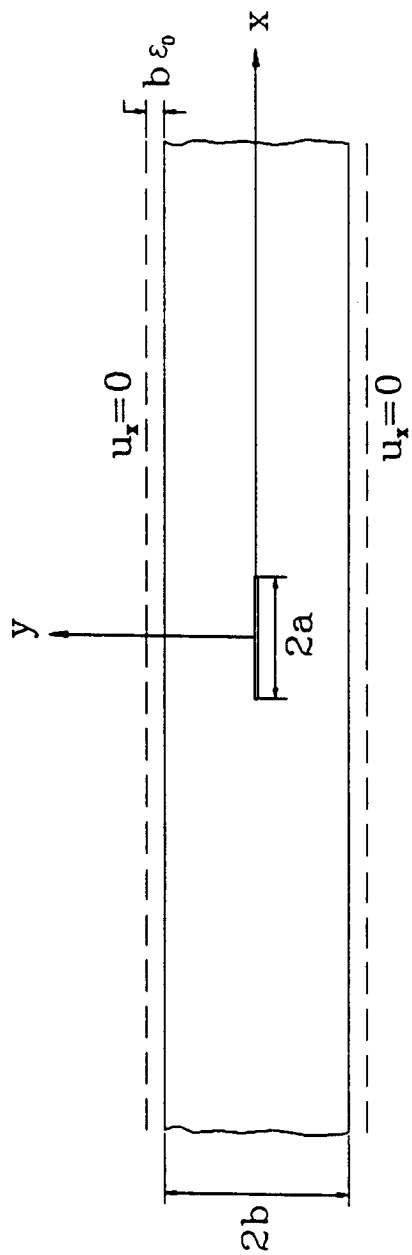

Figure 4

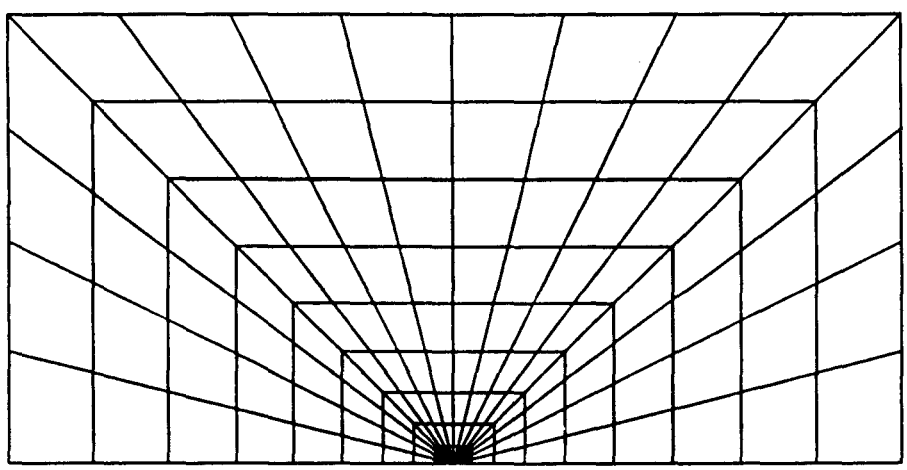

Figure 5

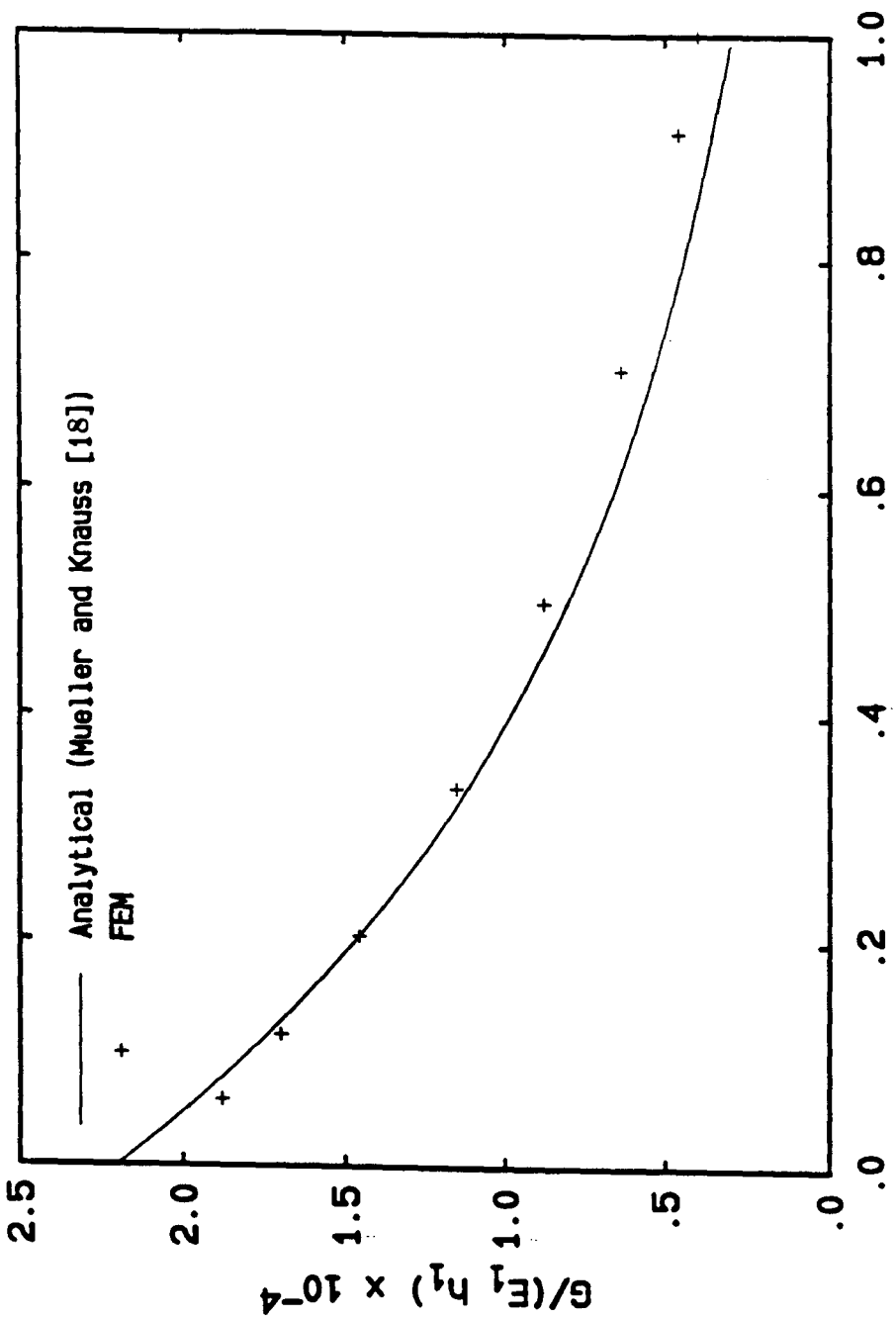
Analytical (Mueller and Knauss [18])
FEM
G/(E1 h1) x 10^-4
t/τ
2.5
2.0
1.5
1.0
.5
.0
.0
.2
.4
.6
.8
1.0

Figure 6

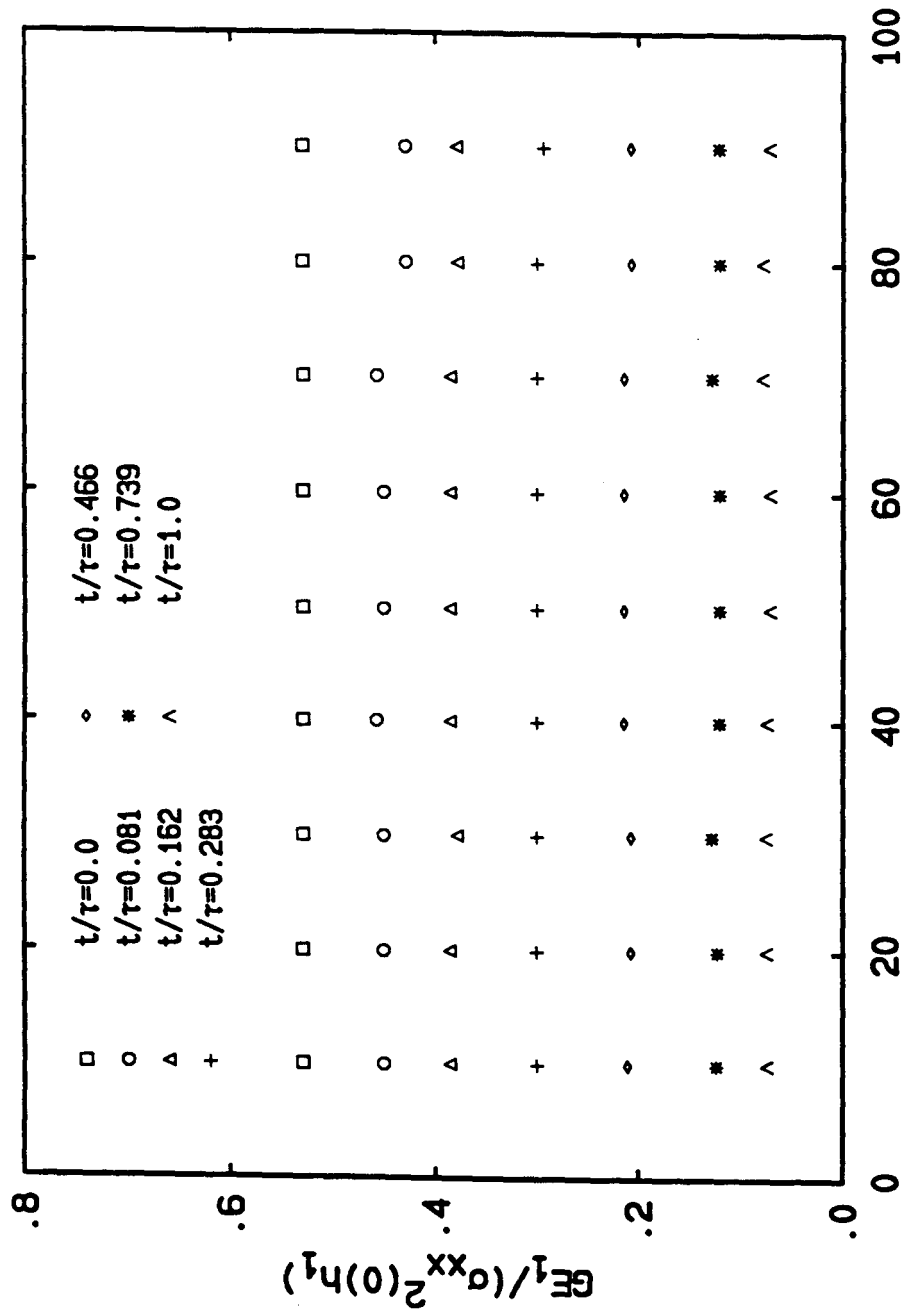
.8
.6
.4
.2
.0
0
20
40
60
80
100
a/h
$GE_1/(\sigma_{xx}^2(0)h_1)$
t/τ=0.0
t/τ=0.081
t/τ=0.162
t/τ=0.283
t/τ=0.466
t/τ=0.739
t/τ=1.0

Figure 7

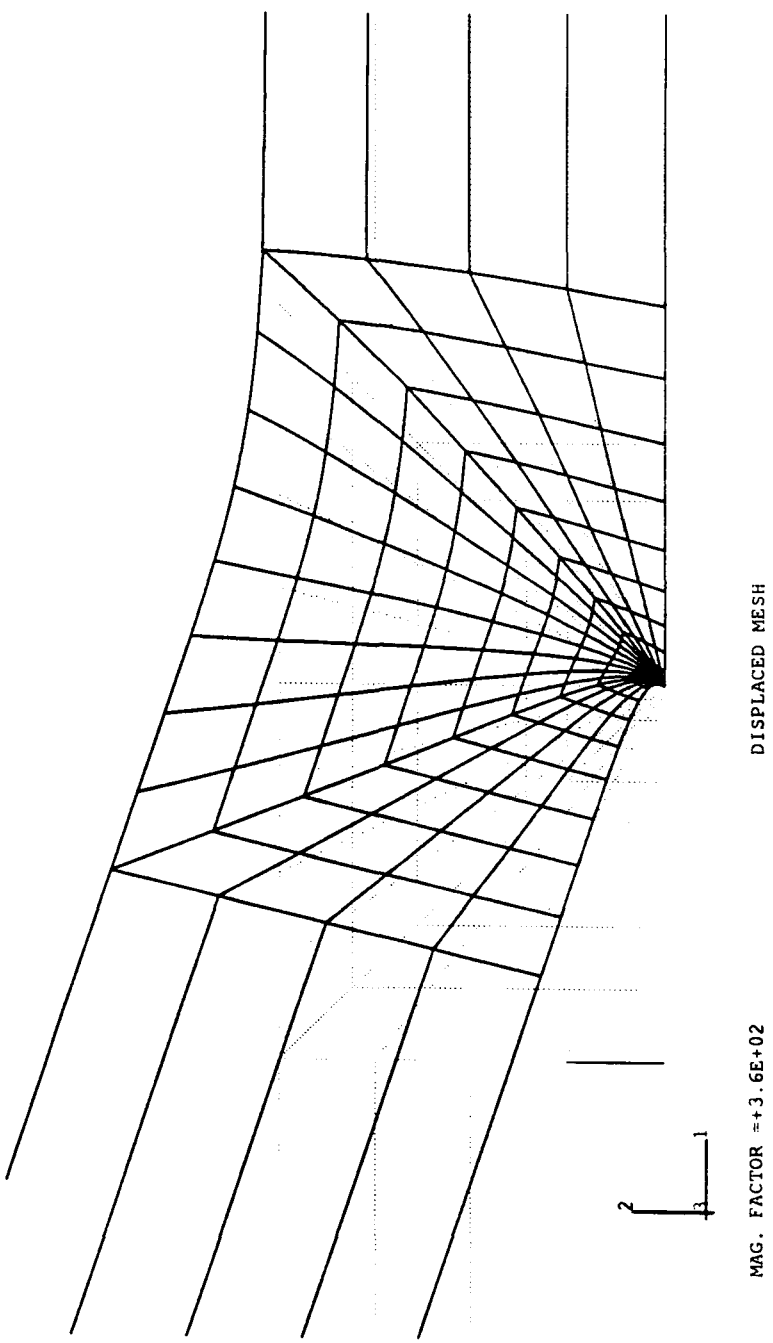

Figure 8

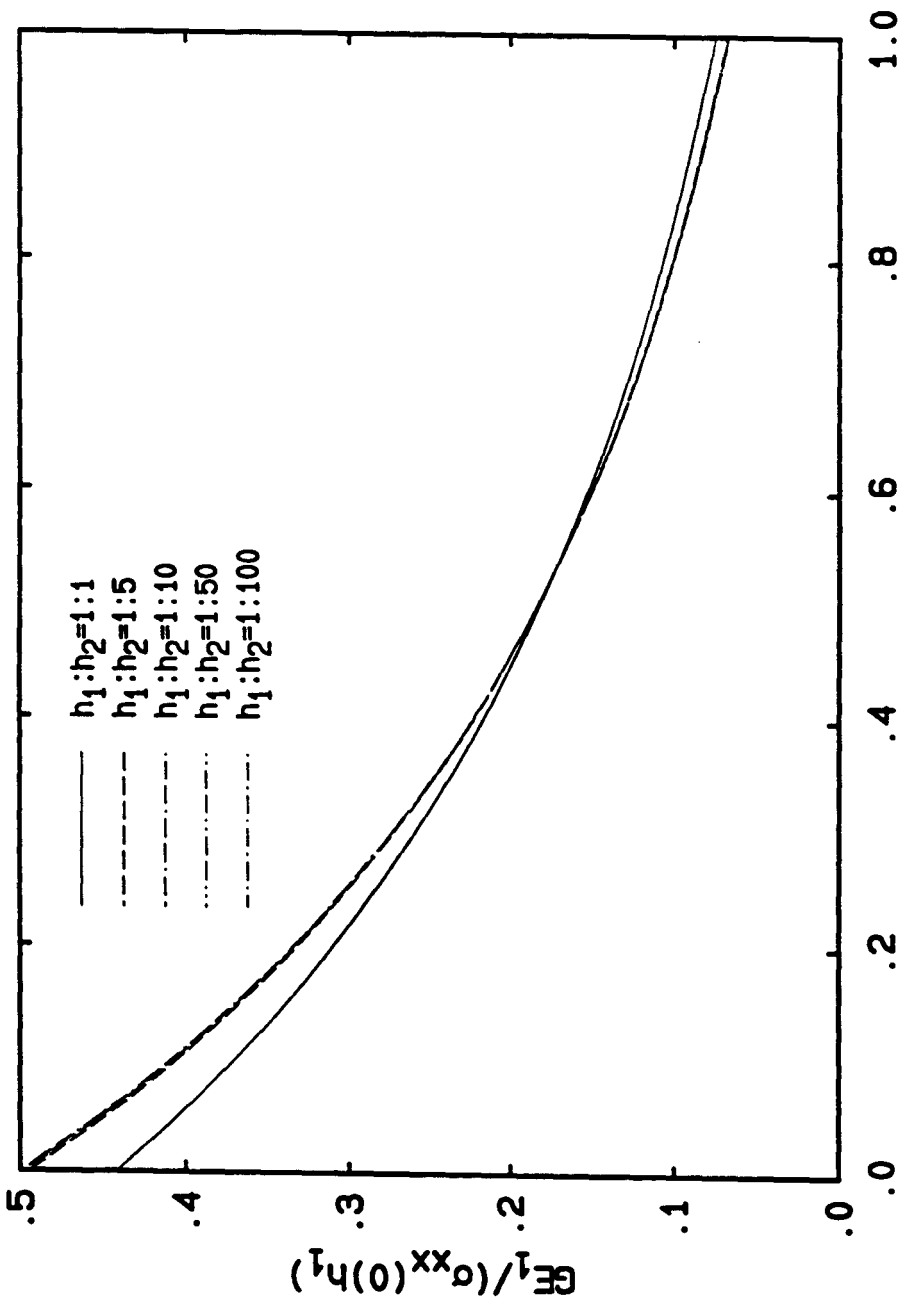
$\delta E_1/(\sigma_{xx}(0)h_1)$
t/τ
h_1:h_2=1:1
h_1:h_2=1:5
h_1:h_2=1:10
h_1:h_2=1:50
h_1:h_2=1:100
.0
.1
.2
.3
.4
.5
.0
.2
.4
.6
.8
1.0

Figure 9

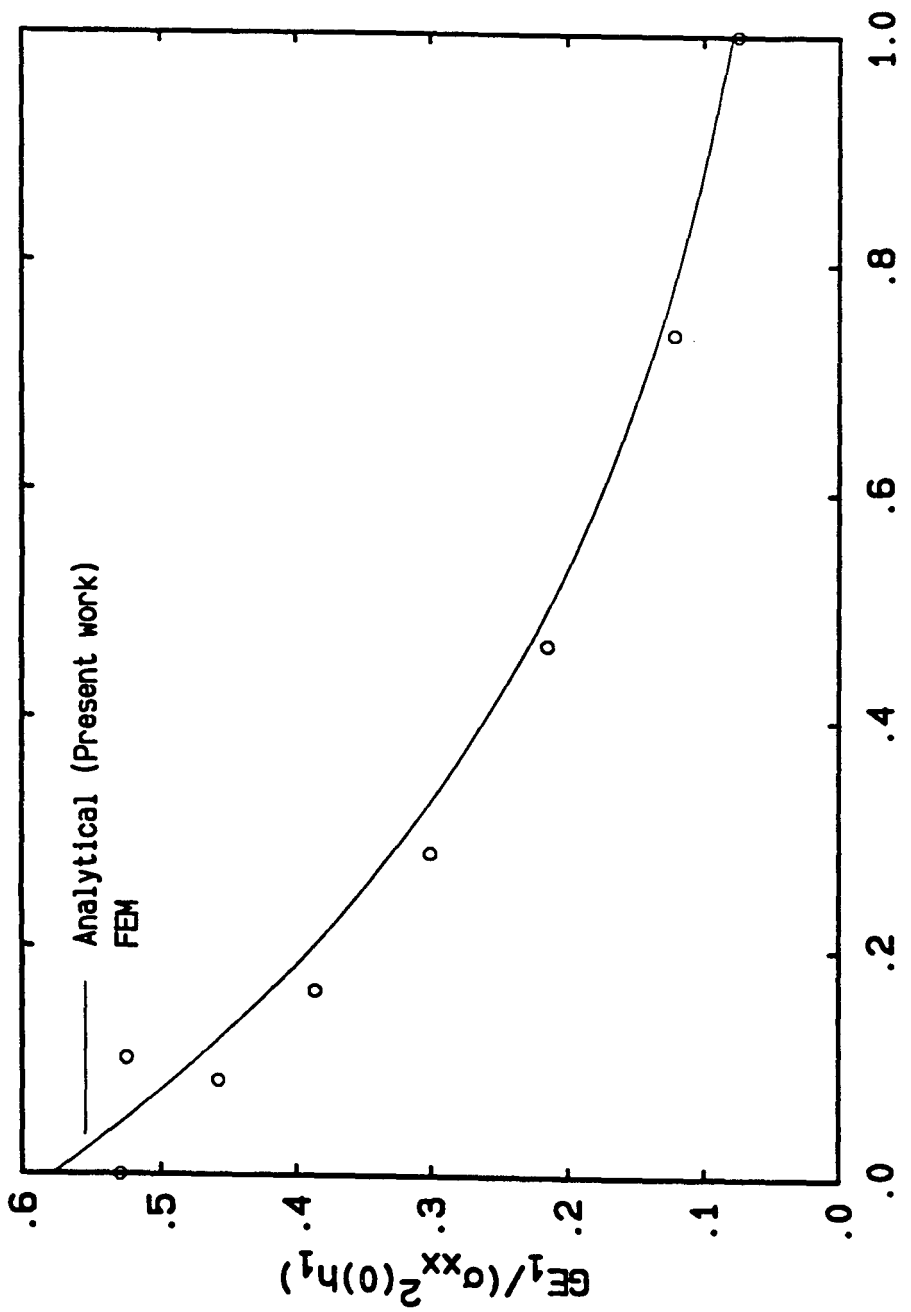
Analytical (Present work)
FEM
$GE_1/(\sigma_{xx}^2(0)h_1)$
t/τ
.0
.1
.2
.3
.4
.5
.6
.0
.2
.4
.6
.8
1.0

Figure 10

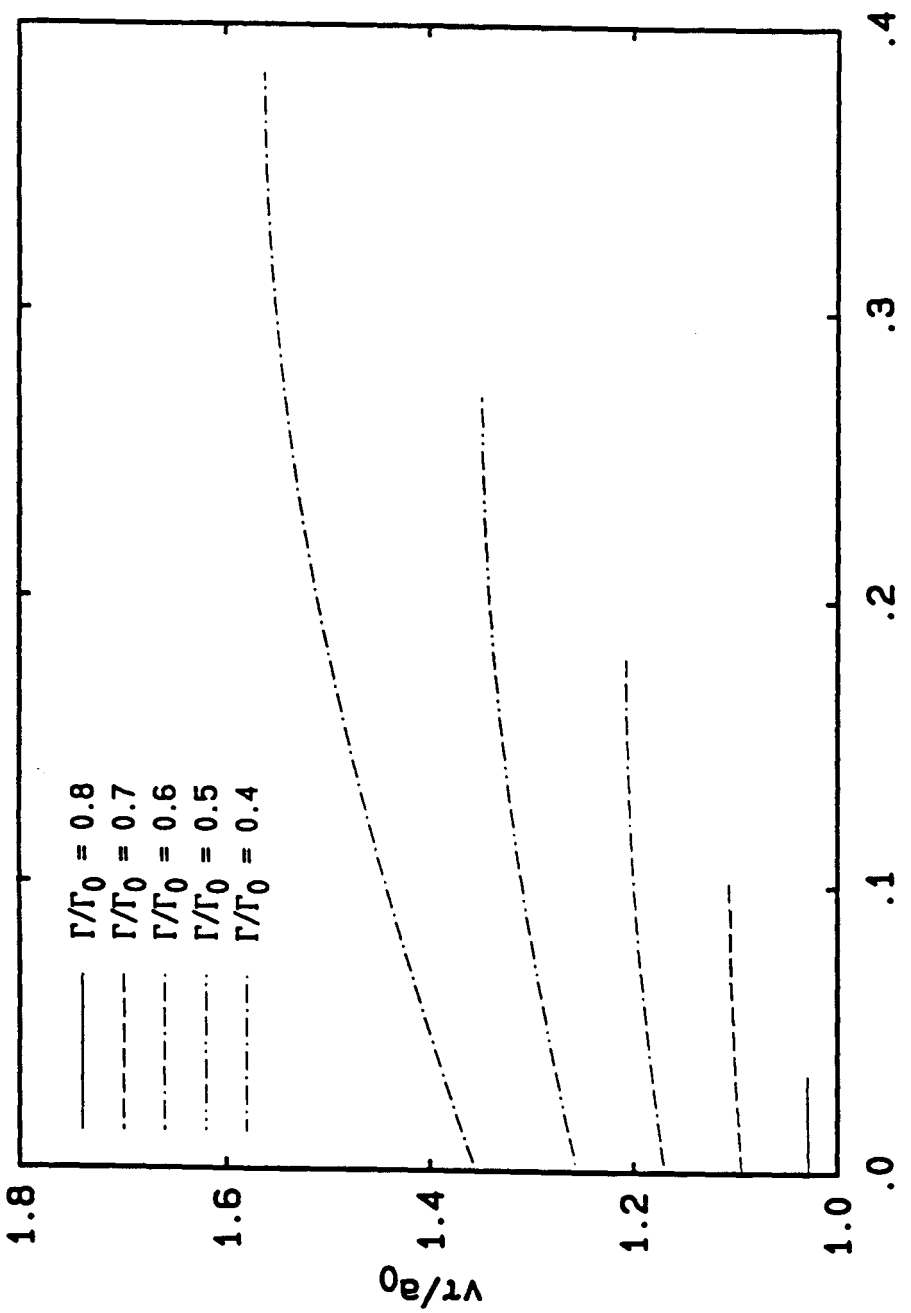

Figure 11

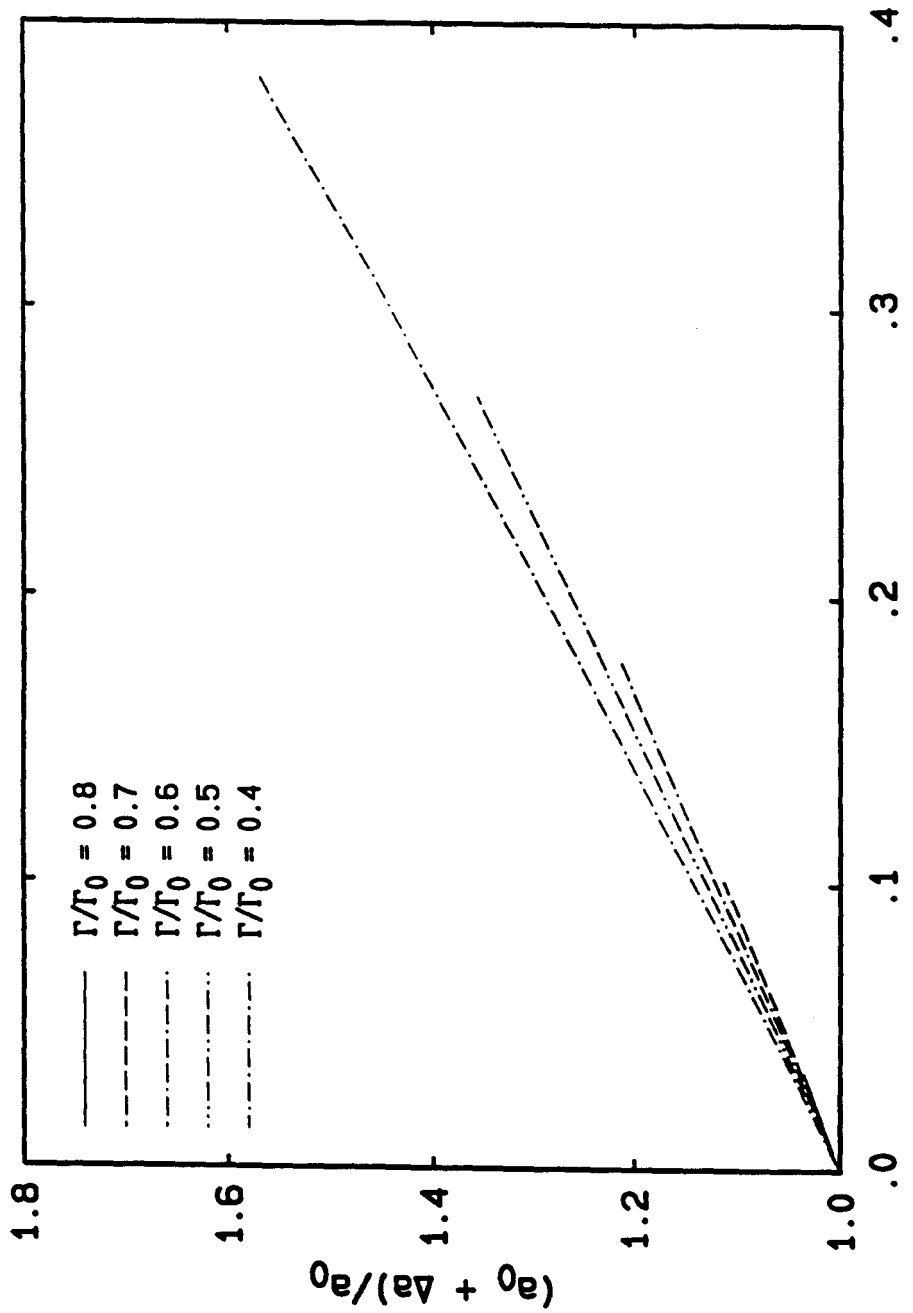

Figure 12

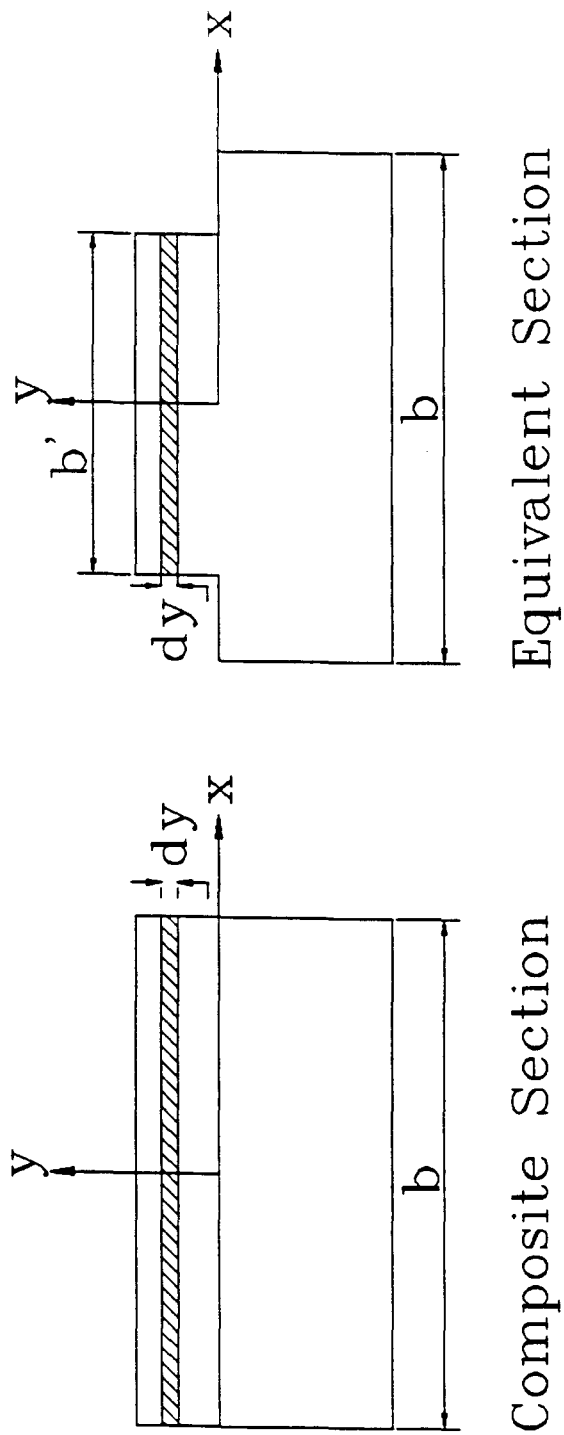

Figure 13